UNITED STATES DEPARTMENT OF THE INTERIOR

GEOLOGICAL SURVEY

Seismic Study of the Agua de Pau Volcano, São Miguel, Açores

by

P .B. Dawson[1], A. M. R. da Silva[2], J. R. Evans[1], and H. M. Iyer[1]

Open-File Report 89-331

Prepared on behalf of the Laboratório de Geociências e Tecnologia
of the Regional Government of the Açores
in cooperation with the
Instituto Nacional de Meterologia and Geofísica, Portugal

[1]Menlo Park, California [2]Ponta Delgada, Açores

1989

Table of Contents

Tables and Appendices

INTRODUCTION

A seismic study of the Agua de Pau volcano on São Miguel Island, Açores, was conducted from June 19, to October 10, 1983 by the United States Geological Survey (USGS) and the Laboratório de Geociências e Tecnologia (LGT) of the Regional Government of the Açores (RGA), in cooperation with the Instituto Nacional de Meterologia e Geofísica (INMG), Açores. The study was part of the LGT program to define the geothermal resources of the Agua de Pau volcano. In 1983 LGT contracted the Office of Earthquakes, Volcanoes, and Engineering, USGS to conduct the seismic study. LGT had previously contracted a comprehensive geoscience assessment of the Agua de Pau geothermal field by members of the USGS from Denver, Colorado, Flagstaff, Arizona, the Hawaiian Volcanic Observatory, and Menlo Park, California. The results of this comprehensive study which was funded by the LGT, USGS, and the United States Agency for International Development (USAID) have been presented by *Silva et al.* [1985].

In this report we present seismic data collected from the central portion of São Miguel using 10 three-channel digital event recorders which were installed by the USGS to augment the 8-station INMG permanent network on São Miguel. Included is a brief review of the geologic and plate tectonic setting of the Açores and the data set, including instrumentation, earthquake location and magnitude determination procedures, temporal and spatial patterns of seismicity, V_p/V_s ratios, and analysis of travel time residuals from regional earthquakes. A review of seismic applications that could serve LGT as a basis for direction in planning future work is included followed by a list of recommendations for upgrading the permanent network and performing further geophysical studies.

GEOLOGIC AND PLATE TECTONIC SETTING

The Açorean archipelago is composed of 9 volcanic islands in the Atlantic Ocean between 37 to 40 degrees north latitude and 25 to 32 degrees west longitude (Figure 1). From a global tectonic point of view the archipelago is located at the westward termination of the Alpide tectonic belt as a triple junction with the Mid-Atlantic Ridge (MAR). The section of this tectonic feature which runs from Gibraltar to the MAR is called the Açores-Gibraltar fracture zone [*Laughton et al.*, 1972]. The Açores-Gibraltar Fracture Zone is characterized by continental collision at the Iberian-African continental margins, and to the west into a deep oceanic basin, a zone of convergence which terminates at about 18°W. From 18°W to 24°W is the 400 km long Gloria fault, an east-west trending strike-slip plate boundary. This lineament continues west as the East Açores Fracture Zone (EAFZ) to an intersection with the MAR. At about 24°W the Terceira Rift [*Machado*, 1972] splits off from the EAFZ to the northwest and continues to the North Açores Fracture Zone (NAFZ) and a triple junction with the MAR at about 39°N. Between the Terceira Rift, EAFZ, and the MAR is the broad Açores plateau (Figure 2).

There are two likely mechanisms for the formation of the present Açores triple junction. *McKenzie* [1972] suggested that the triple junction originated at the junction of the MAR with the EAFZ and then migrated to the north (up the MAR) producing two oblique-spreading arms, one of which would correspond to the Terceira Rift. *Krause and Watkins* [1970] have proposed a similar model. *Searle* [1980] prefers a model in which the triple junction jumps from the MAR-EAFZ intersection to a point farther north on the MAR. The Açores spreading center (Terceira Rift) is then produced, and the EAFZ becomes (relatively) inactive.

The Terceira Rift trends northwest from the Gloria fault at about 36.8°N, 24.5°W to an intersection with the NAFZ near 39.3°N, 28.8°W. The rift is composed of a series of en echelon rifted basins expressed on the islands as grabens where differentiated volcanoes are emplaced, connected by fissural zones where basaltic volcanism occurs. It has been reported that there are chemical differences between volcanic rocks in the fissural zones and the graben zones (where differentiation is occurring), this is verified at least in part on the islands of Faial, Pico, Terceira, and São Miguel (*Silva*, pers. commun. 1986).

São Miguel is the largest island in the archipelago, and lies near the southeast end of the Terceira Rift. Three active trachytic stratovolcanoes are the primary morphologic features on the island (Figure 3). The volcano Furnas and associated Povoção volcanic center comprise the eastern highlands of the island. Agua de Pau volcano, at 950m high, occupies the center of the island and the the volcano Sete Cidades bolsters the western end of São Miguel. All three volcanoes have calderas formed since the late Pleistocene as a result of voluminous eruptions of locally welded pyroclastic flows. Each of these volcanoes have erupted at least once in the last seven hundred years. A 15-km nearly east-west trending zone of fissural basaltic cones runs to Sete Cidades volcano, some 20-km NW of Agua de Pau.

The Agua de Pau volcano lies in a northwest trending graben. The volcano is built on a complex of trachytic welded tuffs, and basaltic and trachytic lava flows which range in age from 300,000 to 100,000 years b.p. The main cone consists of trachytic domes, flows and pyroclastic deposits. C^{14} ages from the pyroclastic flows on Agua de Pau have yielded ages greater than 40,000 years to about 4600 years b.p. The summit of Agua de Pau contains a caldera 3 kilometers wide and 100 to 300 meters deep. The caldera floor is occupied by Logoa do Fogo (Fogo Lake). The caldera is morphologically young and the present relief likely formed during the eruption of 4600 b.p. Several pyroclastic deposits on São Miguel erupted from Agua de Pau suggest earlier caldera forming episodes [*Duffield and Muffler*, 1984]. A trachytic eruption in a. d. 1563 produced the pumice that covers most of the summit and upper flanks of Agua de Pau and mafic lavas were erupted from the flanks of Agua de Pau in a. d. 1563 and 1652.

PREVIOUS WORK ON SAO MIGUEL

As part of the geothermal exploration and development program which was begun in 1976 on São Miguel, many varied geoscience studies have been undertaken by LGT, private contractors, and the USGS [*Geonomics*, 1977; *Gandido et al.*, 1984; *Silva et al.*, 1985]. Prior to 1976 the scientific work on São Miguel was restricted to studies of geologic processes and volcanic histories. Geologic accounts of São Miguel are given by *Jeremine* [1957], *Zbyszewski* [1961], *Walker and Croasdale* [1971], and *Booth et al.* [1978]. Volcanic activity has been documented by *Weston* [1964], and *Machado* in [*Van Padang et al.*, 1967]. The tectonic setting of the Açores has been discussed by *Laughton et al.* [1972], *Feraud et al.* [1980], and *Searle* [1980]. In 1973 a research hole was drilled by scientists from Dalhousie University to obtain information on the volcanic stratigraphy on the north side of Agua de Pau. Temperatures measured in the hole were in excess of 200°C at depths greater than 500m [*Muecke et al.*, 1974] and prompted further research into the geothermal potential of São Miguel. From 1980 to 1984 LGT contracted the USGS to perform a comprehensive study of the geothermal prospects on São Miguel. A review of the geologic, geochemical, and geophysical studies performed by the USGS is given by *Silva et al.* [1985].

The first microearthquake survey on São Miguel was conducted in 1976 on Agua de Pau [*Geonomics*, 1977]. The survey, lasting about 8 weeks and using a portable seismic network, yielded 11 locatable seismic events, most of which were not within the geothermal field. Subsequently, LGT in collaboration with INMG set up a 8-station seismic array on São Miguel. The data from this network has not yet been interpreted.

INSTRUMENTATION

We used 10 Sprengnether DR-100^{TM} portable digital seismographs and two Teledyne Geotech portable drum recorders (Portacorders^{TM}) for the study. Six of the digital recorders and the two drum recorders were installed at sites around the Agua de Pau massif. Three more digital recorders were used at the INMG observatory in Ponta Delgada to record the 8-vertical and 1-horizontal components of the permanent INMG network. The tenth digital instrument was used as a backup and for testing noise levels. Station names and locations are shown Figure 4, and operating parameters are listed in Table 1.

Finding appropriately quiet sites for the portable stations was difficult. Nearly all of São Miguel is under heavy cultivation; where the terrain prohibits farming, cattle are grazed or lumbering operations are present. Pyroclastic flows cover most of the island and rock outcrops are rare. Most outcrops occur in canyons, stream beds, along the coast, or in road cuts and for the most part are inaccessible or seismically noisy. Hence, our seismometer sites were based on compromise between accessibility and best available noise conditions.

The Sprengnether DR-100^{TM} is a 12-bit precision transient-event recorder designed for signals in the frequency range 0-300 Hz and can record up to three components of seismic data. The DR-100^{TM} has an adaptive trigger system and a solid state memory to preserve signal onsets. Channel one is used to activate the trigger. The signal from this channel is rectified and integrated in two averagers giving short-term (STA) and long-term (LTA) average signal levels. STA and LTA averaging periods can be varied and the ratio of these voltages is compared to a user-specified trigger threshold. When the threshold is reached the recorder is turned on. Pre-trigger data is stored in a shift-register memory to preserve pre-trigger signals (event onsets). We used a sample rate of 100 samples/sec and pre-event memory of about 3 seconds. Station CRA and two of the recorders (MI1 and MI2) kept in the INMG observatory had extra memory cards and pre-event memory of 7 seconds.

The DR-100^{TM} has a clock with day/hr/min/sec display derived from a Vectron^{TM} TCXO 1-MHz oscillator. The system ages $2x10^{-9}$ ppm and has a temperature stability of $3x10^{-7}$ sec/deg from 0°C to 50°C. While the system is triggering on an event, timing spikes are added to samples at each odd second on all channels. Before each event is recorded a time code is written containing the system display information, including the time of the first time spike; after each event is recorded a second time code is written containing the time of the last time spike. The header, data, and tailer are recorded on a cassette tape. The recording duration for each event was set for 20 seconds; each tape could hold about 20 events.

The six digital recorders installed on Agua de Pau utilized one vertical and two horizontal L-4 1-Hz geophones and 5-pole low-pass filters with corners at 50 Hz. Gains for the field instruments ranged from 42db to 72db. The seismometer response and the amplifier response are shown in Figure 5. The operating variables depended on the level and type of cultural and natural background noise.

A DP-100^{TM} playback unit and paper chart recorder were also taken to Ponta Delgada to make analog playbacks of the seismograms. Some of the larger local events were timed using

Table 1.

Station Locations and Operating Parameters

Code	Station	Period of Operation (Day/Month/Year)	Latitude (Deg Minutes)	Longitude (Deg Minutes)	Elevation (Meters)	Seismometer Model	Gain (db)
ADA	Agua de Alto	22/06/83 - 12/07/83	37 43.85 N	25 28.59 W	190	S-6000	66**
ADB	Agua de Alto B	12/07/83 - 09/10/83	37 43.98 N	25 28.62 W	200	L-4C	60-66**
CHC	Charcoal	18/06/83 - 06/10/83	37 45.92 N	25 30.59 W	632	L-4C	66
CML*	Pico Cigarreiro	21/06/83 - 12/10/83	37 46.25 N	25 32.76 W	291	S-6000	42
CRA	Cumieira	24/06/83 - 06/10/83	37 45.19 N	25 28.13 W	667	L-4C	66
EPD	Espraiados	22/06/83 - 25/07/83	37 47.72 N	25 23.81 W	506	L-4C	66
EPE	Espraiados	25/07/83 - 07/10/83	37 47.73 N	25 23.76 W	501	L-4C	66
FAC*	Faja de Cima	18/07/83 - 12/10/83	37 46.39 N	25 39.03 W	191	S-6000	42
FRA*	Pico dos Cedros	21/06/83 - 12/10/83	37 44.56 N	25 21.20 W	557	S-6000	42-48
LFA*	Logoa do Fogo	21/06/83 - 12/10/83	37 46.36 N	25 28.99 W	693	S-6000	54
LGD	Logoa do Congro	22/06/83 - 07/10/83	37 45.27 N	25 24.37 W	454	L-4C	66
MTS*	Monte Escuro	21/06/83 - 12/10/83	37 46.86 N	25 26.31 W	826	S-6000	54-60
PFM	Porto Formosa	23/06/83 - 30/09/83	37 48.33 N	25 25.66 W	345	L-4C	66-72
PST	Pasto	20/06/83 - 06/10/83	37 44.16 N	25 31.66 W	265	L-4C	66
PVM	Pico Vermelho	18/06/83 - 23/06/83	37 47.93 N	25 30.93 W	100	L-4C	66
PVN	Pico Vermelho	23/06/83 - 06/10/83	37 47.93 N	25 30.93 W	100	L-4C	60-66**
RIB*	Cerrado Novo	21/06/83 - 12/10/83	37 47.97 N	25 27.66 W	526	S-6000	54
RIBN*	Cerrado Novo	18/07/83 - 12/10/83	37 47.97 N	25 27.66 W	526	S-6000	48
SBA	Santa Barbara	02/10/83 - 12/10/83	37 47.89 N	25 31.00 W	110	L-4C	66
SVA*	Pico Gafanhoto	18/07/83 - 12/10/83	37 47.63 N	25 19.03 W	644	S-6000	48
VIF*	Miradouro	21/06/83 - 12/10/83	37 44.69 N	25 26.38 W	647	S-6000	54

* INMG permanent stations: high cut filter 10 H, low cut filter 0.5 Hz, anti-alias 50, and vertical components except RIBN (N-S horizontal component).

** Portable drum recorders.

All other stations operated with high and low cut filters out, anti-alias 50, and three components (Vertical, N-S, E-W).

P-phases hand picked from the strip charts. We used a HP-85™ microcomputer and computer program HYP85 [*Dawson et al.*, 1985] which is similar to the computer program HYPOINVERSE [*Klein*, 1978] to locate earthquakes while on São Miguel.

The INMG seismic network on São Miguel is centered on Agua de Pau with signals from all stations telemetered to the INMG observatory in Ponta Delgada. There they are decoded and recorded on paper charts at 2 mm/s. The network utilizes Geotech S-6000™, 2-Hz geophones. We monitored all vertical components and one horizontal component (Station RIB) from the INMG network with three of the Sprengnether DR-100's™ at system gains of 36 to 54 db. The 2-Hz seismometers and 10-Hz low-pass filters in the observatory seismographs largely determined the system pass-band for these permanent network stations. The three recorders at INMG were triggered simultaneously by channel one of instrument one (usually station VIF). The INMG recorders were run at low gain levels (24-36 db) because of the extreme cultural and natural noise levels on São Miguel. Two Portacorders™ (ink drum recorders) were operated to provide visual checks of seismic activity in the field and to obtain seismic data for sites too noisy for triggered digital recorders. They utilized L-4 1-Hz vertical geophones, and were operated at gains of 60-72 db.

Two precision clocks (Master Clock II, built by the USGS) were hand carried to the Açores from Menlo Park, California, to provide accurate international time standards for the experiment. The clocks contain an oven-controlled oscillator (aging = 5×10^{-10} ppm, temperature stability = 6×10^{-9} sec/deg from -40°C to +55°C) and were calibrated to the Rubidium time source in Menlo Park, California, before leaving for the Açores. Once in Ponta Delgada one clock was kept stationary for the duration of the experiment and the other clock was used in the field to calibrate the DR-100™ clocks and note the drift rates at every tape change. The field master clock was reset to the stationary master clock once a day. On October 7, 8, and 9, 1983 the master clock was compared to the DCF (Hamburg, Germany) radio time code. The master clock drifted 41.75 ms in 110 days, an average drift rate of 0.36 ms per day (slow compared to the DCF signal). No corrections to earthquake origin times have been applied to compensate for this small drift.

Clocks on each instrument were checked at every tape change and reset to the master time clock. Clock drifts ranged from -13 to +18 ms/day relative to the master clock. Corrections for clock drift were made for each event assuming linear drift, and added to the picked arrival times. Appendix A is a listing of clock drifts for the experiment.

VELOCITY MODELS

A velocity model based on refraction data from the MAR south of the Açores [*Whitmarsh*, 1973] was used for preliminary locations while the experiment was conducted. This simple 3 layer model is shown in Table 2.

Table 2.

3-layer crustal velocity model [*Whitmarsh*, 1973]	
Depth to top (km)	Velocity (km/second)
0.00	4.50
3.80	6.80
8.00	7.50

The model does not allow for thicker crust in the Açores plateau or slow velocities due to near surface pyroclastic deposits.

All events were subsequently relocated using a velocity model derived from seismic refraction data on São Miguel by *Senos and Nunes* [1980] (Table 3). They derived several similar models for São Miguel, the most important features of each being the slow velocities in the upper 2-3 km and the generally thicker (10-11 km) crustal velocities than those derived from seismic refraction profiles at or near the MAR. The low velocities in the top 3 km reflect the near surface pyroclastic flows.

Table 3.

Crustal velocity model based on seismic refraction *Senos and Nunes* [1980]	
Depth to top (km)	Velocity (km/second)
0.00	2.40
0.50	4.10
2.20	5.40
5.40	6.80
11.00	7.80

Final earthquake locations (Appendix B) were derived using the *Senos and Nunes* [1980] model with station delay terms (Table 4) inferred from a study of regional earthquakes referred to later in this paper and applied to the calculated travel times in the location routine. The average root-mean-square residuals in the hypocenter location as well as vertical and horizontal errors were improved 10% using these station terms. Figure 6a is a comparison of epicenters for nine local earthquakes derived from the velocity model without station terms and the velocity model using station terms. Figure 6b is a depth cross-section along A-A' of Figure 6a showing the calculated hypocenters for both models. The most visible difference between the models aside from the improved location residuals is that when applying station terms all epicentral locations are shifted from 0.1 to 2.3 km south and up to 1.3 km deeper.

Table 4.

Station elevations and delays applied in the location routine		
Station	Elevation (m)	Delay*
PVN	100	-0.13
FAC	191	0.05
ADB	200	-0.10
CML	291	-0.02
PST	265	-0.09
PFM	345	-0.17
LGD	454	-0.01
EPE	501	-0.10
RIB	526	-0.05
FRA	557	0.01
CHC	632	0.03
SVA	644	-0.02
VIF	647	0.02
CRA	667	0.05
LFA	693	0.03
MTS	826	0.03
* Delays calculated from a least-squares-fit to regional earthquake data		

MAGNITUDE DETERMINATION

Local earthquake magnitudes can be determined in several ways; we use coda duration (M_D) for all magnitudes listed in this report. The coda-duration magnitude (M_D) is derived by computing the duration of ground motion by employing the relation

$$M_D = a + b \log(\sigma) + c\,\Delta$$

where (σ) is the geometric mean of the total signal duration at all stations recording the event, and Δ is the arithmetic mean distance in kilometers from the epicenter to the recording stations [*Lee et al.*, 1972]. The coda duration is defined as the time from the first motion to where the signal is lost in the background noise. In the absence of any magnitude scale for the Açores, we have used the constants in the scale for California derived by *Lee et al.* [1972]:

$$M_D = -0.87 + 2.00 \log(\sigma) + 0.0035\Delta.$$

Therefore the M_D values presented give only relative magnitudes for the São Miguel area. We used 20 second recording durations (including approximately 3 or 7 second pre-event memory), so only events of less than 13 to 17 seconds duration were used for the coda-duration method. Most of the microseismicity recorded on São Miguel was of 10 to 15 seconds duration so the coda could be measured accurately. Coda durations for the larger

events were taken from the INMG records. *Bakun* [1984] has shown that a close correlation exists in California between M_D and the local magnitude M_L [*Richter*, 1935] for the range $1.5 \approx M_L \approx 3.25$. The M_D values obtained give a first order approximation of the local seismic magnitudes on São Miguel. To develop a magnitude scale that is tuned specifically for the Açores region, many more events must be recorded, including larger-magnitude local events.

DATA

Data from the DR-100™ cassette tapes were read onto a computer system which allowed accurate timing and phase picks of the seismograms, as well as the display of all seismograms for each event (Figure 7). The timing precision of the seismograms is approximately 0.05s. Phase data for each instrument (universal time of the first arrival, direction of first motion, S-arrival time, and coda duration) were then entered into event files. Earthquake hypocenters were obtained using the computer program HYPO71 [*Lee and Lahr*, 1975]. Earthquake hypocenters, program parameters, and symbols used for the HYPO71 location routine are listed in Appendix B,, and Appendix C is a listing of phase data files used for the hypocentral calculation for each event.

There were approximately 7500 station triggers during the experiment. Analog seismograms were made for each event to determine if the triggers were culturally or seismically induced. Approximately 90% of the 7500 triggers appear to have been culturally induced. This means that in order to record small magnitude microseismicity on São Miguel with surficial seismometers one necessarily records a great deal of the human and bovine activity near each station. Over the recording period (June 19 to October 10, 1983), 60 locatable earthquakes, 30 to 40 unlocatable events with arrivals at only two or three stations, and over 300 one station triggers (apparently earthquakes) were recorded. Locatable events averaged one event every seven days. However, microseismic activity was quite high during the entire recording period with several one or two station triggers occurring per day caused by events of $M_D < 1$. Many of the unlocatable events and one station triggers are monochromatic in character. No definite cultural source could be discerned to be causing this type of signal. These small signals are either highly filtered by local velocity structure or are possible B-type volcanic events. At least 60 of the one station events were associated with swarm activity on September 6-7, 1984. Of the 60 located events, 16 are considered regional events (10 km to 140 km outside of the network). The 44 remaining events occurred within and up to 10 km from the network. No teleseisms were recorded because of the high background noise level. Figure 8 is a plot of seismic triggers versus time for the duration of the experiment.

Local Microseismicity

From June 18 to October 10, 1983, 44 local events in the magnitude (M_D) range of 0.6 to 2.3 were located. Ninety five percent of these events occurred to the east of the summit of Agua de Pau. This area is bounded by Lagoa do Fogo on the west, Lagoa de S. Braz on the northeast, and Lagoa do Congro on the south, all occupying Quaternary calderas or trachytic explosion craters. The hypocenters have a horizontal accuracy of about 1.3 km, and a depth accuracy of about 1.6 km. Figure 9a is a map of the earthquake epicenters. Focal depths of these earthquakes (Figure 9b) range from less than 1 to about 12 km depth with only two events occurring deeper than 10 km. The largest events with well constrained focal depths occurred between 2- to 6 km. The events are evenly spread between these depths with no

apparent clustering or linearity. Of significant note is the absence of any located events beneath the summit region of Agua de Pau and the dipping to the east of locatable events with depth. Temporal seismicity patterns were accented by two periods of swarm activity on June 28-29, and September 6-7, 1983 with 50 percent of the located events occurring during the swarms.

Swarm Activity. There were two periods of seismic activity in which locatable events occurred at a higher rate than the background level. On June 28-29, 1983, eight events were located and several unlocatable events occurred. All of the earthquakes during this period were located to the east of Agua de Pau. This increase in seismic activity lasted 28 hours with local magnitudes ranging from M_D 1.1 to 1.5. A larger period of swarm activity with over 200 recorded earthquakes occurred between September 6-7, 1983.

The recording of the seismic swarm on September 6-7, 1983 was enhanced because background noise levels were very low and most stations were running with higher than normal gains. Over 200 events were recorded on the INMG station VIF during a 16-hour period from 1500 UTC September 6, to 0700 UTC September 7, 1983. The digital instruments closest to the swarm area triggered on the numerous events at the beginning of the swarm and ran out of tape before the larger shocks of the sequence occurred. Digital recorders further than 5-6 km from the swarm triggered only on the larger events. Altogether digital records of at least 64 of the swarm events were obtained. Many of the events triggered only one or two stations and the INMG paper records were not clear enough to pick reliable arrivals for the small events. Twenty three events were large enough to be located, 11 by digital records alone, 6 by digital and paper records, and 6 by paper records alone. Magnitudes during this time ranged from M_D 0.6 to 2.3 and focal depths ranged from 0.1 to 12 km. Figure 10 is a plot of the 23 events located during the September 6-7, 1983 swarm.

The swarm of September 6-7, 1983 (Figure 10) began with numerous small events recorded just above the background noise level. The earthquakes increased in magnitude and rate of occurrence for eight hours, with at least 146 events recorded during this prograde period, until 2310 UTC, September 6, 1983 when a M_D 2.1 event occurred. Seismic activity incrementally dropped off after the 2310 event, with 75 events occurring through 0600 UTC, September 7, 1983. At 0555 UTC September 7, 1983 the largest locatable event of the swarm was recorded at M_D 2.3. Two more locatable events were recorded at 0606 and 0635 UTC, after which activity remained very low for three days with only a few one and two station events recorded until September 11, 1983. Figure 11 is a plot of total events versus time for the swarm activity and Figure 12 is a plot of magnitude versus time for the September swarm.

There are several possible explanations for the seismic activity on the east side of Agua de Pau. First, the activity could be associated with the geothermal system described by *Duffield and Muffler* [1984], although no surface manifestations of the system are visible in the area of seismic activity and seismic activity is sparse near known manifestations on the north slope of Agua de Pau. Fumaroles and hot springs, such as Lombadas and Caldeiras, occur at the intersection of faults and deeply eroded canyons on the north slope of Agua de Pau. The east side of Agua de Pau is not deeply eroded so the geothermal system may be masked by overlying deposits. Second, the activity could be due to regional stress being released along the Terceira Rift. The structure of the rift zone is not well defined through Agua de Pau because recent volcanic deposits cover most structure and faults. Third, many of the studies concerning São Miguel suggest that a large rhyolitic magma chamber underlies the

central and eastern portion of São Miguel [*Booth et al.*, 1978; *Duffield and Muffler*, 1984; *Gandido et al.*, 1984]. The seismic activity could be associated with minor inflation or deflation of the postulated magma chamber or with movement of magma in fractures. The absence of seismic activity beneath the summit of Agua de Pau and the sharp delineation of the activity at an angle away from the summit of the volcano (to the east) may be reflecting the "shadow" of a magmatic, partially molten, or hot plutonic heat source. This boundary may reflect a difference in temperature and or pressure which corresponds to an elastic-anelastic transition zone. Another interpretation of the demarcation of seismicity is that it may delineate the east side of the Agua de Pau graben, although the dip of the interface is in the wrong sense for a graben structure. *Anderson* [1936] predicted with mathematical analysis that outward dipping caldera fault structures would result from cauldron subsidence. The most prominent example of outward dipping caldera faults is seen at Rabaul caldera, Papau New Guinea [*Mori and McKee*, 1987]. The observed depths of earthquakes at Rabaul only extend to about 4 km depth, while at Agua de Pau the seismicity extends to greater than 10 km. It is not known if the caldera ring fault system extends to these depths, so the magmatic or regional tectonic interpretations discussed above may be more likely sources for the seismic activity.

Regional Seismicity

Sixteen regional earthquakes were recorded over the period of the experiment. Since these events occurred well outside our seismic network, their epicenters and depths could not be determined accurately and magnitudes are taken from codas on the paper INMG records. Several of these events had emergent P-phases and poor S-phases, and were monochromatic in character. It is possible that these events could be local B-type volcanic events. A typical regional event located using good arrivals is shown in Figure 13. Figure 14 shows the epicenters of the 16 regional earthquakes. The epicenters are scattered over a broad area about São Miguel. At least 12 of the 16 events fall along a northwest striking zone, reminiscent of the 10-year regional pattern of seismicity shown in Figure 15, which delineates the Terceira Rift, North Açores Fracture Zone, and the Mid-Atlantic Ridge.

V_p/V_s AND POISSON'S RATIO

In the hypocenter location program (HYPO71), a constant V_p/V_s ratio is assumed. Since only a P-velocity model is specified, the program assumes that the S-velocity is $1/\sqrt{3}$ of P-velocity, corresponding to a Poisson's ratio of 0.25. However, significant V_p/V_s variations have been found in active geothermal areas, such as Yellowstone National Park, Wyoming [*Chatterjee et al.*, 1985]. These variations are thought to be caused by pore-fluid and steam-filled fractures in geothermal reservoirs.

V_p/V_s can be determined by using the Wadati method in which arrival times of P-waves (t_p) are plotted as the abscissa and the difference of arrival time between the P and S-phases (T_{p-s}) as the ordinate. If Poisson's ratio

$$\sigma = \frac{1}{2} \left((V_p / V_s)^2 - 2\right) / \left((V_p / V_s)^2 - 1\right)$$

is constant along the travel path of the seismic ray, the relation (T_{p-s}) versus t_p will be a straight line for any given event with a slope equal to (V_p/V_s)-1 [*Wadati*, 1933; and *Kisslinger and Engdahl*, 1973]. Alternately, one can plot a modified Wadati diagram in which

instead of plotting T_{p-s} versus T_p, the P-wave travel time T_p is plotted as abscissa against the S-wave travel time T_s as ordinate. Earthquake location and origin time errors do not affect the slope in either method if Poisson's ratio is constant in the volume sampled by the seismic rays. The slope of the line through the T_p versus T_s travel time plot gives V_p/V_s directly. The advantage of the latter method is that travel time data from several earthquakes can be plotted simultaneously to derive an average of V_p/V_s for the study area. Hypocentral errors only weakly effect such plots.

Local events

We chose to use the modified Wadati method of plotting T_p versus T_s to derive a V_p/V_s ratio for the local events rather than the standard Wadati method because the limited number of stations recording individual events exhibited a large range of scatter in obtained V_p/V_s values in the standard method. Two modified Wadati diagrams were plotted, the first using data from vertical and horizontal geophones, the second using data from only horizontal geophones. Figure 16a is a modified Wadati diagram for 37 local events using 84 readings from vertical and horizontal components. Figure 16b is a subset of this data in which readings from the three-component instruments only are plotted. A least-squares fit was made for each plot and the V_p/V_s ratios and Poisson's ratios were calculated. Confidence intervals of 90, 95, and 99 percent for V_p/V_s were also determined [*Graybill*, 1976]. Table 5 is a summary of the results. Figure 16a, plotted using S-phases weighted 3 or better for 37 of the local events, gives $V_p/V_s = 1.52 \pm 0.09$ and Poisson's ratio of 0.11 ± 0.05. The correlation coefficient is 0.95 which indicates that a linear fit is appropriate. To check the reliability of the V_p/V_s value (1.52 is quite low compared with the global average of 1.73), we plotted S data picked from just the horizontal components (Figure 16b) since possible systematic errors introduced in reading S arrival times from vertical components could lower the value of V_p/V_s. V_p/V_s from these data is 1.53 ± 0.12 and the Poisson's ratio 0.13 ± 0.06. The correlation coefficient is 0.96 indicating a good linear relationship between P and S. Figures 16a and b demonstrate that the arrival times of S-phases picked using the vertical geophones are within the error limits of the S picks from the horizontal geophones.

Table 5.

V_p/V_s and Poisson's ratio in the São Miguel region

Area	V_p/V_s	Correlation	σ	Confidence Interval		
				90%	95%	99%
Agua de Pau*	1.52	0.963	0.11	0.09	0.11	0.14
Agua de Pau **	1.53	0.963	0.13	0.12	0.14	0.20
Regional events	1.62	0.984	0.19	0.05	0.07	0.09
* Data from vertical and horizontal geophones for 35 local events						
** Data from only horizontal geophones for 27 local events						

Regional events

V_p/V_s ratios for the regional events were derived using Wadati's original method for four of the best-recorded regional events. The resulting V_p/V_s ratios are widely scattered in the range of 0.91-1.98, reflecting the poor resolution resulting from using a limited number of data points over a limited aperture range for each event. To find an average V_p/V_s value for the regional events we plotted the phase data from nine regional events on a modified Wadati plot using only arrivals weighted 3 or better (Figure 16c). The resulting best fit line for the regional events gives a value of 1.62 ± 0.05 for V_p/V_s and Poisson's ratio of 0.19 ± 0.02. The correlation coefficient for the data is 0.98. The data for the regional events are summarized in Table 5. Figure 16d is a bar graph showing the error limits of V_p/V_s for two local event data sets and the regional event data set.

Observations

Two key observations can be made of our V_p/V_s measurements: (1) there is a 7% difference between V_p/V_s values computed using local and regional events; and (2) low V_p/V_s values prevail for both regional- and local-event data sets, compared with the global average value of 1.73. We are unable to assign a high level of confidence to the difference between V_p/V_s for local and regional events, as can be seen from the bar graph in Figure 16d. However, the difference, if real, is not surprising since the local events represent V_p/V_s in a crustal volume of complex volcanic rock around the Agua de Pao volcano, whereas the V_p/V_s value using regional events are for the sub-moho ray paths of Pn and Sn phases of the regional events. One expects the regional V_p/V_s value to correspond to that for fairly homogeneous upper mantle, however, the V_p/V_s value for basaltic samples from the Pacific Ocean measured in the laboratory is about 1.86 [*Christensen*, 1972], a value much higher than our observed 1.62.

A plausible explanation for the low V_p/V_s value in the crust beneath Agua de Pao can be given in terms of the presence of a fractured geothermal reservoir in which the temperatures are close to that at water-steam transition. A steam-water phase-transition anelastic mechanism should affect compressibility more than shear modulus, lowering V_p/V_s. The presence of partial melt is not an acceptable explanation since melt inclusions tend to reduce S-wave velocity more than P and increase V_p/V_s. Mineralogical anomalies [*Kern and Richter*, 1981] between the summit and flanking volcanic materials could produce a lower V_p/V_s ratio, or erroneous identification of the S-phases are possible explanations. However, the consistent correlation of S between events (Table 5), indicates we are accurately identifying the S-phase.

REGIONAL TRAVEL TIME RESIDUAL ANALYSIS

Teleseismic P-residual and attenuation studies have been used extensively in the United States to delineate zones of anomalous seismic-wave velocities associated with magmatic heat sources (Yellowstone: [*Iyer et al*, 1981]; The Geysers-Clear Lake area: [*Oppenheimer and Herkenhoff*, 1981, and *Ward and Young* 1980]; Long Valley-Mono Craters: [*Achauer et al.*, 1986]; Coso Hot Springs: [*Reasenberg et al.*, 1980, and *Young and Ward*, 1980]; Roosevelt Hot Springs: [*Robinson and Iyer*, 1981]; San Francisco Mountain: [*Stauber*, 1982]; Newberry Volcano: [*Stauber et al.*, 1988]; and Medicine Lake Volcano: [*Evans*, 1982]). On São Miguel, due to the high ambient seismic noise level, we did not record any teleseisms, however, we were able to use the regional events to map P-residual patterns in the Agua de

Pau area using a modified version of the teleseismic experiment. The term "P-delay" refers to the increase in travel time as seismic P-waves traverse a low-velocity body, such as a magma chamber. If the P-waves travel through a homogeneous, isotropic medium the arrival times of P-phases at a seismograph array reflect a constant velocity of travel and no travel time residuals (advances or delays) are observed. On the other hand, if the waves sample an anomalous high- or low-velocity zone the arrival-times give measurable travel time residuals. Positive residuals or P-delays are associated with low-velocity or low-density bodies and negative residuals or P-advances are associated with high-velocity or high-density bodies beneath the array.

Travel time residuals were calculated for P-arrival times from nine of the regional events by using a least squares fit to the plane wave-front. Average apparent velocity and azimuth of travel to the source were also calculated. The travel time residuals at each station are simply the deviation of the observed arrival times from the predicted least-squares-fit arrival times. Note that the residuals calculated using this method are independent of the earthquake locations and origin times and do not account for wave front curvature. Azimuths of the events measured from the network ranged from 91° to 314°. Apparent velocities, azimuths, and residuals are shown in Table 6. Residuals from all azimuths, except the event at 263°, show positive residuals (delays) around the summit of Agua de Pau. Superimposed on this central delay is a pattern of azimuthally varying residuals. To highlight the azimuthally invariant component of the residual pattern, we have averaged the residuals from all events (Figure 17). The azimuthally invariant pattern is dominated by an east-west elongate zone of P-delays (with an amplitude of 0.1 to 0.2 seconds) centered on Agua de Pau volcano.

Table 6.
Plane Wave Station Residuals

Event	Azimuth	App. Vel.	Station															
	(degrees)	(km/sec)	ADB	CHC	CML	CRA	EPE	FAC	FRA	LFA	LGD	MTS	PPM	PST	PVN	RIB	SVA	VIF
2752157	314**	6.23	-0.08	-	-0.05	-	-	0.02	-	0.00	-	0.03	-	-	-0.08	0.00	-0.01	0.03
1820533	293**	6.82	-	-	-	0.13	-	-	0.04	-	-	-0.02	-	-	-0.17	-	-	-0.14
2220040	193	6.85	0.01	0.04	-0.07	-0.04	-	0.33*	0.54*	0.07	-	0.18	-	-0.05	-0.21	-0.08	0.42*	0.19
2750543	159***	7.19	-0.16	-	-0.08	-	-	0.21*	0.06	0.03	-	-0.01	-	-	-0.19	0.07	-0.19	0.04
2250214	149***	5.45	-0.15	-	-2.20*	-	-	0.01	-	-0.06	-0.01	-0.02	-	-0.03	-0.72*	0.02	-	0.16
1832229	131***	7.52	-	0.02	0.10	-	-0.10	-	0.01	0.09	-	0.09	-0.17	-0.18	-0.03	-0.06	-	-0.01
2242236	130***	8.35	0.58*	-	0.00	-	-	0.47*	1.07*	0.10	-	-0.03	-	-	-0.01	-0.09	0.06	-0.06
2820421	127***	7.71	-0.26*	-	-0.06	-	-	0.13	-0.07	0.10	-	0.09	-	-	-0.38	-0.15	-0.02	0.02
1792217	91	7.14	-	-	0.04	-	-	-	0.79*	-0.10	-	0.00	-	-	-	-0.13	-	-0.05
Average		7.72	-0.10	0.03	-0.02	0.05	-0.10	0.05	0.01	0.03	-0.01	0.03	-0.17	-0.09	-0.13	-0.05	-0.02	0.02
Average	NW**	6.53	-0.08	-	-0.05	0.13	-	0.02	0.04	0.00	-	0.01	-	-	-0.13	0.00	-0.01	-0.06
Average	SE***	7.24	-0.16	0.02	-0.01	-	-0.10	0.07	0.00	0.05	-0.01	0.02	-0.17	-0.11	-0.15	-0.04	-0.05	0.04

* 4 qualities not used in the analysis

Assuming that the averaged residuals reflect velocity anomalies in the top layers of the

crust, the residuals remaining when the average residual is removed should approach zero if all variations in P-wave velocities are due to structure in the top crustal layers (because residuals caused by shallow anomalies are azimuthally invariant). Figures 18a-i are plots of the residuals for each event minus the average residuals. The patterns show clear evidence for azimuthal variation – the delays shift away from the source direction for different events.

There are several possible explanations for this pattern of delays including elevation effects, composition effects (trachytic volcano versus mafic crust), or anomalies due to steam or melt in the upper. Simple elevation effects can account for most of the delays observed near the summit of Agua de Pau. Figure 19 shows station elevation versus the average residual. Except for FAC and CML, the two stations on the western extension of the anomaly, the data fit a line indicating an elevation correction velocity of 5 km/s should be applied as a station term. The observed P-delays of 0.1 to 0.2 seconds require 0.5 to 1 km station elevation, which is the range of elevation for the stations. Since the average station residuals seem to reflect structure observed from all azimuths, they have been applied as station term input to HYPO71 for locating the regional and local earthquakes.

The difference in composition from the Agua de Pau massif to the surrounding crust could also contribute to the delay pattern. A complex of trachytic tuffs and flows imbedded in a basaltic medium could cause a delay of P-wave arrivals at stations on the massif. Another explanation for the delays is to assume that the linear relationship between residuals and elevation is caused by an extended crustal low-velocity zone. Since the seismic waves used in this study are probably Pn phases with an emergent angle of about 23°, the observed delays could be interpreted to have been caused by a low-velocity body, elongate in an east-west direction, beneath the Agua de Pau volcano. The body could be 10 km long and 5 km wide, extending from the surface to a depth of about 5 km. The resultant velocity decrease (using 0.1-0.2 second delay) within the body from the surrounding rock would be about 10%. One example of such a low-velocity body could be a large steam reservoir within the upper crust. The presence of a large geothermal system in the area of Agua de Pau is also suggested by the geochemical and geophysical studies performed by the USGS, the presence of hot springs such as Lombadas and Caldeiras, of producing geothermal wells, and the low V_p/V_s ratios discussed earlier. A steam reservoir can explain the low V_p/V_s and low P-wave velocities inferred from the delays because steam-filled fractures in rock volumes result in lower than normal P-velocities [*Ito et al.*, 1979]. Another explanation for a crustal low-velocity body is the presence of partial melt [*Iyer and Stewart*, 1977]. Relating detailed surface lithology with the observed residuals, and further detailed geophysical studies are needed to discriminate between these proposed delay-causing mechanisms.

DISCUSSION

The significant finding of this study is that the seismic activity recorded for the duration of the experiment was centered on the east slope of Agua de Pau and extended into the topographic low between the Agua de Pau and Furnas volcanoes. Little seismicity was recorded directly under the Agua de Pau caldera and no seismicity occurred near any known geothermal manifestations such as Lombadas or Caldeiras. It must be noted that only the larger events (M>1.5) which occurred within the network triggered 50 per cent or more of the portable stations. Station VIF triggered the recording of the 8 INMG vertical seismometers so there is a bias toward locating events occurring in the vicinity of station VIF. Few events occurred south of VIF, however, indicating that there is a real southern boundary of seismic

activity in the vicinity of VIF. We estimate that events with $M_D < 2$ and occurring more than 15 km from the center of our network would not be sensed by the number of stations required to locate the event. Thus, if activity is present at the Cete Cidades and Furnas volcanoes, it is on the order of that about Agua de Pau or less. The large number of seismic triggers for which no location was possible indicates that the seismicity of São Miguel is probably much higher than that implied by the small number of events located in this study.

The comprehensive study of the Agua de Pau volcano conducted by the USGS indicates an active geothermal system exists under the upper portion of Agua de Pau, with the most likely prospects on the north and east sides of the volcano. The low V_p/V_s ratio of 1.52 for local earthquakes and 1.62 for regional earthquakes suggest a zone of anomalous P-velocity exists beneath Agua de Pau. Most of the receivers are west, north, and south from the local earthquakes sources used in the V_p/V_s study. Clearly a zone of low V_p/V_s exists above and to the west of the area of seismic activity, which corresponds to the summit area of Agua de Pau. High temperature and pore pressure could affect V_p/V_s as could differences in composition between the summit material and flanking material of Agua de Pau or the presence of slow surficial pyroclastic deposits. However, it has been shown that low values for V_p/V_s in a geothermal regime are indicative of a steam reservoir. *Senos and Nunes* [1980] cite evidence of a zone of attenuation under the Furnas volcano and low (1.58) V_p/V_s values in a similar geological setting 20 km from Agua de Pau.

Residuals from P-wave travel times calculated from 9 regional events show slower arrivals about the summit of Agua de Pau than around the flanks. The difference is on the order of 0.1 to 0.2 s which does not indicate the presence of a large magma chamber. The residual pattern could be due to simple elevation effects, partial melt, or a low velocity anomaly such as a steam reservoir which affects the P-wave travel time.

Silva et al. [1985] and *Duffield and Muffler* [1984] have reviewed the geologic, geophysical, and hydro-geochemical data from the USGS studies and conclude that a high-temperature magmatic or plutonic heat source is driving a hydrothermal-convection system with upflow near the summit of the volcano at temperatures near 300°C. Figure 20 is a depth cross-section plotted along A-A' of Figure 9 showing the local seismicity, the likely area affecting V_p/V_s, and the zone of P-delays. Also plotted on this figure is the schematic from [*Silva et al.*, 1985] showing the geothermal system inferred by other USGS studies. It is apparent that several plausible theories can be forwarded to explain the location of seismicity, low V_p/V_s values, and P-delays, so clearly more geophysical studies need be done to prove or disprove these alternatives. However, the agreement between this study and that of *Silva et al.* [1985] is quite good, supporting the presence of a hydrothermal system beneath the summit of the Agua de Pau volcano.

Earthquake and Volcanic Hazards

It must be stressed that the seismic activity present on and near São Miguel is an ongoing process. The possibility of large magnitude events is low in any given year, but must not be discounted. The January 1, 1980, M 7.2 event [*Hirn et al.*, 1980] that destroyed many buildings on the island of Terceira is an example of the type of tectonic event associated with the Terceira Rift which could occur under or near São Miguel . However, the short duration of our seismic study does not permit definitive conclusions on the recurrence intervals or other statistics of destructive earthquakes near the island.

The youthful calderas and historical volcanic activity at all of the volcanic centers on São Miguel, as well as the ages of eruptions documented by *Booth et al.* [1978] indicate future eruptions can be expected. The eruptive histories of the volcanoes on São Miguel document recurrence intervals of 500 years for a magnitude 6 eruption and 200 years for a magnitude 5 eruption. Swarm activity is often observed in active volcanic systems and the occurrence of two such swarms of seismic activity in three months suggests the presence of an active volcanic system at the Agua de Pau volcano. Seismic monitoring of the microearthquake activity on São Miguel must be upgraded so that an accurate record of activity can be built for future reference. Deviations from the normal pattern of seismicity should be noted so that possible impending eruptions could be prepared for.

Magma Chamber

One of the purposes of our study was to detect any magma chamber present beneath the Agua de Pau volcano. Travel time residuals obtained from the regional events do not definitively define a magma chamber, though they could be interpreted as due to a crustal low-velocity body in which the P-wave velocity is lower than normal by about 10%. The body could be a result of a dry-steam reservoir or a partially molten magma chamber beneath Agua de Pau or simply reflect the silicic composition of the massif.

The low V_p/V_s ratios of local events can be attributed to slow surficial deposits, but are more likely due to a steam-charged geothermal system. Since the geologic and geophysical evidence indicate the presence of a steam reservoir beneath the central and eastern portion of São Miguel, then the magmatic system that drives the system should be located. *Booth et al.* [1978] have shown that between about 5000 and 7000 a.B.P. there were at least 13 basaltic eruptions around the flanks of Agua de Pau and Furnas. During the past 5000 years there have been no basaltic flank eruptions in the same area. They suggest that a lateral spreading of the trachytic magma chamber that supplies Agua de Pau occurred at about the time of the "Fogo A" eruption (4550 a.B.P.). The subsequent termination of basaltic flank eruptions may be a result of the inability of the basaltic magma to penetrate the overlying trachytic magma chamber. Lagoa do Congro and Logoa de S. Braz (Figure 3) occupy craters between Agua de Pau and Furnas. Both are post "Fogo A" trachytic eruption centers indicating a trachytic magma chamber or feeder system exists under the central and eastern area of São Miguel.

Our study indicates the existence of an anomalous zone, most likely a steam-charged geothermal system, beneath most of Agua de Pau. The abrupt delineation of seismic activity from the summit of Agua de Pau eastward with depth may outline the eastern edge of the magma chamber which drives the geothermal system.

REVIEW OF SEISMIC APPLICATIONS AND RECOMMENDATIONS FOR FUTURE STUDIES

Seismic Studies

Seismic studies are important for the Açores in general and for São Miguel in particular for the following reasons:

1. *Earthquake hazards evaluation and monitoring.*

2. *Volcanic hazards evaluation and monitoring.*
3. *Geothermal exploration and environmental monitoring of geothermal development.*

Earthquake hazards evaluation and monitoring.

The Açores are situated at the intersection of two active seismic zones, the Mid-Atlantic Ridge and the Açores-Gibraltar Fracture Zone (Figure 2). Reports of historical seismicity [*Machado*, 1966; *Machado*, 1973; and *Machado and Forjaz*, 1965] describe the frequent occurrence of felt earthquakes and less-frequent occurrence of destructive earthquakes in the Açores archipelago. The potential for large earthquakes in the Açores was demonstrated by the occurrence of the destructive Terceira earthquake (M_D7.2) of January 1, 1980. São Miguel was last subjected to a destructive earthquake in 1522 near the town of Villa Franca do Campo. The island appears not to have had a major earthquake since then. The many kilometers of old hand erected stone walls that traverse the landscape of São Miguel indicate that major seismic events are fairly uncommon. Therefore, the importance of monitoring seismicity is vital for the understanding of the tectonic and volcanic processes occurring on São Miguel.

Volcanic hazards evaluation and monitoring.

In addition to the potential seismic risk, volcanic hazards provide a compelling reason for seismic monitoring of all the Açores islands, and in particular, the highly populated São Miguel. The three active stratovolcanoes of São Miguel, (Sete Cidades, Agua de Pau, and Furnas; Figure 3) have a long record of explosive eruptions. *Booth et al.* [1978] have documented a total of 57 volcanic eruptions during the past 5000 years on São Miguel using tephrachronology. "Of the 28 trachytic and 29 basaltic eruptions known to have occurred during this period, ten were of magnitude 6, twenty-six of magnitude 5, and at least 9 of magnitude 4 or less (in Tsuya's scale based on total volumes of material erupted). ...Although no eruptions of magnitude 7 have occurred during this period, such eruptions are no doubt possible on the island. ...An eruption of magnitude 6 thus takes place on an average every 500 years in São Miguel, one of magnitude 5 every 200 years..." The most recent trachytic eruptions were in 1562 at Fogo (magnitude 6) and in 1640 at Furnas (magnitude 5).

Even though information on the seismic activity preceding any of these eruptions is sparse, we think it is reasonable to assume that volcanic eruptions in the Açores are preceded by intense seismic activity as in other major volcanoes of the world. The 1957-1958 Capelinhos eruption on Ihla Faial was documented by *Machado et al.* [1962]. No seismic monitoring devices were located on the island at the onset of the eruption so the pre-eruptive seismicity is unknown. A Bosch-Omori seismograph was installed several months after eruptive activity began and was operating during a seismic swarm in May, 1958. From May 12 to May 13, 450 earthquakes were felt on Faial, many of intensity X on the modified Mercalli scale [*Machado et al.*, 1962]. In this brief period of time over 500 homes were destroyed. *Araujo* [1801] documented the seismic and eruptive history of the Açores from their discovery to 1801. He describes several volcanic eruptions and intense accompanying seismicity. Therefore, we believe that continuous seismic monitoring of the Açores volcanoes is an absolute necessity. Particularly for São Miguel, a properly operating state of the art seismic network giving precise locations of seismic activity in and around the island could save lives and property by providing an early warning of a volcanic eruption.

Geothermal exploration and environmental monitoring of geothermal development.

Seismic techniques used in geothermal studies fall into two categories, active techniques, in which controlled explosions or vibrators are used to generate seismic waves, and passive techniques, in which earthquakes are used as the sources. Active studies are mainly concerned with modeling the fine structure of the crust using refraction and reflection surveys and are not discussed here. Passive studies mainly consist of microearthquake surveys to establish a seismo-tectonic framework of the geothermal area under investigation and to model the three-dimensional structure of the area. Seismic waves from local, regional, and distant earthquakes can be used to model anomalous physical properties of the underlying rock, such as those caused by hydrothermal activity or partial melting. Following is a brief review of the application of passive seismic methods in geothermal studies.

Microearthquakes

Microearthquake studies in geothermal areas can be divided into several categories:

a. *Exploration.*
b. *Tectonic evolution.*
c. *Detection of zones of anomalous physical properties in the upper crust (due to the presence of geothermal reservoirs, magma pockets etc.).*
d. *Environmental monitoring.*

a. *Exploration.* Geothermal prospects are invariably located in areas of active tectonism, hence it is not surprising that most of them are quite seismically active. *Ward and Jacob* [1971] showed how a microearthquake survey can be used as a geothermal exploration tool to delineate fracture zones which provide paths for hot water to reach the surface. There have been numerous microearthquake surveys in geothermal areas for geothermal exploration [*Ward and Bjornsson*, 1971; *Marks et al.*, 1978; and *Walter and Weaver*, 1980].

b. *Tectonic evolution.* Whether microearthquake surveys are useful for siting geothermal drill-holes or not, their study forms an important and integral part of the process of understanding the volcanic and tectonic evolution of geothermal areas. Clear examples of the utility of tectonic studies for geothermal exploration are provided by studies at Brawley and Coso geothermal areas, California [*Weaver and Hill*, 1979]. In both these areas it has been demonstrated that the geothermal zones occur at miniature continental spreading centers.

c. *Detection of zones of anomalous physical properties.* Microearthquakes can be used to look for velocity and attenuation anomalies associated with hydrothermal reservoirs and magma pockets in geothermal areas. *Chatterjee et al.* [1985] found abnormally low V_p/V_s (and low Poisson's ratio) beneath the geyser basins of Yellowstone National Park, Wyoming. They attributed this to the presence of hydrothermal reservoirs in which the temperatures were close to those needed for the transition of water to steam. *Sanders and Ryall* [1983] used the observed strong attenuation of S-waves from microearthquakes along certain paths to map the

subsurface geometry of magma bodies in Long Valley, California. In the same region *Kissling et al.* [1984], using local earthquake data and a tomographic inversion method, have delineated a zone of low P-wave velocity in the depth range of 3 to 7 km beneath the resurgent dome and the south moat of the Long Valley caldera.

d. *Environmental monitoring.* In general, seismic activity occurs in many geothermal areas of the world. *Ward* [1972] discussed the problem of earthquake risks associated with geothermal activity. A primary concern is whether the extraction of fluids and reinjection of spent fluids could trigger a moderate earthquake. There is clear evidence that modifying fluid pressure can alter seismicity patterns. In particular, seismic activity seems to be triggered by injection of fluids at high pressure into the ground [*Raleigh et al.*, 1976]. *Eberhart-Phillips and Oppenheimer* [1984] showed, by careful relocation of earthquakes in the Geysers geothermal area, California, that seismic activity tends to cluster near production wells in the steam field. They could not find statistically significant results to show whether seismicity was indeed induced by the reinjection of spent fluids. They postulate that the seismic activity associated with geothermal production could be a result of perturbation of the regional stress field due to volumetric contraction caused by steam withdrawal.

Regional Earthquakes and Teleseisms

An important constituent of a geothermal system is the heat source that activates it, usually some form of magmatic intrusion. In order to estimate the longevity of a geothermal system and to understand its volcanic setting, it is important to detect and delineate these magmatic intrusions. The technique of measurement of teleseismic travel time residuals has been successfully used to make three-dimensional models of velocity anomalies in the crust and upper mantle of the earth [*Aki*, 1982] and has been used by *Iyer et al.* [1979, 1981], *Reasenberg et al.* [1980], *Robinson and Iyer* [1981], and *Steeples and Iyer* [1976], among others, to map magma chambers in several geothermal areas in the United States. (For a review of geophysical detection of magma chambers, see [*Iyer*, 1984].) Regional earthquakes can be used in a similar way to locate anomalous low-velocity zones in the earth's crust.

Recommendations

The level of seismic activity on São Miguel leads us to recommend several studies which would help characterize the active geothermal, seismic, and volcanic processes occurring there.

(1). The first, and most important, recommendation is to upgrade the existing seismic network. The paper recorders now used do not have the sensitivity to detect small-magnitude microearthquakes. An island-wide network that would enable the detection and location of events to the M_D=1 level would greatly improve the understanding of seismic activity on the island. Because of the high level of noise on the island we recommend that the present stations and any future stations be installed in boreholes to reduce the problem of surficial noise and to enhance the detection capabilities of the network. Such a network should provide, (a) a background seismicity level with which to compare seismicity changes associated with future geothermal development, (b) seismic monitoring for detecting seismic activity preceding hazardous volcanic eruptions, and (c) seismicity studies for earthquake prediction and

earthquake hazard evaluation. It is also recommended that a state-of-the-art computer-oriented seismic data analysis center be set up to process the data from the seismic array and that it be staffed by professional seismologists, at least one of whom should have a Ph.D. Any such network must operate with high reliability - an electrical engineer should also be employed to maintain and modify the network under the seismologists direction. Such a network would also be of tremendous scientific interest, potentially attracting visiting scientists to extend the research opportunities and capability of the laboratory.

(2). The effectiveness of a seismic network depends on how precisely earthquake hypocenters can be determined. For all the studies mentioned above, earthquake location accuracy to a fraction of a kilometer is required. The critical data to achieve such precision are detailed velocity models commonly derived from seismic refraction experiments. The available refraction data for São Miguel [*Senos and Nunes*, 1980] is a good beginning but is inadequate for this application; we propose a comprehensive refraction experiment. Instruments, field procedures, and analysis techniques for such an experiment are highly developed in many institutions of the world including the U.S. Geological Survey [*Zucca et al.*, 1982; and *Fuis et al.*, 1984]. The small dimensions of São Miguel (60 km x 15 km) permit deployment of dense profiles of portable seismic stations on the island and detonation of seismic-source explosions in the ocean to evolve detailed velocity models.

(3). An extension of the seismic refraction study is to conduct an active source seismic tomography imaging experiment to model in three dimensions both lateral and vertical velocity and attenuation heterogeneities associated with the geothermal and volcanic systems in the Agua de Pau-Furnas area of São Miguel. Such an experiment would consist of deploying a two-dimensional array of about 120 seismographs over an 10 x 10 km area with average instrument spacing of about 1 km, and setting off seismic-source explosions (in the ocean) around the array. This method has proved very successful in providing images of upper crustal magma chamber at two volcanoes in the Cascade Range, USA [*Achauer et al.* 1988, and *Evans and Zucca*, 1988].

(4). We strongly recommend a teleseismic P-residual study of the whole of São Miguel, The strategy would be to supplement the proposed seismic network with several portable stations to achieve an average instrument spacing of about 5 km. Collection of teleseismic and regional event data requires several months of recording. The analysis of data from such a study would provide a 3-dimensional model of the crust and upper mantle to depths of about 60 km beneath São Miguel with a resolution as good as 5 km. This model would complement the high-resolution model from the seismic imaging experiment proposed under (3). This type of experiment could be expected to provide a wealth of data to explore in detail the seismicity, V_p/V_s, and residual anomalies discussed earlier in this report. The data set thus collected can be used for numerous studies related to the seismicity, tectonics, volcanology, and geothermal potential of São Miguel.

ACKNOWLEDGEMENTS

The staff of LGT provided full logistic support and negotiated with landowners for field deployments. Laboratory space was provided by LGT and INMG provided access to their permanent network. Louis and Roberto Amaral participated in all aspects of our activities and in addition to the long and hard hours of field work acted as interpretors and guides. They very quickly grasped the principles of the operation of our seismic system and provided invaluable help as field and laboratory technicians. Finally, we acknowledge full support and

help from the numerous officials of the Regional Government of the Açores, the U.S. Consulate in São Miguel, the USAID missions in Ponta Delgada and Lisboa, and the Office of International Geology of the U.S. Geological Survey.

REFERENCES

Achauer, U., J. R. Evans, and D. S. Stauber, High-resolution seismic tomography of compressional wave velocity structure at Newberry Volcano, Oregon Cascade Range, *J. Geophys. Res.*, *93*, 10,135–10,147, 1988.

Achauer, U., L. Greene, J. R. Evans, and H. M. Iyer, Nature of the magma chamber underlying the Mono Craters area, eastern California, as determined from teleseismic travel time residuals, *J. Geophys. Res.*, *91*, 13,873–13,891, 1986.

Aki, K., Three-dimensional seismic inhomogeneities in the lithosphere and asthenosphere: evidence for decoupling in the lithosphere and flow in the asthenosphere, *Reviews of Geoph. etc*, *20*, 161–170, 1982.

Anderson, E. M., The dynamics of the formation of cone–sheets, ring–dykes and caldron–subsidences, *Proc. Royal Soc. Edinburgh*, *56*, 128–157, 1936.

Bakun, W. H., Seismic moments, local magnitudes, and coda-duration magnitudes for earthquakes in central California, *Bull. Seism. Soc. Am.*, *74*, 439–458, 1984.

Booth, B., R. Croasdale, and G. P. L. Walker, A quantitative study of five thousand years of volcanism on Sao Miguel, Azores, *Philos. Trans. R. Soc. London*, *288*, 271–319, 1978.

Chatterjee, S. N., A. M. Pitt, and H. H. Iyer, Vp/Vs ratios in the Yellowstone National Park region, Wyoming, *J. of Volcan. and Geotherm. Res.*, *26*, 213–230, 1985.

Christensen, N. I., Compressional and shear wave velocities at pressures to 10 kilobars for basalts from the East Pacific Rise, *Geophy. J. R. Astron. Soc*, *28*, 425–429, 1972..

Conde Senos, M. L. and J. A. F. Costa Nunes, Report of seismic refraction on Isla Sao Miguel, *Servico Meteorologica Nacional*, 1980.

Dawson, P. B., R. Cutler, and J. R. Evans, HP-85 computer program HYP85; an earthquake location program, *U.S. Geol. Surv. Open File Rep.*, *85-243*, 33 pp., 1985.

da Silva, A. M. R., W. A. Duffield, and L. J. P. Muffler, Geothermal studies of Agua de Pau Volcano, Sao Miguel, Azores,, *Trans. Geothermal Resources Coun.*, *9*, part II, p. 401–406., 1985.

de Araujo, L. A., Memoria chronologica dos tremores mais notaveis, *Na Typographia Chalcographica e Litteraria*, 24 pp., 1801.

Duffield, W. A. and L. J. P. Muffler, Geothermal Resources of Sao Miguel, Azores, *A summary report for USAID.*, 1984.

Eberhart-Phillips, D. and D. H. Oppenheimer, Induced seismicity in the Geysers geothermal area, California, *J. Geophys. Res.*, *89*, 1191–1207, 1984.

Evans, J. R., Compressional-wave velocity structure of the Medicine Lake volcano and vicinity from teleseismic relative traveltime residuals, *Tech. Prog. Abs. and Biog., 52nd Annual Meeting*, 482–485 , Soc. Explor. Geophys., Tulsa, OK, 1982.

Evans, J. R. and J. J. Zucca, Active high-resolution seismic tomography of Compressional wave velocity and attenuation structure at Medicine Lake Volcano, Northern California Cascade Range, , *93*, 15016–15036, 1988.

Feraud, G., I. Kaneoka, and C. J. Allegre, K/Ar ages and stress pattern in the Azores: geodynamic implications, *Earth and Planetary Science Letters, 46*, 275–286, 1980.

Fuis, G. S., W. D. Mooney, J. H. Healy, G. A. McMechan, and W. J. Lutter, A seismic refraction survey of the Imperial Valley Valley Region, California, *Journal of Geophys. Res., 89*, 1165–1189, 1984,.

Gandido, A., M. Guidi, C. Merlo, L. Mete, R. Rossi, C. Sommaruga, and L. Zan, Preliminary model of the Ribeira Grande geothermal field (Azores Islands), *United Nations Economic Commission for Europe Seminar on Utilization of Geothermal Energy for Electric Power Production and Space Heating*, Florence, Italy., 1984.

Geonomics, Inc., , *Microearthquake seismology survey, Task IV, of the Sao Miguel geothermal project, submitted to IGA, Azores.*, 1977.

Graybill, F. A., *Theory and application of the linear model*, Duxbury Press, 1976.

Hirn, A., H. Haessler, P. Hoang-Trong, G. Wittlinger, and L. A. Mendes Victor, Aftershock sequence of the January 1st, 1980, earthquake and present-day tectonics in the Azores, *Geophyisical Research Letters, 7*, 501–504, 1980.

Ito, H., J. DeVilbiss, and A. Nur, Compressional and shear waves in saturated rock during water-steam transition, *J. Geophys. Res., 84*, 4731–4735, 1979.

Iyer, H. M., Geophysical evidence for the locations, shapes and sizes, and internal structure of magma chambers beneath regions of Quaternary volcanism, *Phil. Trans. Roy. Soc. London, A310*, 473–510, 1984.

Iyer, H. M., J. R. Evans, G. Zandt, R. M. Stewart, J. M. Coakley, and J. N. Roloff, A deep low-velocity body under the Yellowstone caldera, Wyoming: delineation using teleseismic P-wave residuals and tectonic interpretation, *Geol. Soc. Am. Bull., 92*, Part I: 792–798, Part II: 1471–1646, 1981.

Iyer, H. M., D. H. Oppenheimer, and T. Hitchcock, Abnormal P-wave delays in the Geysers-Clear Lake geothermal area, California, *Science, 204*, 495–497, 1979.

Iyer, H. M. and R. M. Stewart, Teleseismic technique to locate magma in the crust and upper mantle, *Bulletin 96*, edited by H. J. B. Dick, 281–299 , Oregon Department of Geology and Mineral Industries, Portland, 1977.

Jeremine, E., Etude microscopique des roches de la region de Furnas (S. Miguel, Acores), *Com. Serv. Geol. Portugal, 38*, 65–90, 1957.

Kern, H. and A. Richter, Temperature derivatives of compressional and shear wave velocities in crustal and mantle rocks at 6 kbar confining pressure, *J. Geophys., 49*, 47–56, 1981.

Kissling, E., W. L. Ellsworth, and R. S. Cockerham, Three-dimensional structure of the Long Valley caldera, California, region by geotomography, *U.S. Geol. Surv. Open File Rep., 84–939*, 188–220, 1984.

Kisslinger, C. and E. R. Engdahl, The interpretation of Wadati diagram with relaxed assumptions, *Bull. Seism. Soc Am., 63*, 1723–1736, 1973.

Klein, F. W., Hypocenter location program HYPOINVERSE, Part 1: Users guide to versions 1, 2, 3, and 4, *U.S. Geol. Surv. Open File Rep.., 78–694*, 113 pp., 1978.

Krause, D. C. and N. D. Watkins, North Atlantic crustal genesis in the vicinity of the Azores, *Geophys. J. R. astr. Soc., 19*, 261–283, 1970.

Laughton, A. S., R. B. Whitmarsh, J. S. M. Rusby, M. L. Somers, J. Revie, B. S. McCartney, and J. E. Nafe, A continuous east-west fault on the Azores-Gibraltar ridge, *Nature, 237*, 217–220, 1972.

Lee, W. H. K., R. E. Bennett, and K. L. Meagher, A method of estimating magnitude of local earthquakes from signal duration, *U.S. Geol. Surv. Open File Rep., XX*, 37 pp., 1972.

Lee, W. H. K. and J. C. Lahr, HYPO71 (Revised); A computer program for determining hypocenter, magnitude and first motion pattern of local earthquakes, *U.S. Geol. Surv. Open File Rep., 75–311*, 1975.

Machado, F., Anomalias das Intensidades do Terramoto de S. Miguel, Acores em 1522, *Bol. Mus. Lab. Miner. Geol. Fac. Ciencas, 10*, 109–117, 1966.

Machado, F., Periodicidade sismica nos Acores, *Ministerio da Industria e Technologia, Direccao-Geral dos Servicos Electricos, Direccao Geral dos Combustiveis, Comissao para o Estudo de Geotermia dos Acores-S. Miguel, Documentacao.*, 1973.

Machado, F. and V. H. Forjaz, A crise sismica de S. Jorge, de Fevereiro de 1964, *Bol. Soc. Geol. Port., 16*, 19–36, 1965.

Machado, F., W. H. Parson, A. F. Richards, and J. W. Mulford, Capelhinos eruption of Fayal Volcano, Azores, 1957-1958, *J. Geophys. Res., 67 (9)*, 3519–3530, 1962.

Machado, F., J. Quintino, and J. H. Monteiro, Geology of the Azores and the Mid-Atlantic rift, *Proc. 24th Int. Geol. Congr., Sect. 3*, 134–142, 1972.

Marks, S. M., R. S. Ludwin, K. B. Louie, and C. G. Bufe, Seismic monitoring at the Geysers geothermal field, California, *U.S. Geol. Surv. Open File Rep., 78–798*, 1978.

McKenzie, D., Active tectonics of the Mediterranean region, *Geophys. J. R. Astron. Soc, 30*, 109–185, 1972.

Mori, J. and C. McKee, Outward-dipping ring-fault strucutre at Rabaul caldera as shown by earthquake locations, *Science, 235*, 193–195, 1987.

Muecke, G. K., J. M. Ade-Hall, F. Aumento, A. MacDonald, P. H. Reynolds, R. D. Hyndman, J. Quintino, N. Opdyke, and W. Lowrie, Deep drilling in an active geothermal area in the Azores, *Nature, 252*, 281–285, 1974.

Neumann Van Padang, M., A. F. Richards, F. Machado, T. Bravo, P. E. Baker, and R. W. Le Maitre, Atlantic Ocean, *Inter. Volcan. Assoc., Catalogue of active volcanoes-Pt 21.*, 1967.

Oppenheimer, D. H. and K. E. Herkenhoff, Velocity-density properties of the lithosphere from three-dimensional modeling at the Geysers-Clear Lake region, California, *J. Geophys. Res., 86*, 6057–6065, 1981.

Raleigh, C. B., J. D. Healy, and J. D. Bredehoeft, An experiment in earthquake control at Rangely, Colorado, *Science, 191*, 1230–1237, 1976.

Reasenberg, P., W. Ellsworth, and A. Walter, Teleseismic evidence for a low-velocity body under the Coso geothermal area, *J. Geophys. Res., 85*, 2471–2483, 1980.

Richter, C. F., An instrumental earthquake magnitude scale, *Bull. Seism. Soc. Am.*, *25*, 1–32, 1935.

Robinson, R. and H. M. Iyer, Delineation of a low-velocity body under the Roosevelt Hot Springs geothermal area, Utah, using teleseismic P-wave data, *Geophysics*, *46*, 1456–1466, 1981.

Sanders, C. O. and F. Ryall, Geometry of magma bodies beneath Long Valley, California determined from anomalous earthquake signals,, *Geophysical Research Letters*, *10*, 690–692, 1983.

Searle, R. C., Tectonic pattern of the Azores spreading centre and triple junction, *Earth and Planetary Science Letters*, *51*, 415–534., 1980.

Stauber, D. A., Two-dimensional compressional wave velocity structure under San Francisco volcanic field, Arizona, from teleseismic P-residual measurements, *J. Geophys. Res.*, *87*, 5451–5459, 1982.

Stauber, D. A., S. M. Green, and H. M. Iyer, Three-dimensional P velocity structure of the crust below Newberry volcano, Oregon, *J. Geophys. Res.*, *93*, 10,059–10,107, 1988.

Steeples, D. W. and H. M. Iyer, Low-velocity zone under Long Valley as determined from teleseismic events, *J. Geophys. Res.*, *81*, 849–860, 1976.

Wadati, K., On travel time of earthquake waves, Part II, *Geophys. Mag.*, *7*, 101–111, 1933.

Walker, G. P. L. and R. Croasdale, Two plinian-type eruptions in the Azores, *J. Geol. Soc. London*, *127*, 17–55, 1971.

Walter, A. W. and C. S. Weaver, Seismicity of the Coso Range, California, *JGR*, *85*, 2441-2458, 1980.

Ward, P. L., Microearthquakes: prospecting tool and possible hazard in the development of geothermal resources, *Geothermics*, *1*, 3–12, 1972.

Ward, P. L. and S. Bjornsson, Microearthquakes, swarms, and the geothermal areas of Iceland, *J. Geophys. Res.*, *76*, 3953–3982, 1971.

Ward, P. L. and K. H. Jacob, A study of microearthquakes and ground noise in the Ahuachapan geothermal field, El Salvador, Central America,, *Final Report to the United Nations Resources and Transport Division, Energy Section.*, 1971.

Ward, R. W. and C. Young, Mapping seismic attenuation within geothermal systems using teleseisms with application to the Geysers-Clear Lake region, *J. Geophys. Res.*, *85*, 5227–5236, 1980.

Weaver, C. S. and D. P. Hill, Earthquake swarms and local crustal spreading along major strike slip faults in California, *Pageoph*, *117*, 51-64, 1979.

Weston, F. S., List of recorded volcanic eruptions in the Azores with brief reports, *Bol. Mus. Lab. Miner. Geol. Fac. Ciencas*, *10*, 3–18, 1964.

Whitmarsh, R. B., Median valley refraction line, Mid-Atlantic ridge at 37 N, *Nature*, *246*, 297–299, 1973.

Young, C. and R. W. Ward, Three-dimensional Q model of the Coso Hot Springs known geothermal resource, *J. Geophys. Res.*, *85*, 2459–2470, 1980.

Zbyszewski, G., Etude geologique de l'Ile de S. Miguel (Acores), *Com. Serv. Geol. Portugal, 45*, 5–79, 1961.

Zucca, J. J., D. P. Hill, and R. L. Kovach, Crustal structure of Mauna Loa Volcano, Hawaii, from seismic refraction and gravity data, *Bull. Seis. Soc. Am., 72*, 1535–1550, 1982.

FIGURE CAPTIONS

Figure 1. Generalized map of the regional tectonic structures in the region of the Açores. Shown are the Mid-Atlantic Ridge (MAR), the Açores-Gibraltar Fracture Zone (AGFZ), and the Gloria Fault (GF).

Figure 2. Bathymetric map (after Tolstoy, 1951) of the Açores Plateau. The plateau is bounded on the west by the Mid-Atlantic Ridge, on the south by the East Açores Fracture Zone, and on the northeast by the Terceira Rift and North Açores Fracture Zone. Bathymetry is in meters.

Figure 3. São Miguel island. Shown are the three main volcanic centers, Sete Cidades, Água de Pau, and Furnas. Calderas are indicated by hatched lines. Fissural basalt cones are shaded. Dots indicate the principle towns of Sete Cidades, Ponta Delgada, Ribeira Grande, Vila Franca do Campo, Furnas, Povoção, and Nordeste. Dots with tails show existing thermal springs on Agua de Pau including Caldeiras and Lombadas. Dashed lines are inferred faults from geophysical surveys. Lakes are indicated by script type. Solid diamonds are seismic station locations.

Figure 4. Seismic network used for the experiment. Solid diamonds are the INMG permanent network stations with signals telemetered to Ponta Delgada. Open diamonds indicate USGS digital recorder locations except for PVN and ADB which were paper drum recorders.

Figure 5. Frequency response curves for a) L4-C 1Hz geophone, and b) AS-110 high gain amplifier (not including the 50 Hz 5-pole anti-alias filters) employed in the DR-100.

Figure 6. Map (a) and cross section A-A' (b) of 8 selected local events. Open circles are events located without station terms, solid circles are the same events located with station terms.

Figure 7. Typical seismograms for a local event: a) the vertical component with the P-arrival indicated by the dashed line and timing marks for the first (1) and second (2) odd seconds after instrument trigger indicated by solid lines; b) horizontal component for the same event with the S-arrival indicated by the dashed line; and c) output of the plotting routine showing seismograms from 6 stations for the same event.

Figure 8. Total seismic triggers from June 20 to October 12, 1983 determined from analog records of approximately 7500 station triggers.

Figure 9. Final location map for local events using the velocity model of *Senos and Nunes* [1980] with station terms. b) Shows the events in a depth cross-section. Magnitude and depth symbols are shown in (a). Diamonds indicate station locations.

Figure 10. Epicenters (a) and depth cross-section (b) for the events located during the September 6-7, 1983 swarm. Symbols are the same as Figure 9.

Figure 11. Bar graph of seismic events against time for the September 6-7, 1983

seismic swarm. Time period is 24 hours from 1000 (UTC) September 6. Events are grouped into 15 minute intervals.

Figure 12. Calculated magnitudes versus time for the September 6-7, 1983 seismic swarm. The largest recorded event was M_D 2.34 at 0555 (UTC) September 7, 1983.

Figure 13. Plot of seismograms for a typical regional event which occurred approximately 35 km SE of São Miguel. Solid lines through the middle of the seismograms are the odd second spikes from the DR-100 record.

Figure 14. Regional earthquakes located from June 19 to October 10, 1983 by the INMG and USGS network. São Miguel is shown in outline. Locations are approximate because of the small aperture of the network. Local events are also plotted.

Figure 15. Regional earthquakes recorded by NOAA for the years 1970 to 1980 near the Açores Plateau (from the World Data Center A for Solid Earth Geophysics, National Geophysical Data Center). Shown by dashed lines are the approximate locations of the Mid-Atlantic Ridge (MAR), North Açores Fracture Zone (NAFZ), Terceira Rift (TR), East Açores Fracture Zone (EAFZ), and the Gloria Fault (GF). Islands are shaded.

Figure 16. Modified Wadati diagrams with S-travel time plotted against P-travel time for a) 37 local events with data from vertical and horizontal geophones, b) 27 local events with P from vertical geophones and S from horizontal geophones only, c) 9 regional events using data from vertical and horizontal components, and d) error estimates for the 90% confidence level for (A) local event data from 16a, (B) local event from 16b, and (C) regional event data from 16c.

Figure 17. Average (invariant) residuals calculated from 9 regional events. The contour which approximates 0 s delay is shown with a solid line.

Figure 18. a-i) Residuals at each station minus the invariant residual for the 9 regional events. 0 s contour is shown with a solid line. Arrow indicates approximate approach azimuth of event.

Figure 19. Average station residuals versus station elevation. Line A is a least-squares fit to all stations, Line b is a least- squares fit to all stations accept FAC and CML, and line C is the slope of the velocity in the top layer of the velocity model used in the hypocentral location routine.

Figure 20. Depth cross-section plotted along line A-A' of Figure 9. Vertical exaggeration is 2x. Shown are the areas of P-wave delay and low V_p/V_s. The dashed line indicates the zone of low V_p/V_s and P-wave attenuation from *Senos and Nunes* [1980]. Locations of seismic events are shown as solid circles. Shown is the proposed geothermal model of Agua de Pau *Silva et al.*, [1985].

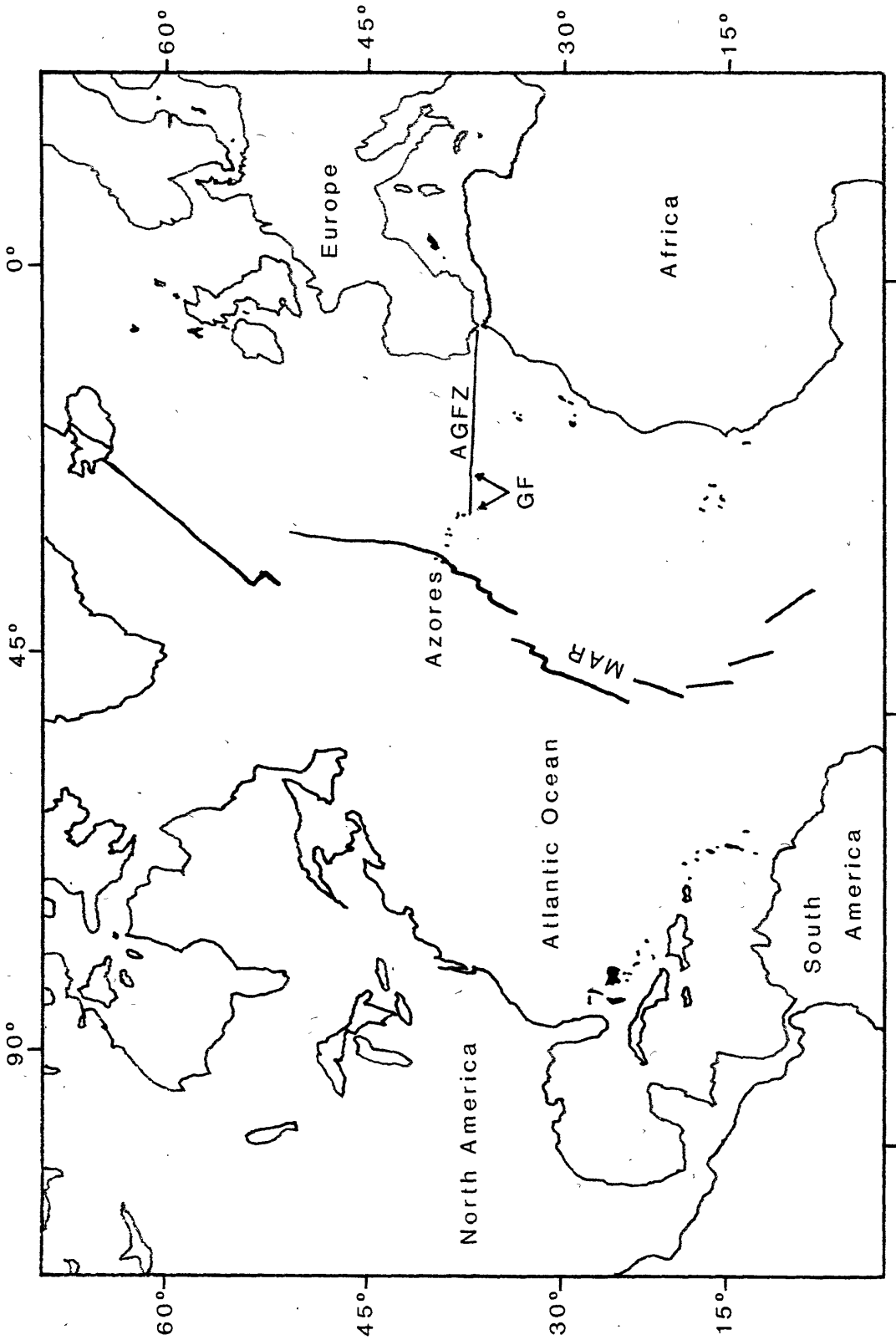
60°
45°
30°
15°
0°
45°
90°
Europe
Africa
AGFZ
GF
Azores
MAR
Atlantic Ocean
North America
South America

Figure 1

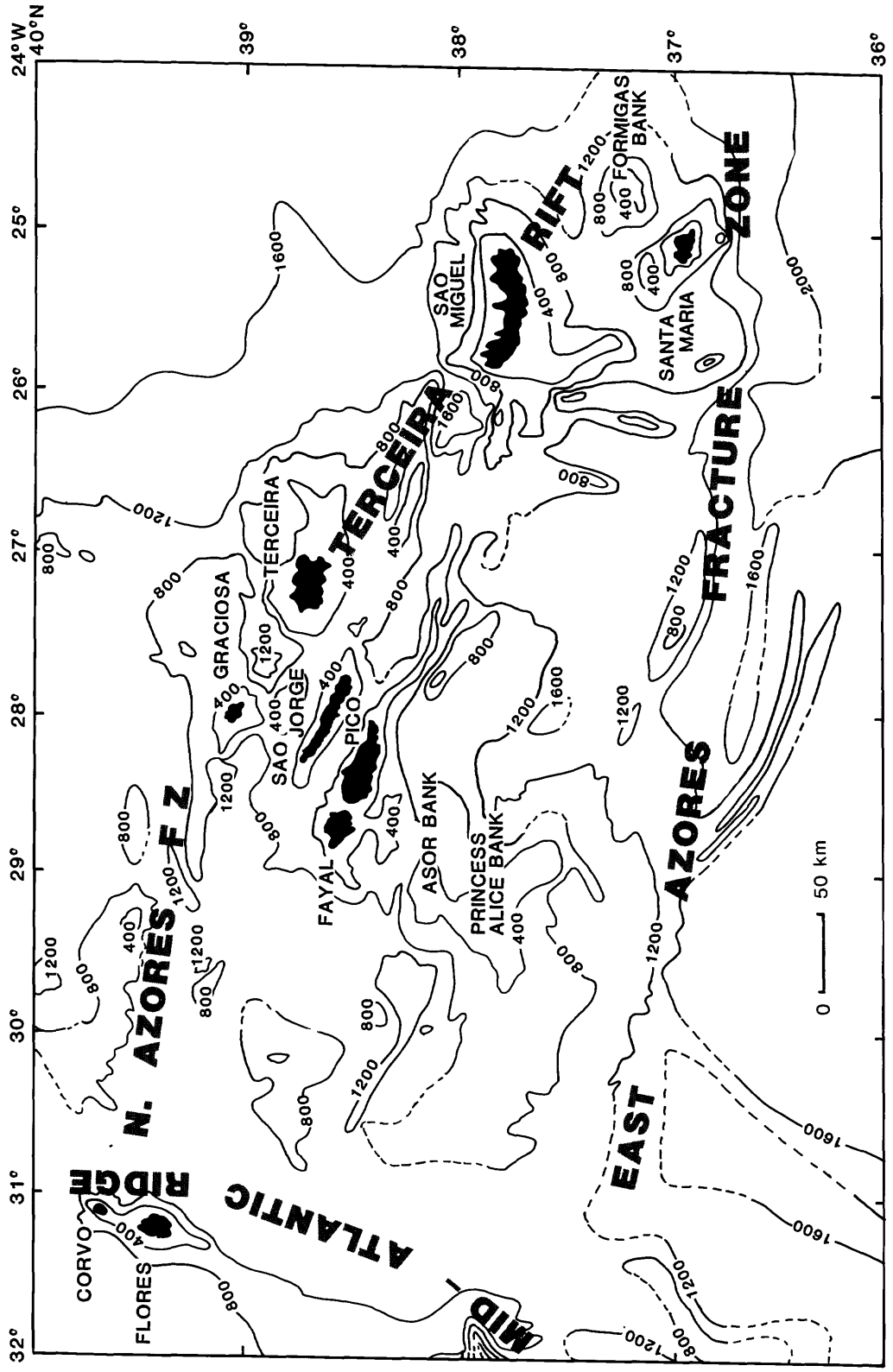
24°W
40°N
39°
38°
37°
36°
25°
26°
27°
28°
29°
30°
31°
32°
N. AZORES F.Z.
AZORES TRIPLE JUNCTION
MID ATLANTIC RIDGE
CORVO
FLORES
GRACIOSA
TERCEIRA
SAO JORGE
PICO
FAYAL
ASOR BANK
PRINCESS ALICE BANK
TERCEIRA RIFT
SAO MIGUEL
FORMIGAS BANK
SANTA MARIA
EAST AZORES FRACTURE ZONE
0
50 km

Figure 2

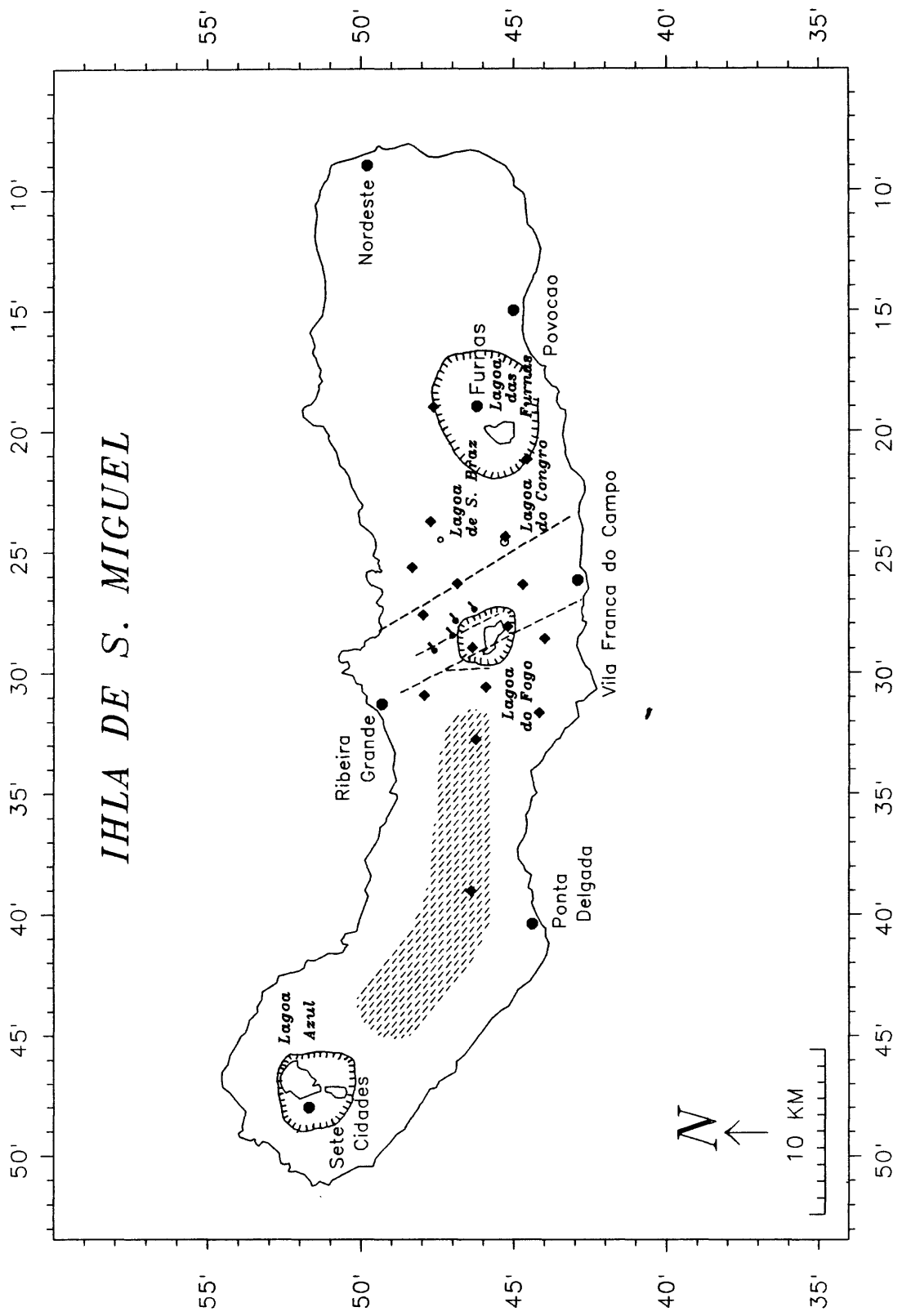
IHLA DE S. MIGUEL
Nordeste
Povoacao
Furnas
Lagoa das Furnas
Lagoa do Congro
Lagoa de S. Braz
Vila Franca do Campo
Ribeira Grande
Lagoa do Fogo
Ponta Delgada
Lagoa Azul
Sete Cidades
10 KM
N
55'
50'
45'
40'
35'
10'
15'
20'
25'
30'
35'
40'
45'
50'

Figure 3

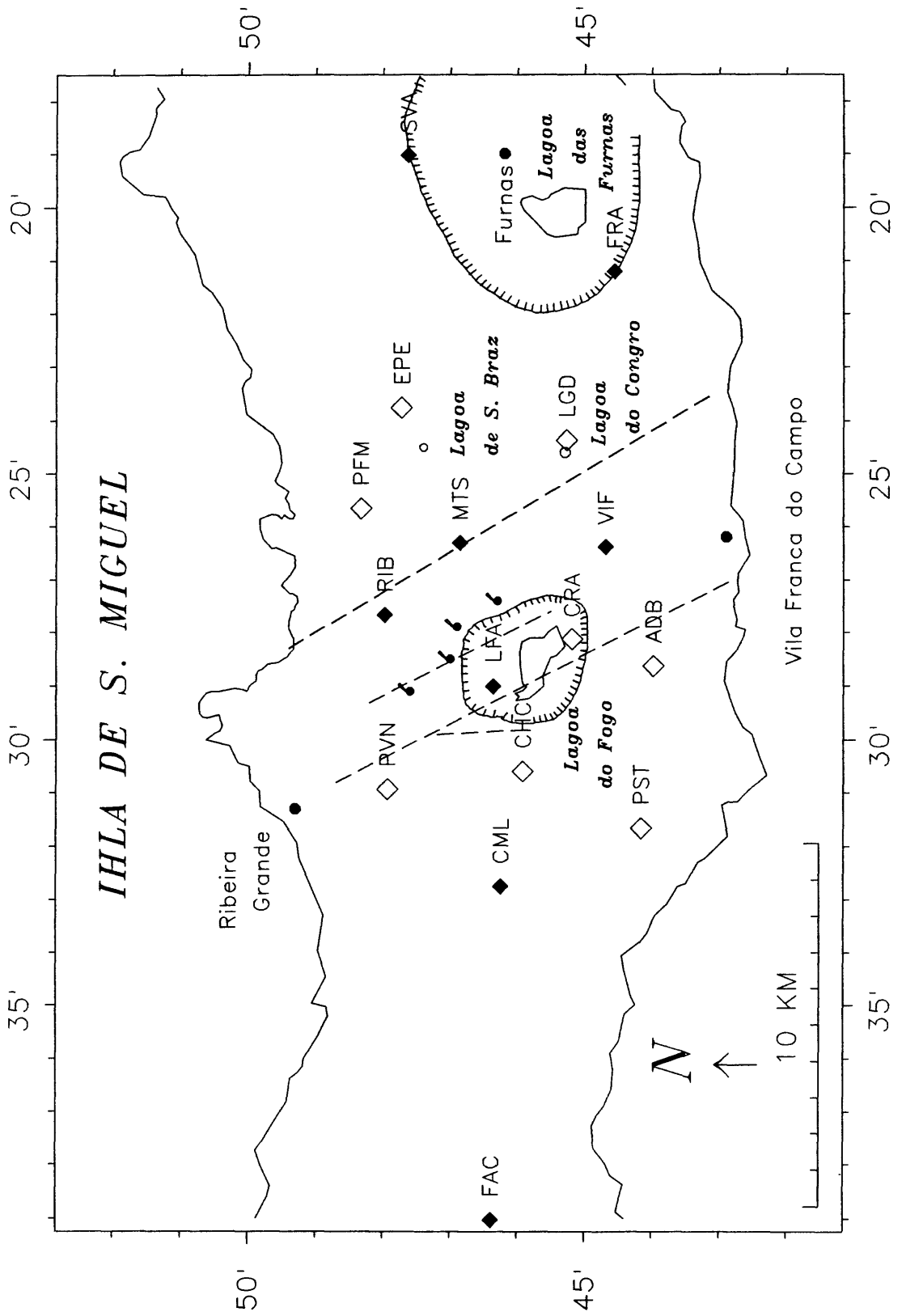
ILHA DE S. MIGUEL
50'
45'
20'
25'
30'
35'
Ribeira Grande
Vila Franca do Campo
SVA
Furnas
Lagoa das Furnas
FRA
EPE
PFM
MTS
Lagoa de S. Braz
LGD
Lagoa do Congro
VIF
RIB
RVN
LRA
CRA
CHC
Lagoa do Fogo
ADB
PST
CML
FAC
N
10 KM

Figure 4

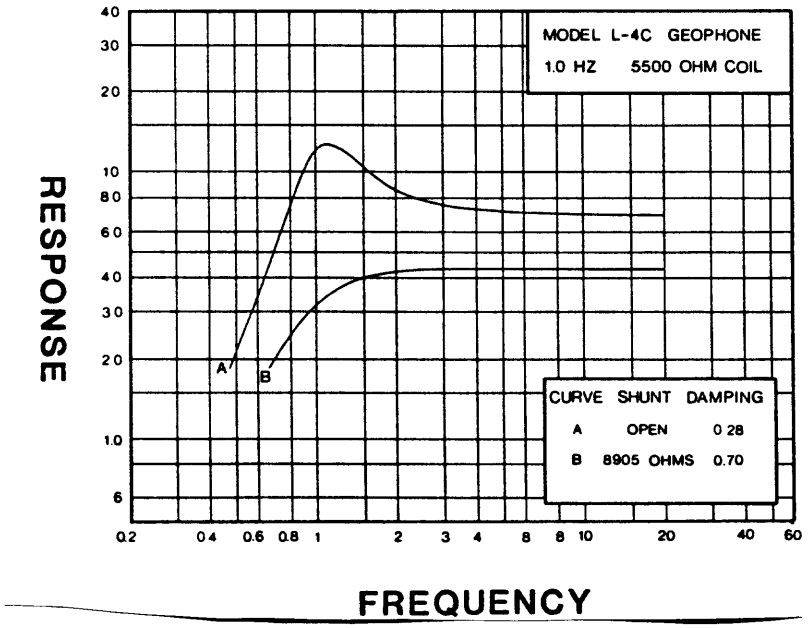
MODEL L-4C GEOPHONE
1.0 HZ 5500 OHM COIL
CURVE SHUNT DAMPING
A OPEN 0.28
B 8905 OHMS 0.70
A
B
RESPONSE
FREQUENCY

(a)

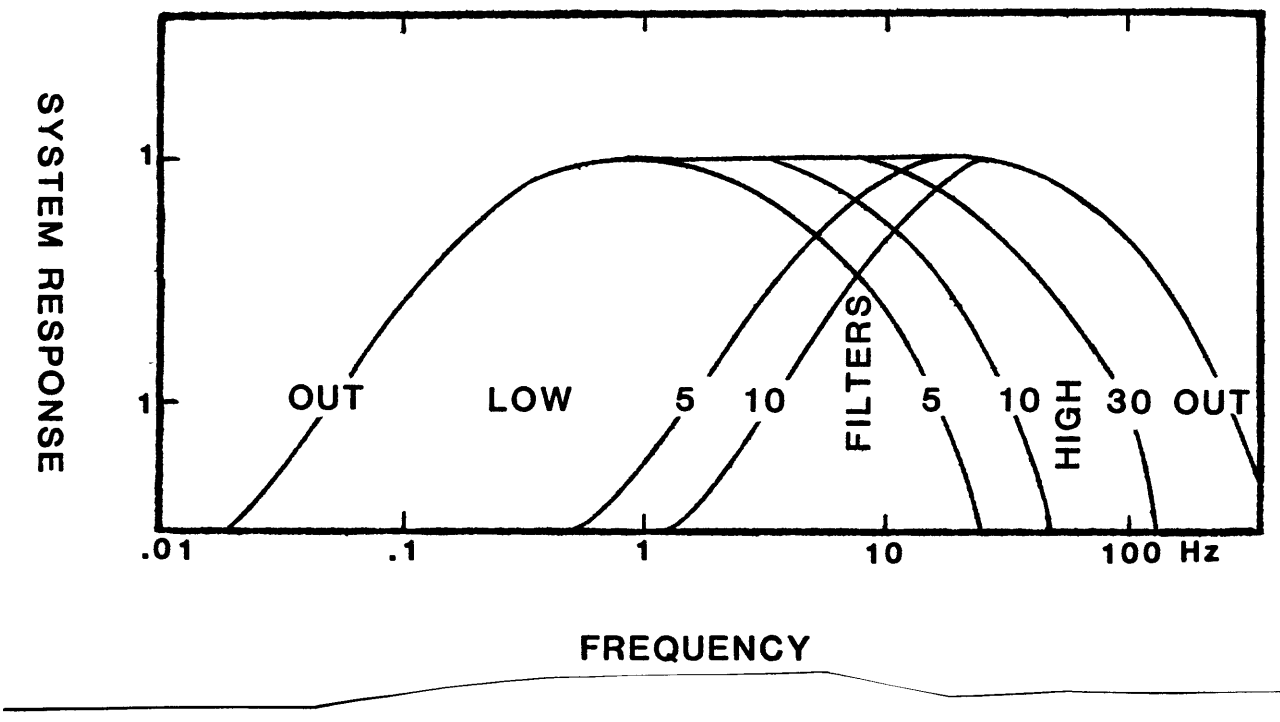
SYSTEM RESPONSE
OUT
LOW
5
10
FILTERS
5
10
HIGH
30
OUT
.01
.1
1
10
100 Hz
FREQUENCY

(b)

Figure 5

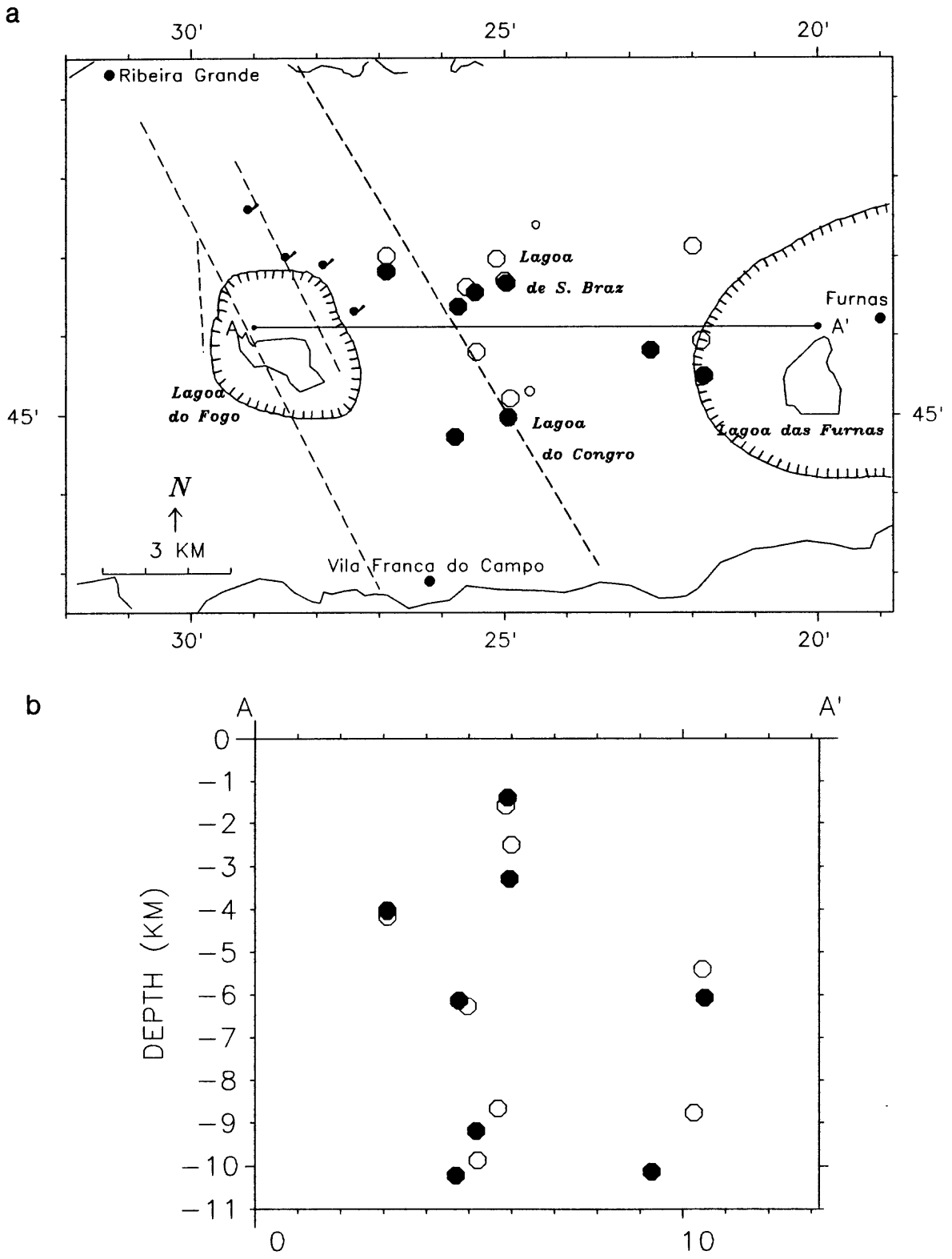
a
30'
25'
20'
Ribeira Grande
Lagoa
de S. Braz
Furnas
A
A'
Lagoa
do Fogo
Lagoa
do Congro
Lagoa das Furnas
45'
45'
N
3 KM
Vila Franca do Campo
30'
25'
20'
b
A
A'
DEPTH (KM)
0
−1
−2
−3
−4
−5
−6
−7
−8
−9
−10
−11
0
10

Figure 6

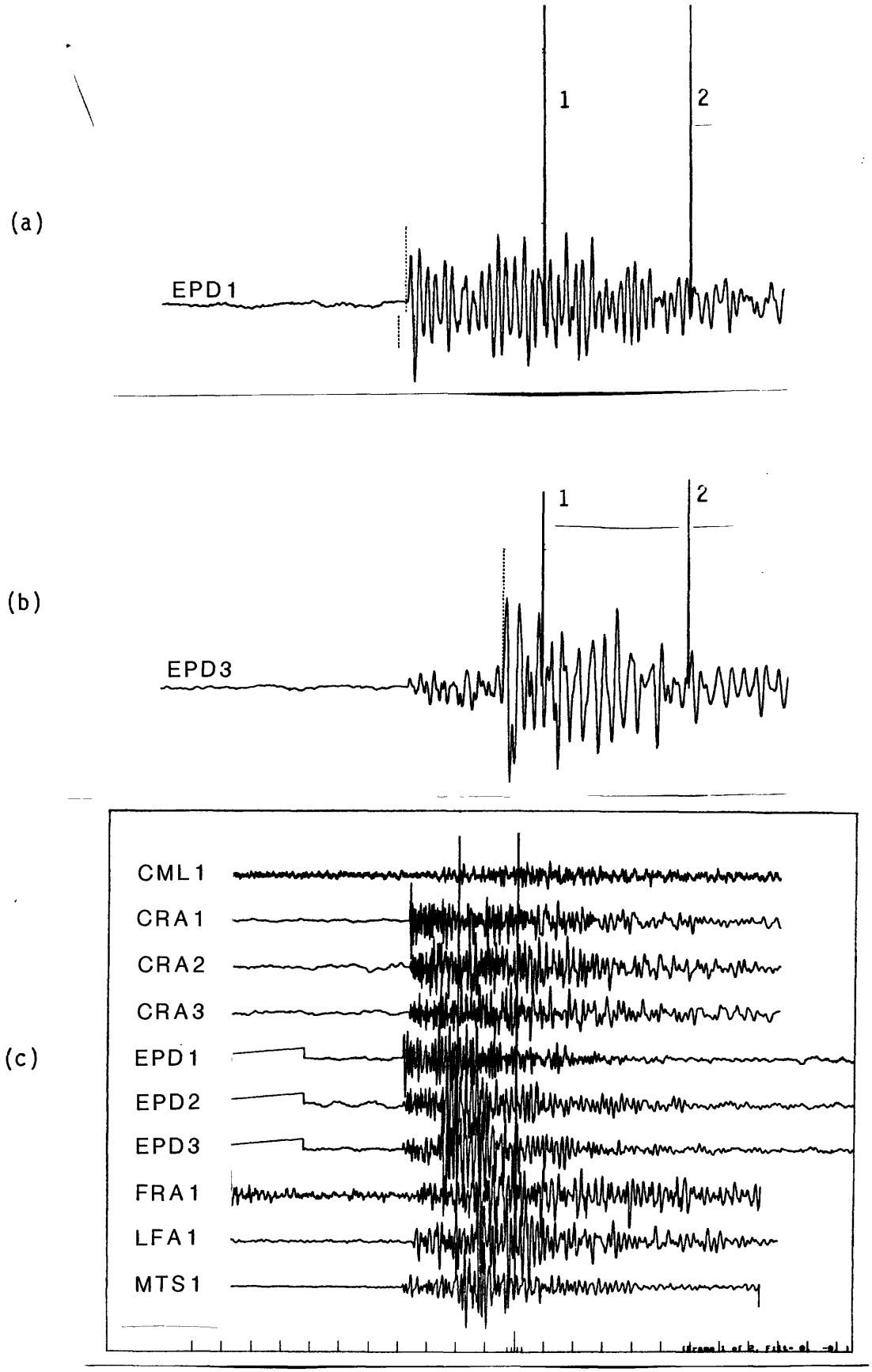
(a)
1
2
EPD1
(b)
1
2
EPD3
(c)
CML1
CRA1
CRA2
CRA3
EPD1
EPD2
EPD3
FRA1
LFA1
MTS1

Figure 7

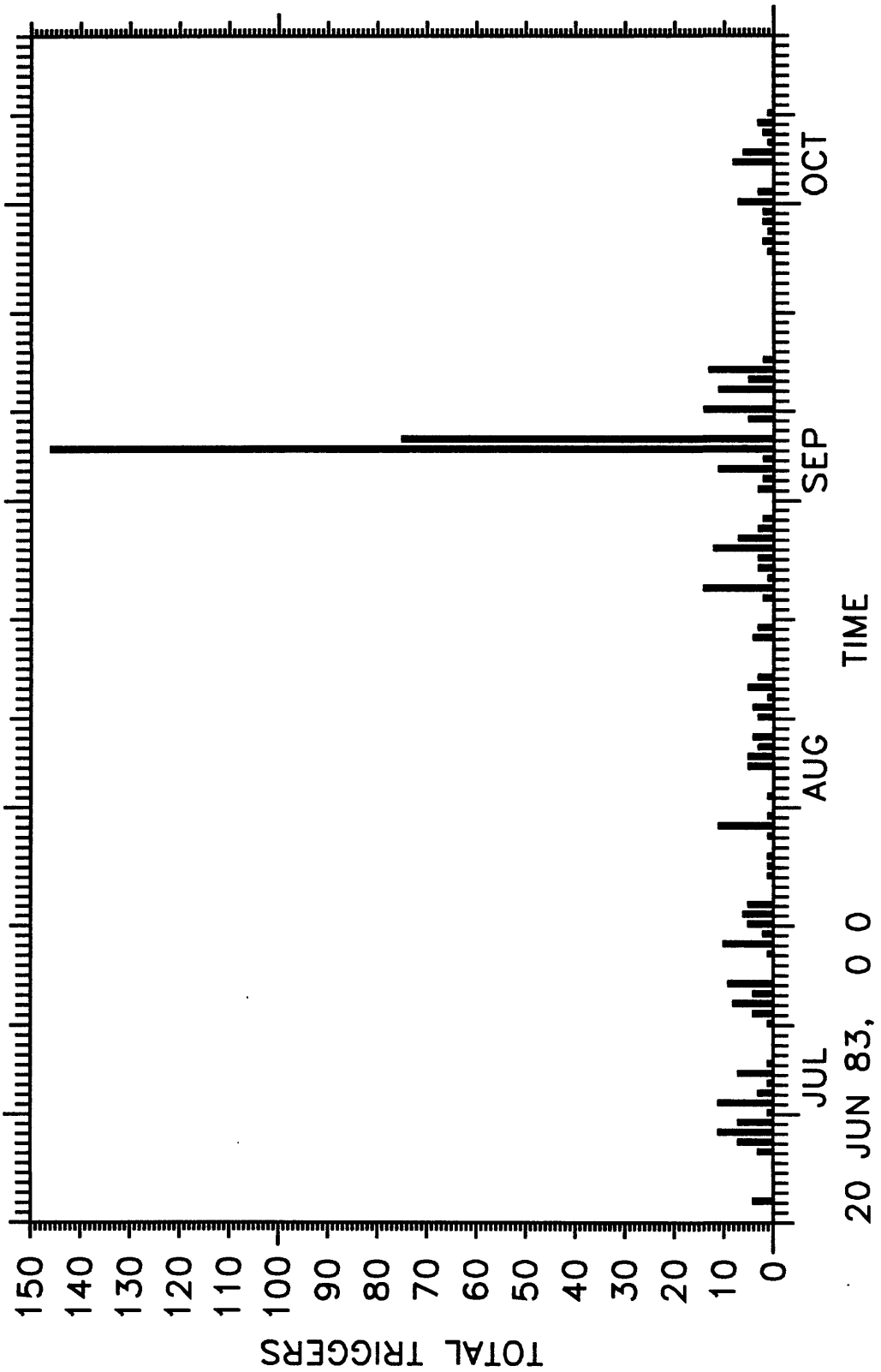
TOTAL TRIGGERS
150
140
130
120
110
100
90
80
70
60
50
40
30
20
10
0
20 JUN 83, 0 0
JUL
AUG
SEP
OCT
TIME

Figure 8

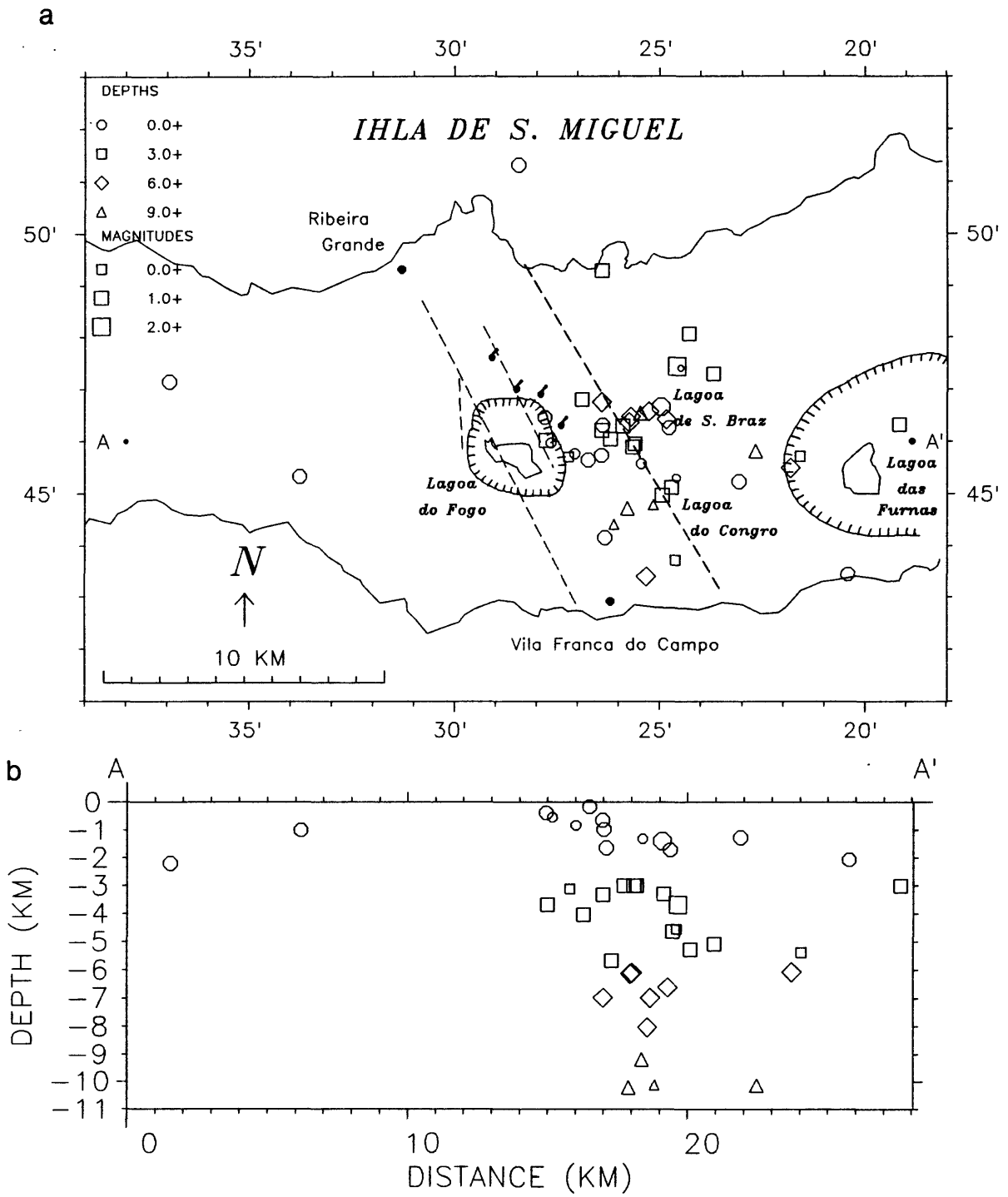
a
35'
30'
25'
20'
DEPTHS
0.0+
3.0+
6.0+
9.0+
MAGNITUDES
0.0+
1.0+
2.0+
IHLA DE S. MIGUEL
Ribeira Grande
50'
45'
A
A'
Lagoa de S. Braz
Lagoa do Fogo
Lagoa do Congro
Lagoa das Furnas
N
10 KM
Vila Franca do Campo
b
A
A'
DEPTH (KM)
0
−1
−2
−3
−4
−5
−6
−7
−8
−9
−10
−11
0
10
20
DISTANCE (KM)

Figure 9

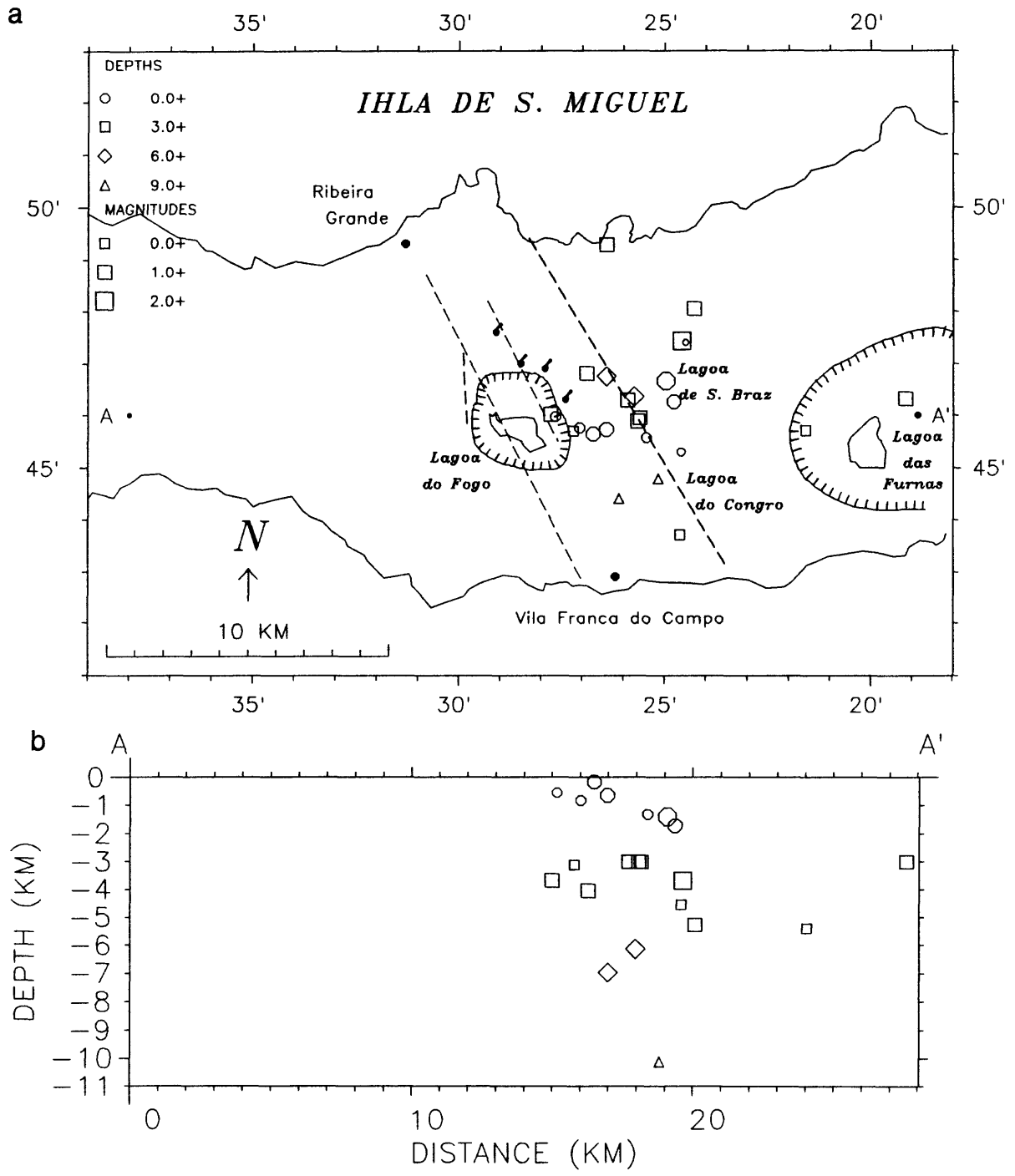
a
35'
30'
25'
20'
DEPTHS
0.0+
3.0+
6.0+
9.0+
MAGNITUDES
0.0+
1.0+
2.0+
IHLA DE S. MIGUEL
Ribeira Grande
50'
45'
A
A'
Lagoa de S. Braz
Lagoa do Fogo
Lagoa do Congro
Lagoa das Furnas
N
10 KM
Vila Franca do Campo
b
DEPTH (KM)
0
-1
-2
-3
-4
-5
-6
-7
-8
-9
-10
-11
0
10
20
DISTANCE (KM)

Figure 10

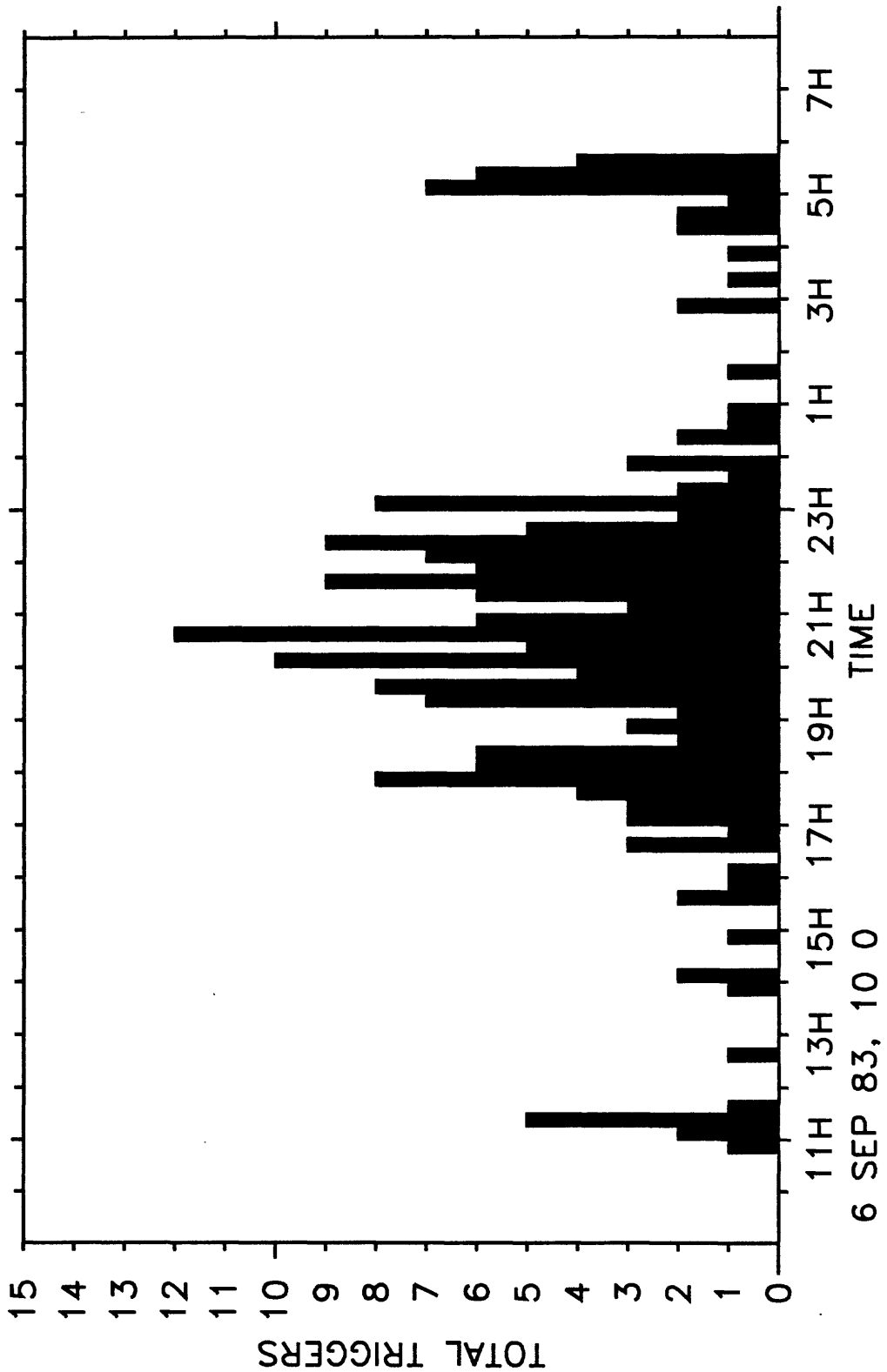
TOTAL TRIGGERS
0
1
2
3
4
5
6
7
8
9
10
11
12
13
14
15
11H 13H 15H 17H 19H 21H 23H 1H 3H 5H 7H
TIME
6 SEP 83, 10 0

Figure 11

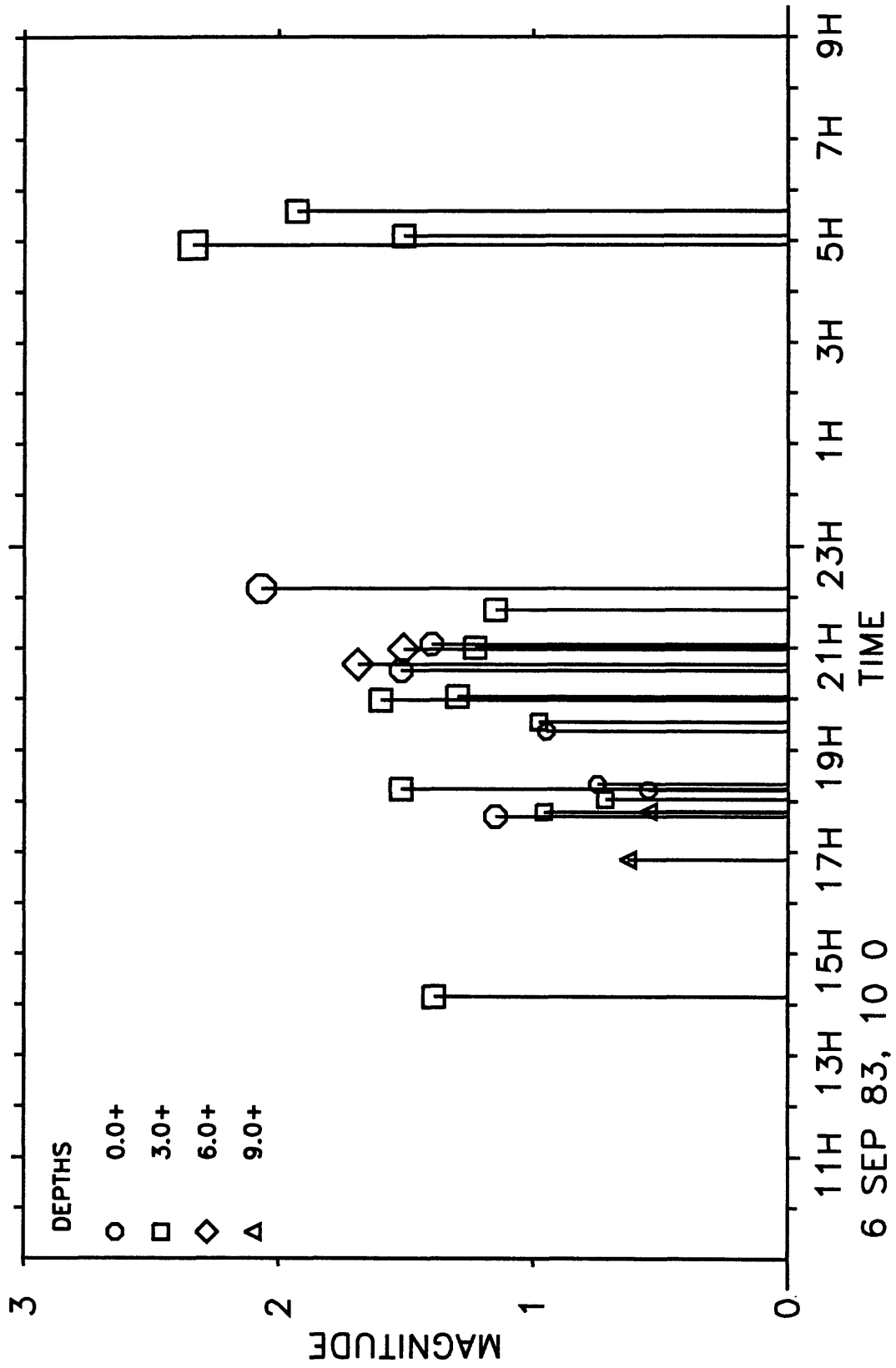
MAGNITUDE
3
2
1
0
DEPTHS
0.0+
3.0+
6.0+
9.0+
11H 13H 15H 17H 19H 21H 23H 1H 3H 5H 7H 9H
TIME
6 SEP 83, 10 0

Figure 12

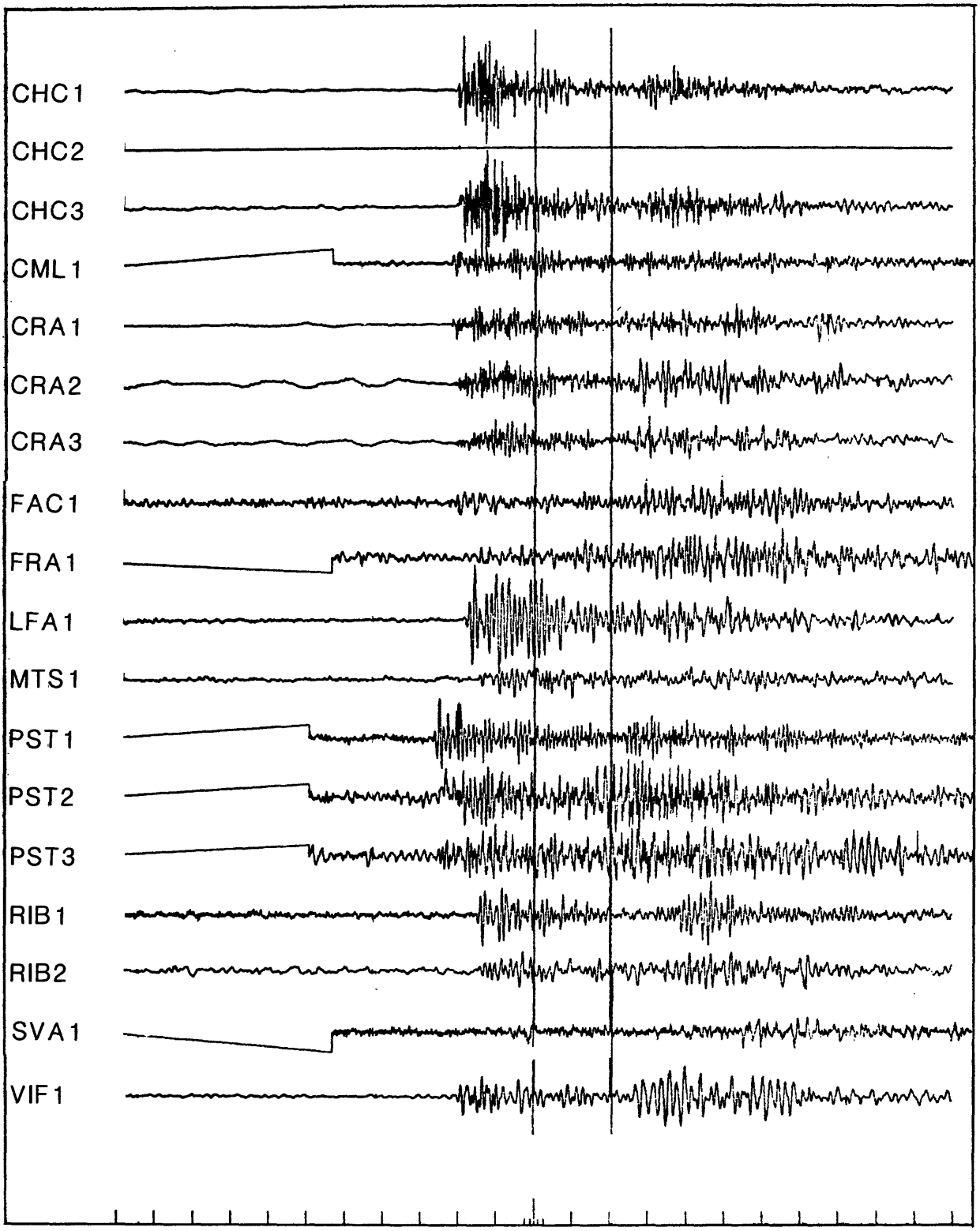
CHC1
CHC2
CHC3
CML1
CRA1
CRA2
CRA3
FAC1
FRA1
LFA1
MTS1
PST1
PST2
PST3
RIB1
RIB2
SVA1
VIF1

Figure 13

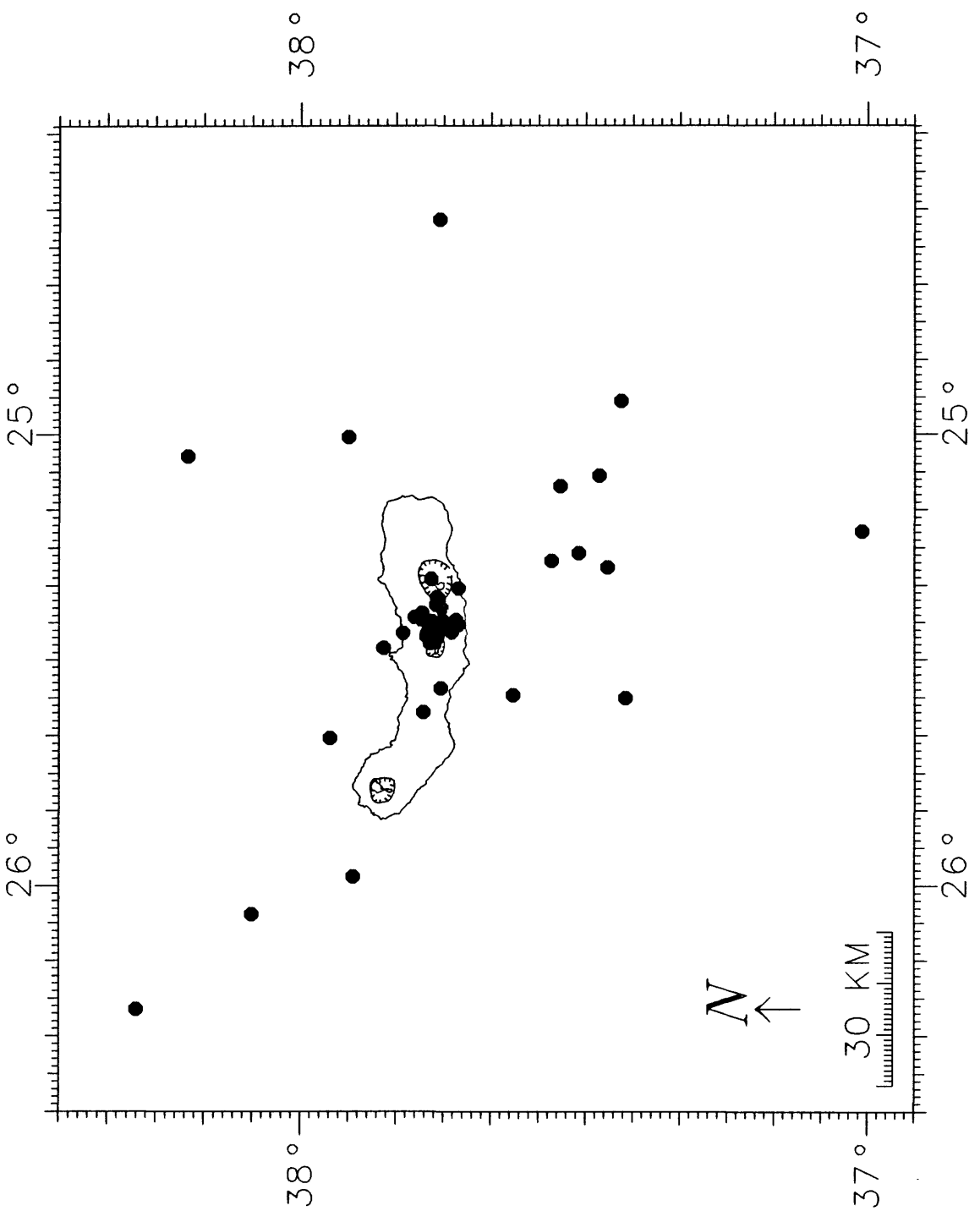

Figure 14

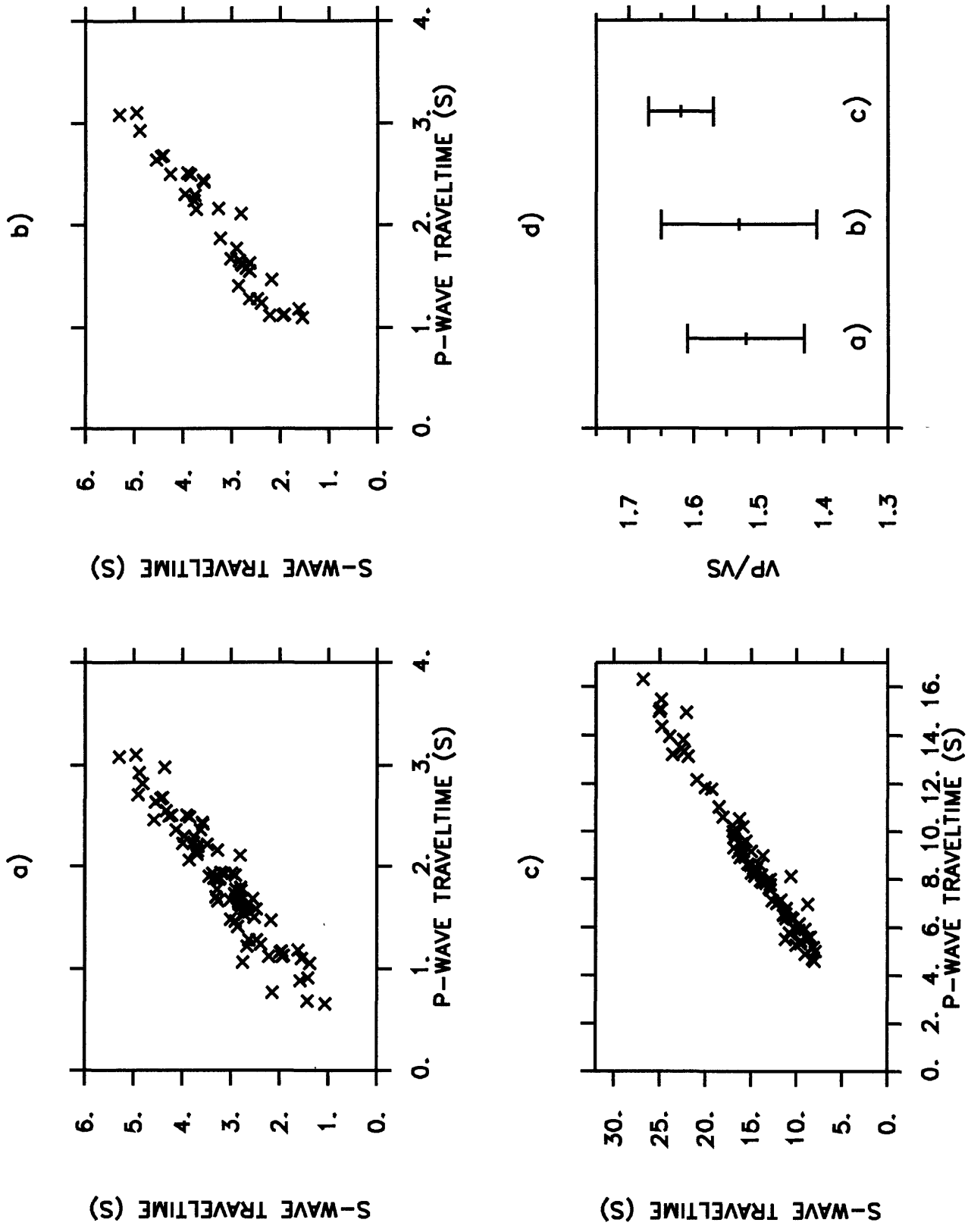
a)
b)
c)
d)
S-WAVE TRAVELTIME (S)
P-WAVE TRAVELTIME (S)
VP/VS
0.
1.
2.
3.
4.
5.
6.
10.
15.
20.
25.
30.
1.3
1.4
1.5
1.6
1.7

Figure 16

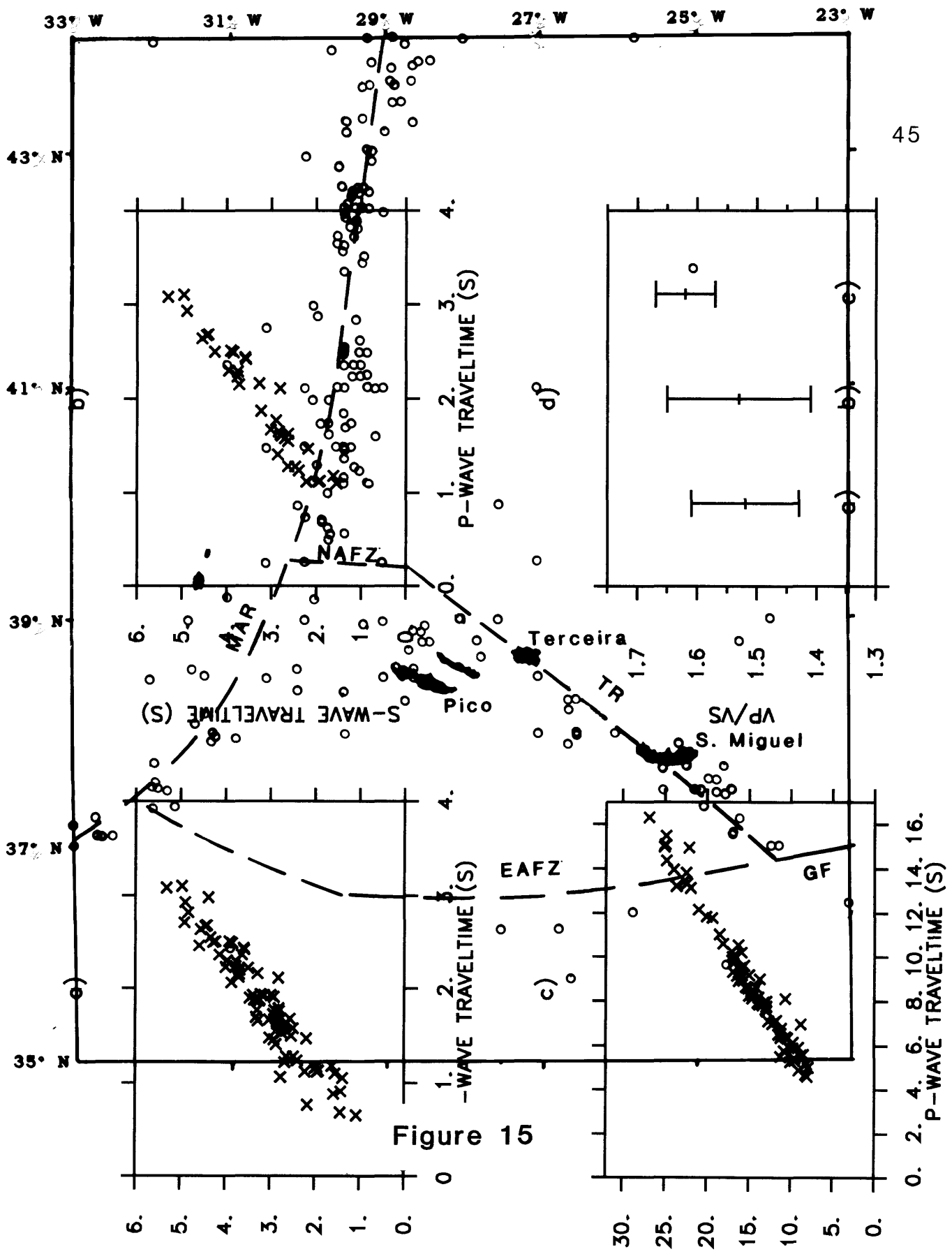
33° W
31° W
29° W
27° W
25° W
23° W
43° N
41° N
39° N
37° N
35° N
MAR
NAFZ
EAFZ
TR
GF
Terceira
Pico
S. Miguel
a)
b)
c)
d)
e)
S-WAVE TRAVELTIME (S)
P-WAVE TRAVELTIME (S)
Vp/Vs

Figure 15

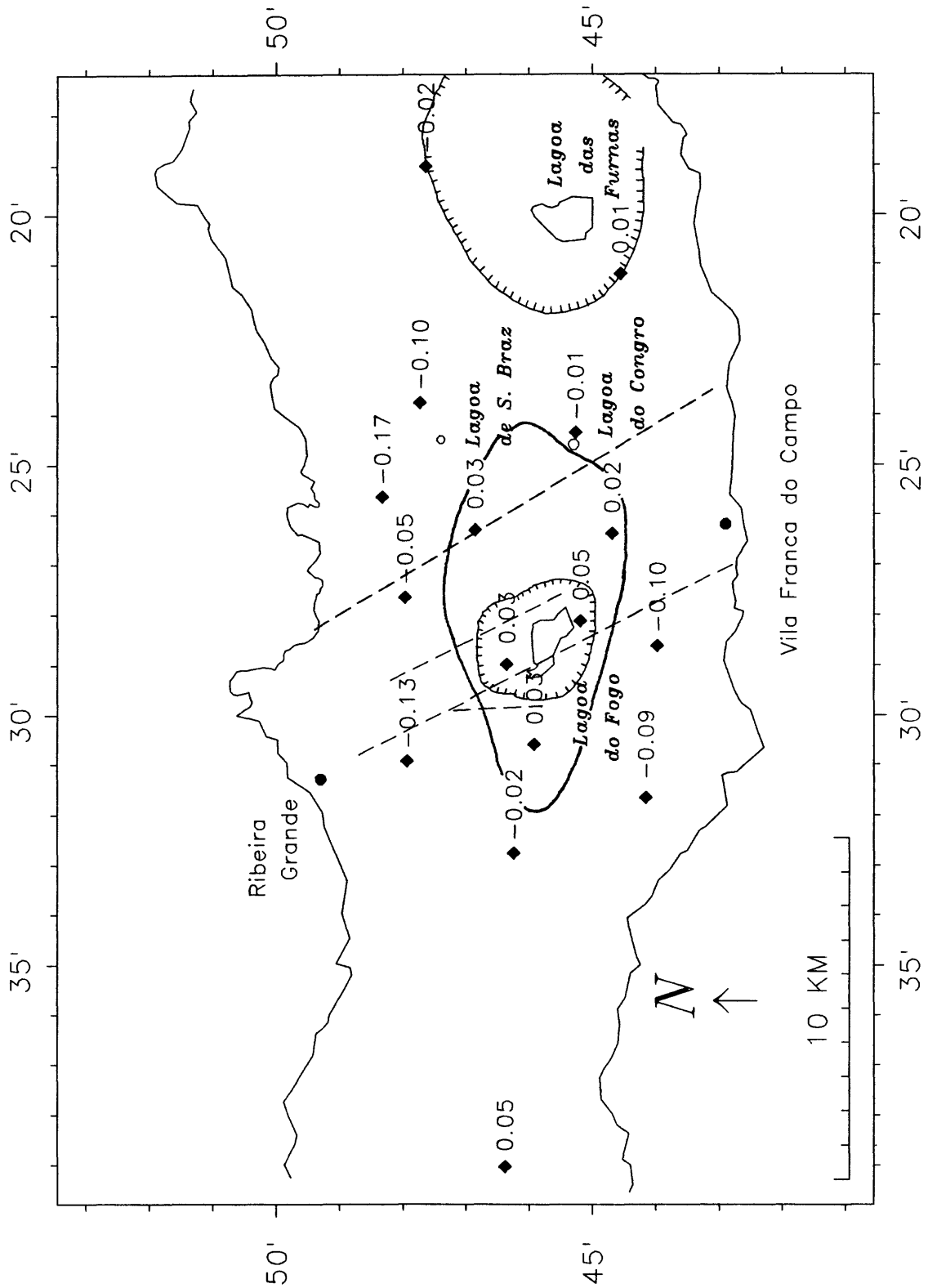
50'
45'
20'
25'
30'
35'
Ribeira Grande
Vila Franca do Campo
Lagoa das Furnas
Lagoa de S. Braz
Lagoa do Congro
Lagoa do Fogo
-0.02
-0.10
-0.17
-0.05
-0.13
0.05
0.03
-0.01
0.02
-0.09
0.01
0.05
10 KM
N

Figure 17

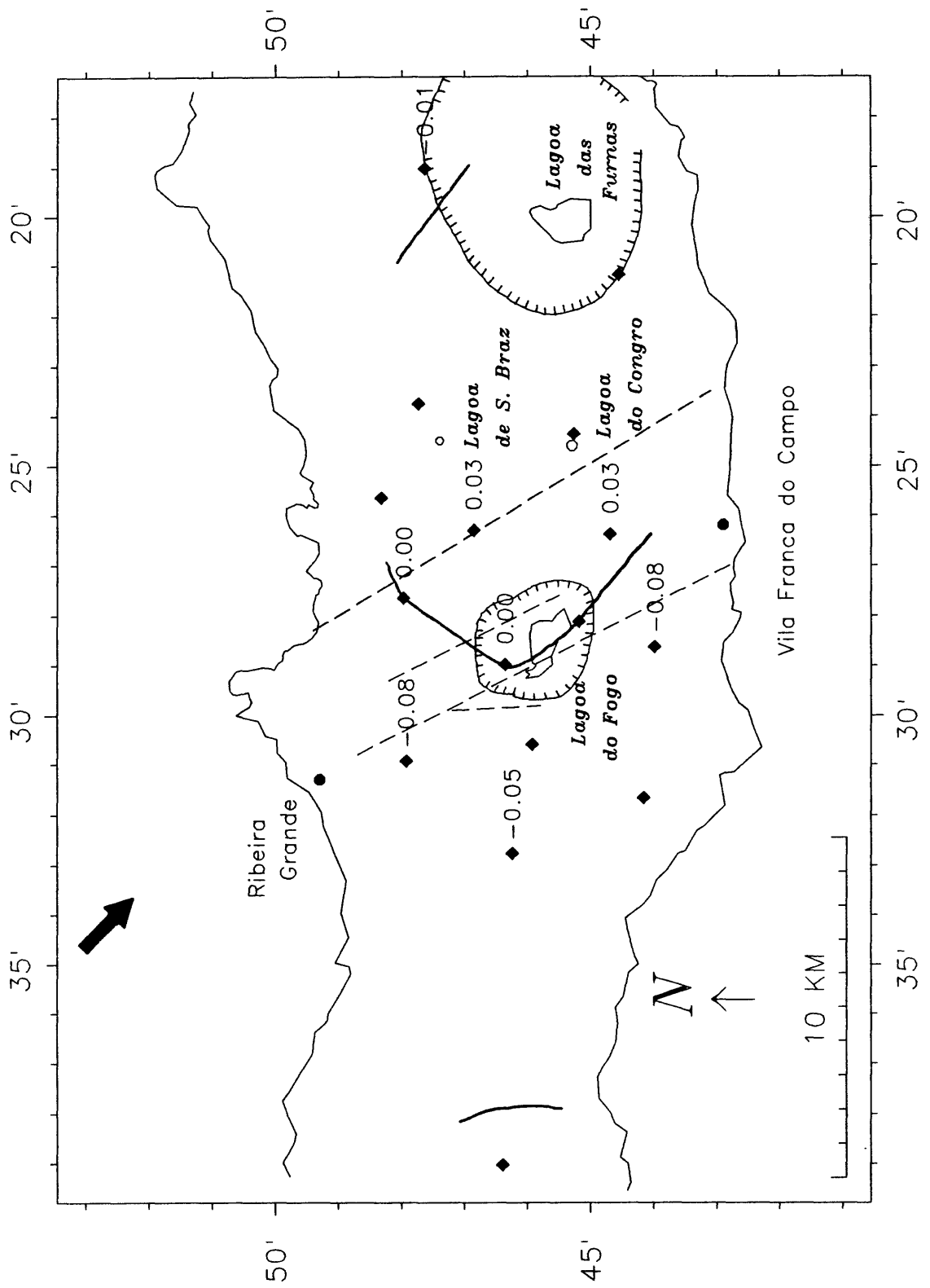
50'
45'
20'
25'
30'
35'
Ribeira
Grande
Vila Franca do Campo
Lagoa
das
Furnas
Lagoa
de S. Braz
Lagoa
do Congro
Lagoa
do Fogo
0.01
0.03
0.03
0.00
0.00
-0.08
-0.08
-0.05
N
10 KM

Figure 18a

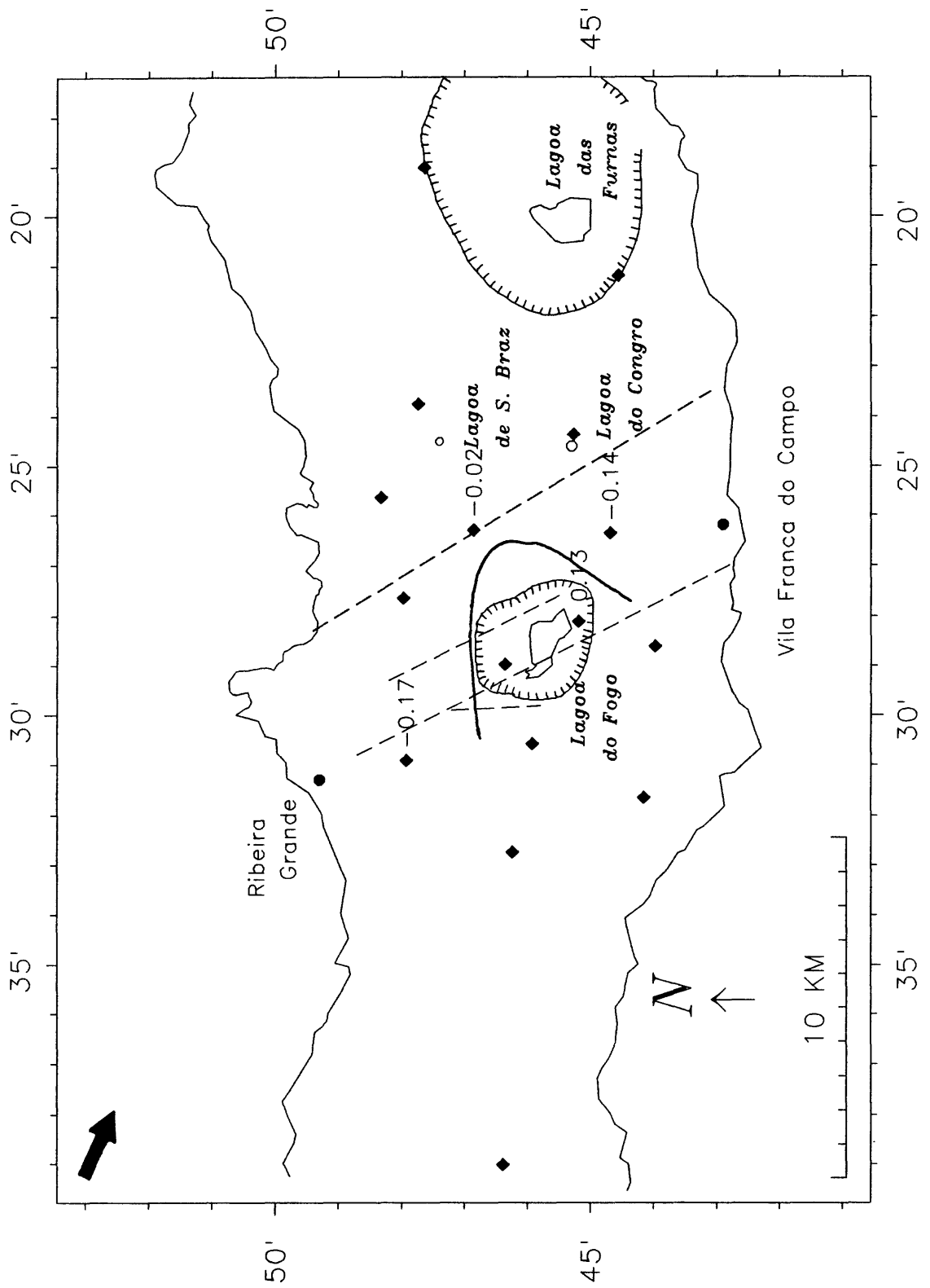
50'
45'
20'
25'
30'
35'
Lagoa das Furnas
Lagoa de S. Braz
Lagoa do Congro
Lagoa do Fogo
-0.02
-0.14
-0.13
-0.17
Ribeira Grande
Vila Franca do Campo
10 KM
N

Figure 18b

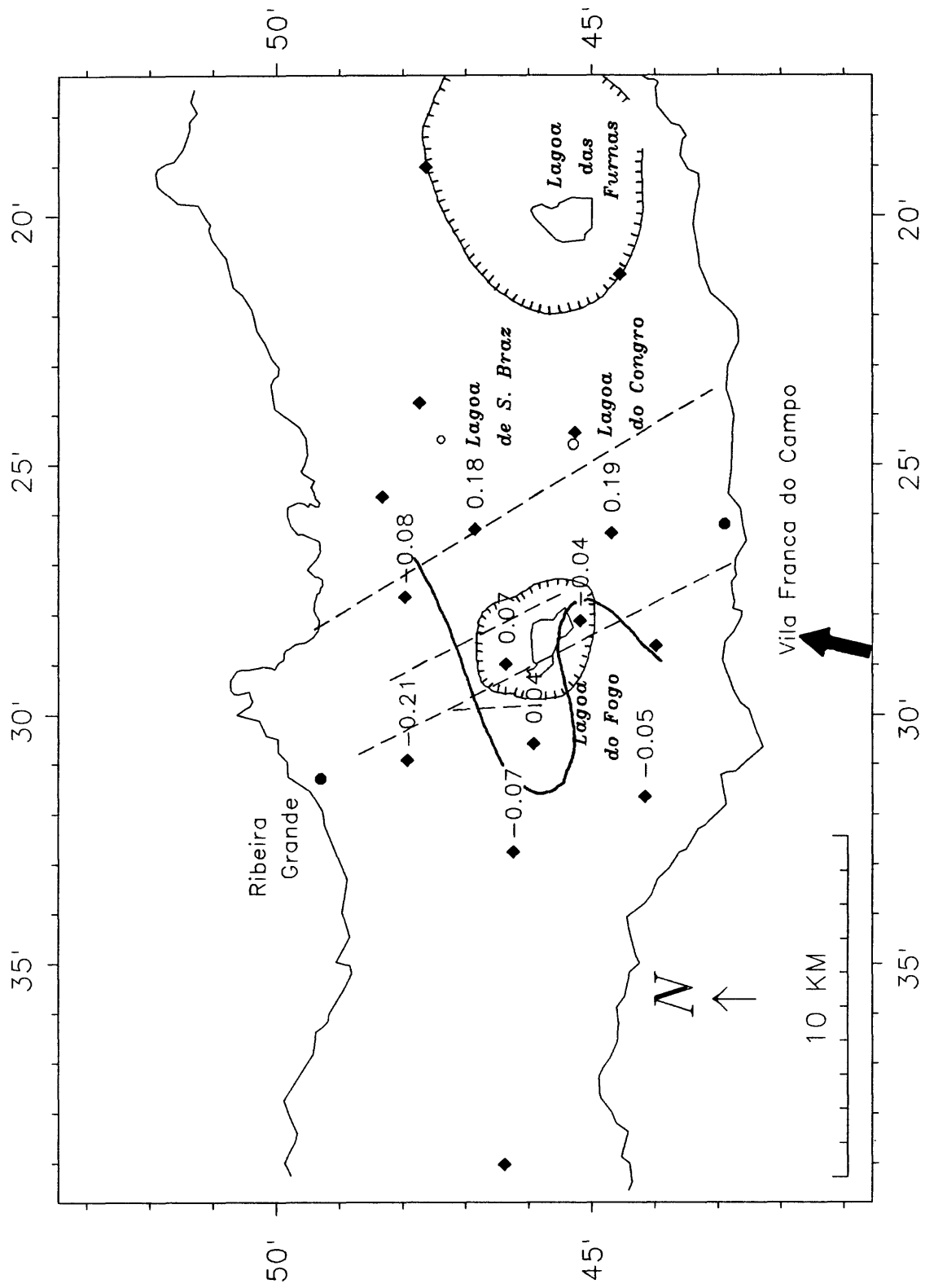
50'
45'
20'
25'
30'
35'
Lagoa das Furnas
Lagoa de S. Braz
Lagoa do Congro
Lagoa do Fogo
0.18
0.19
0.08
0.04
0.07
0.04
-0.21
-0.07
-0.05
Ribeira Grande
Vila Franca do Campo
N
10 KM

Figure 18c

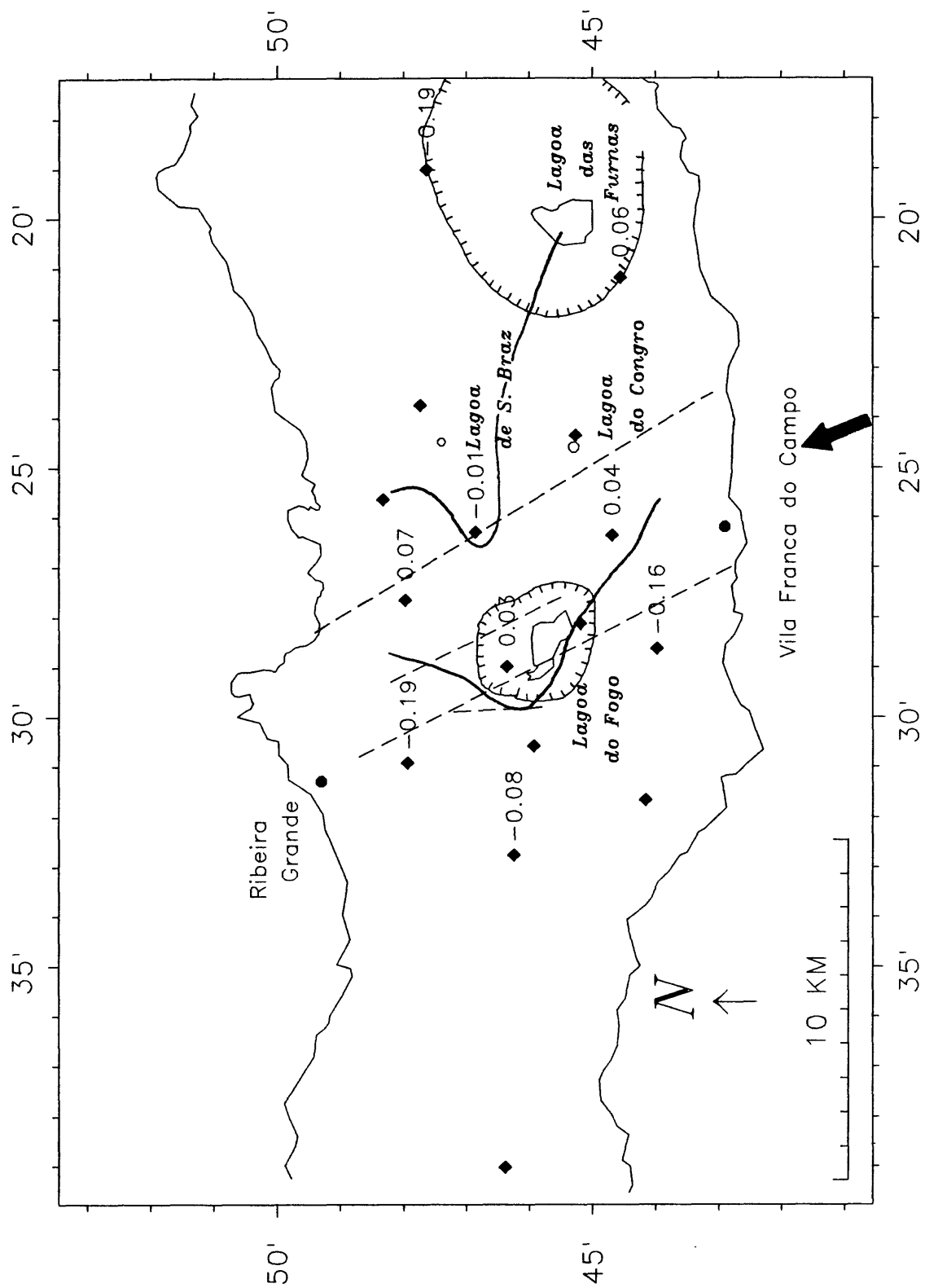
50'
45'
20'
25'
30'
35'
-0.19
Lagoa das Furnas
0.06
Lagoa de S.Braz
-0.01
Lagoa do Congro
0.04
0.07
0.03
-0.16
-0.19
Lagoa do Fogo
-0.08
Ribeira Grande
Vila Franca do Campo
N
10 KM

Figure 18d

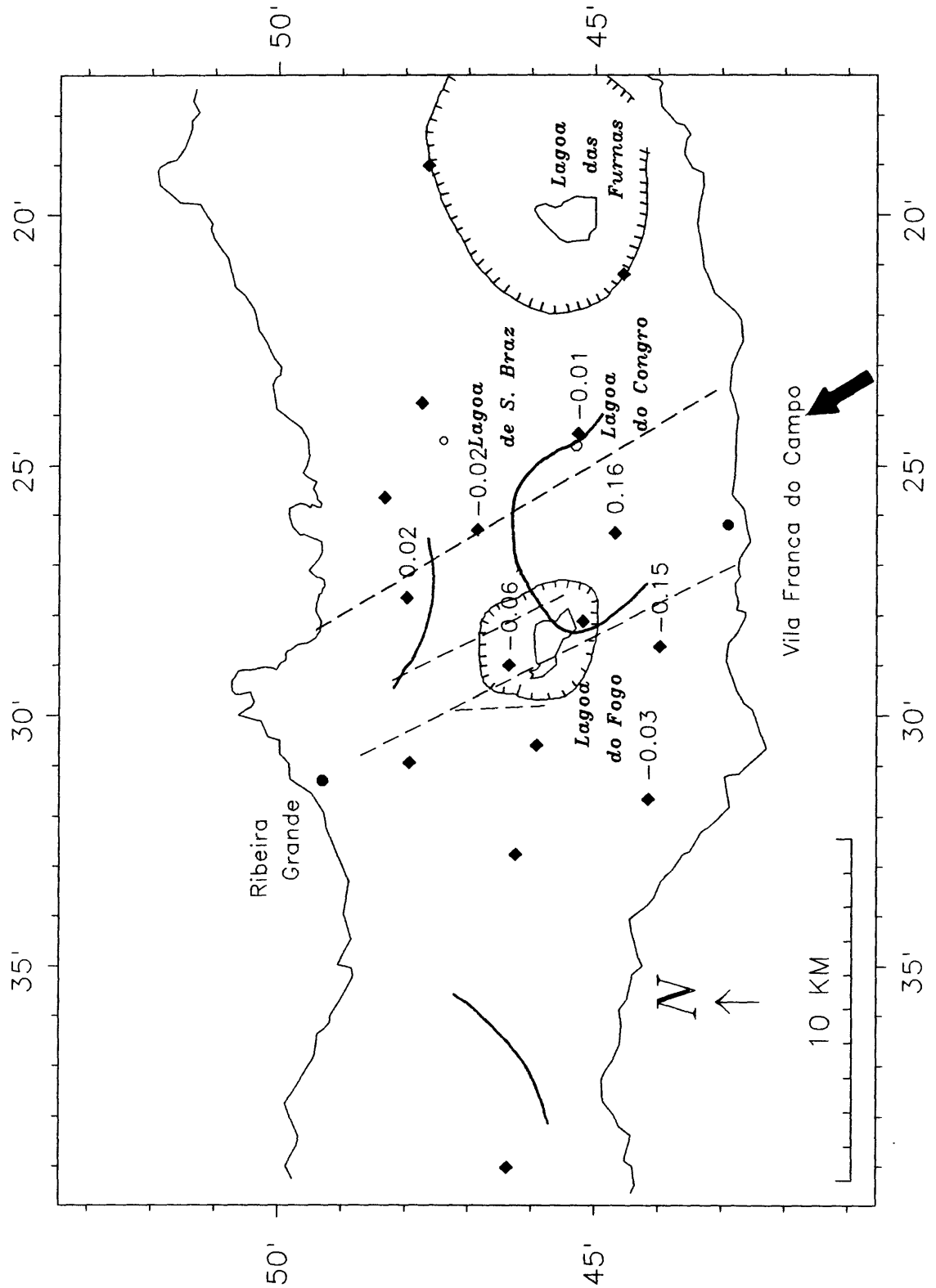
50'
45'
20'
25'
30'
35'
Lagoa das Furnas
Lagoa de S. Braz
Lagoa do Congro
Lagoa do Fogo
-0.02
-0.01
0.16
0.02
-0.06
-0.15
-0.03
Ribeira Grande
Vila Franca do Campo
N
10 KM

Figure 18e

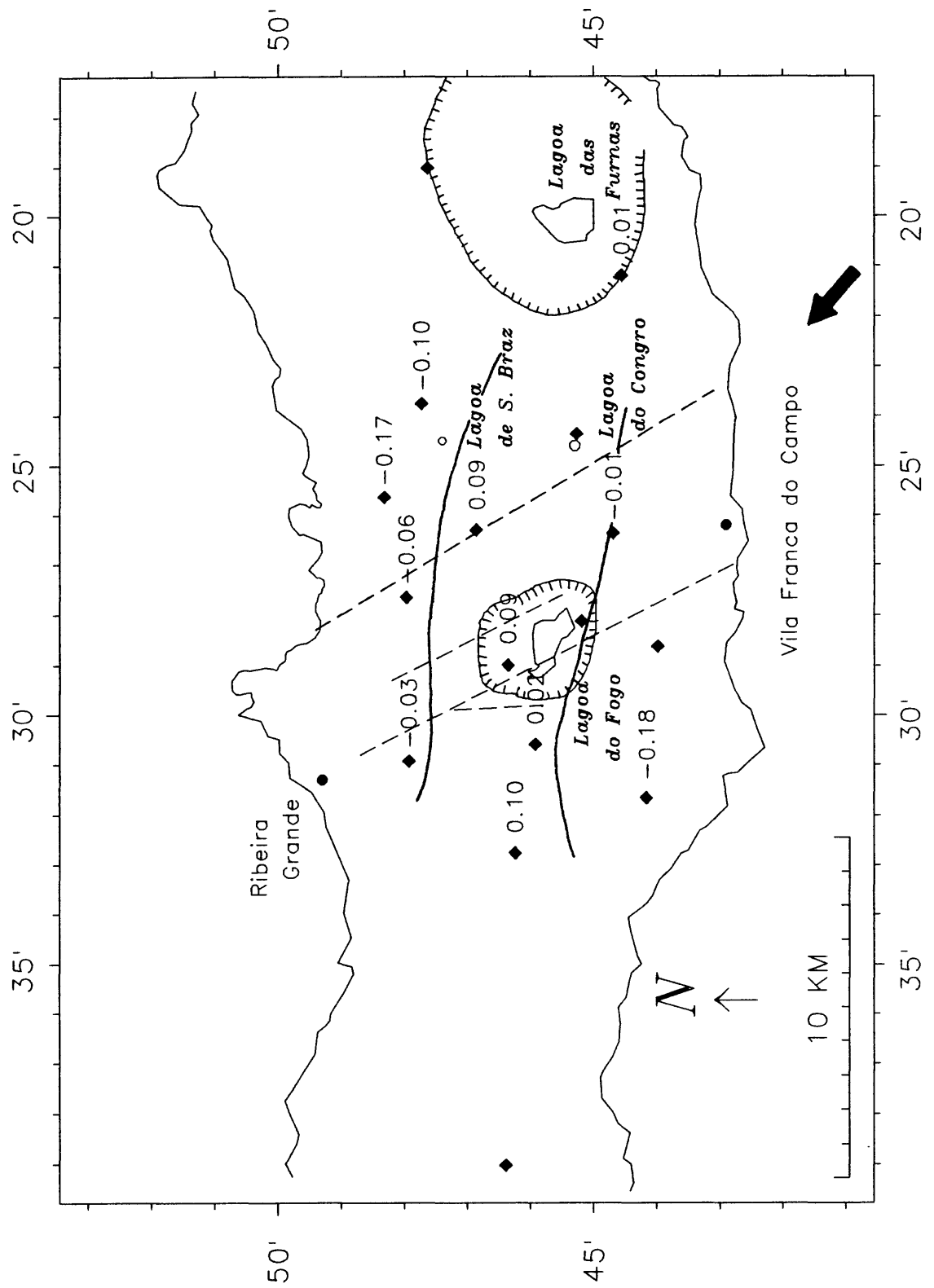
50'
45'
20'
25'
30'
35'
Lagoa das Furnas
Lagoa de S. Braz
Lagoa do Congro
Lagoa do Fogo
Ribeira Grande
Vila Franca do Campo
-0.10
-0.17
0.09
-0.06
-0.03
0.10
0.09
0.02
-0.01
-0.18
0.01
N
10 KM

Figure 18f

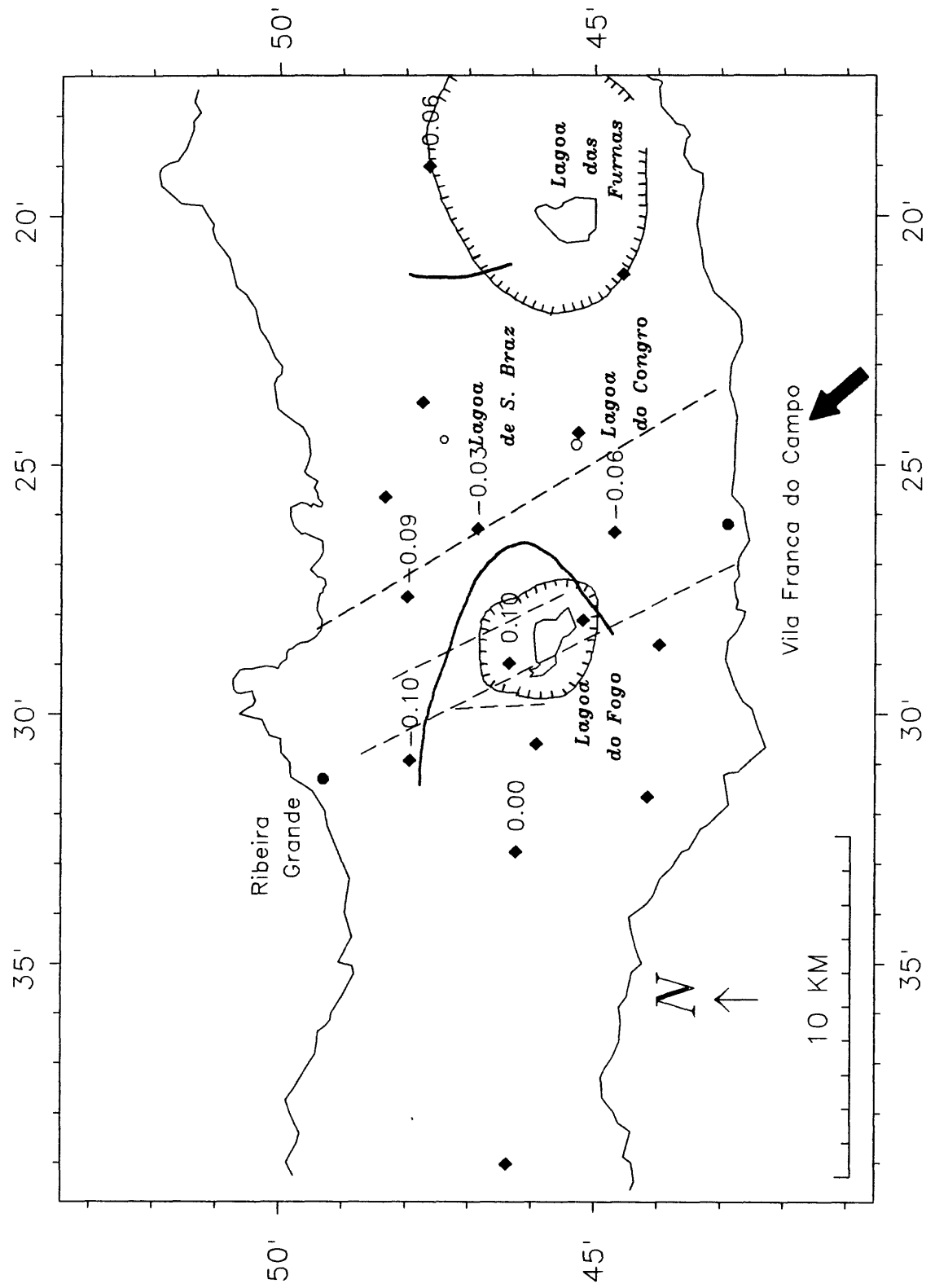
50'
45'
20'
25'
30'
35'
Lagoa das Furnas
Lagoa de S. Braz
Lagoa do Congro
Lagoa do Fogo
Ribeira Grande
Vila Franca do Campo
-0.06
-0.03
-0.06
+0.09
-0.10
0.10
0.00
N
10 KM

Figure 18g

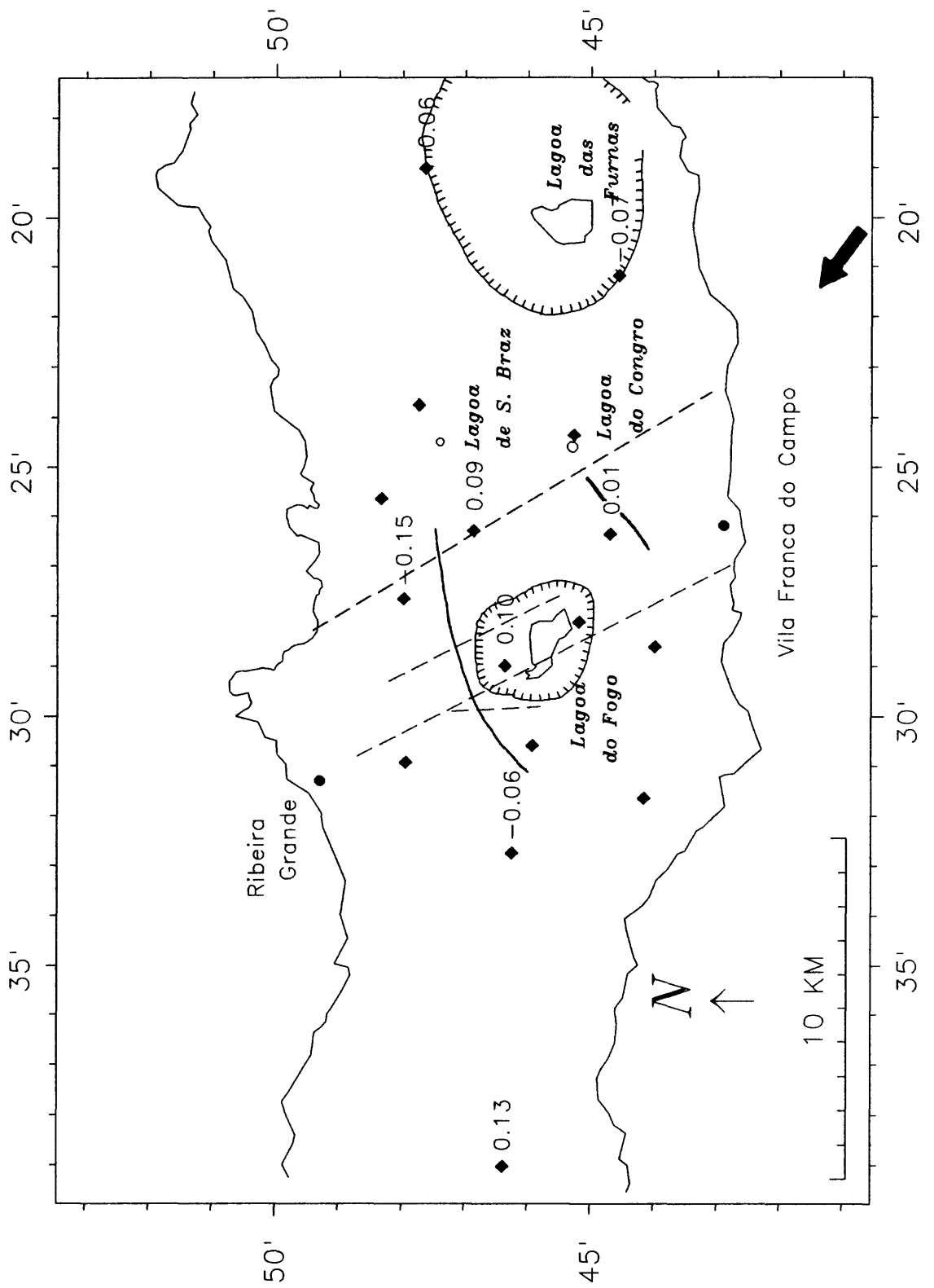
50'
45'
20'
25'
30'
35'
Ribeira
Grande
Vila Franca do Campo
Lagoa
de S. Braz
Lagoa
do Congro
Lagoa
do Fogo
Lagoa
das
Furnas
+0.06
0.09
+0.15
0.10
0.01
−0.06
0.13
−0.07
N
10 KM

Figure 18h

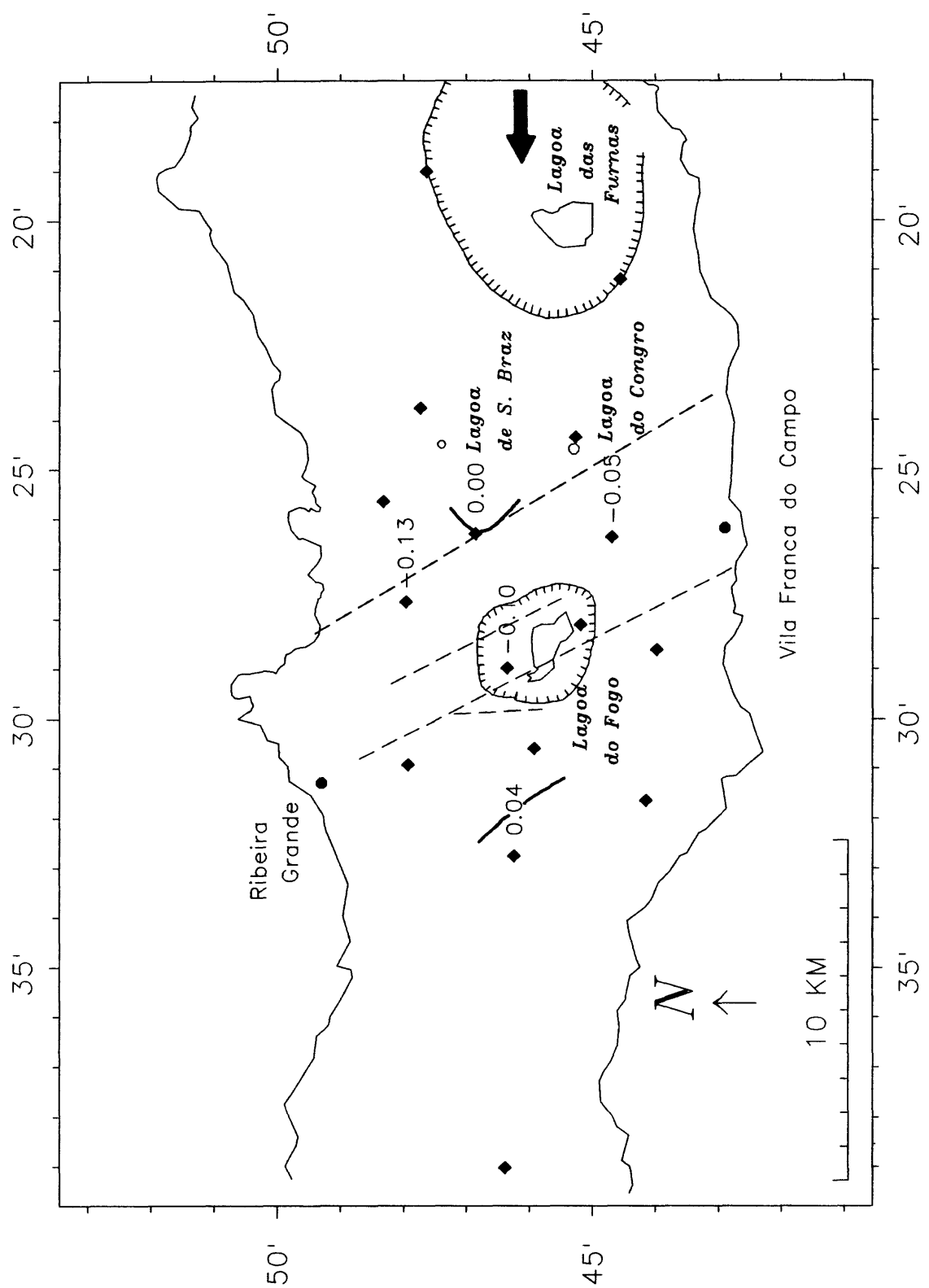
50'
45'
20'
25'
30'
35'
Lagoa das Furnas
Lagoa de S. Braz
Lagoa do Congro
Lagoa do Fogo
0.00
+0.13
-0.05
-0.10
0.04
Ribeira Grande
Vila Franca do Campo
N
10 KM

Figure 18i

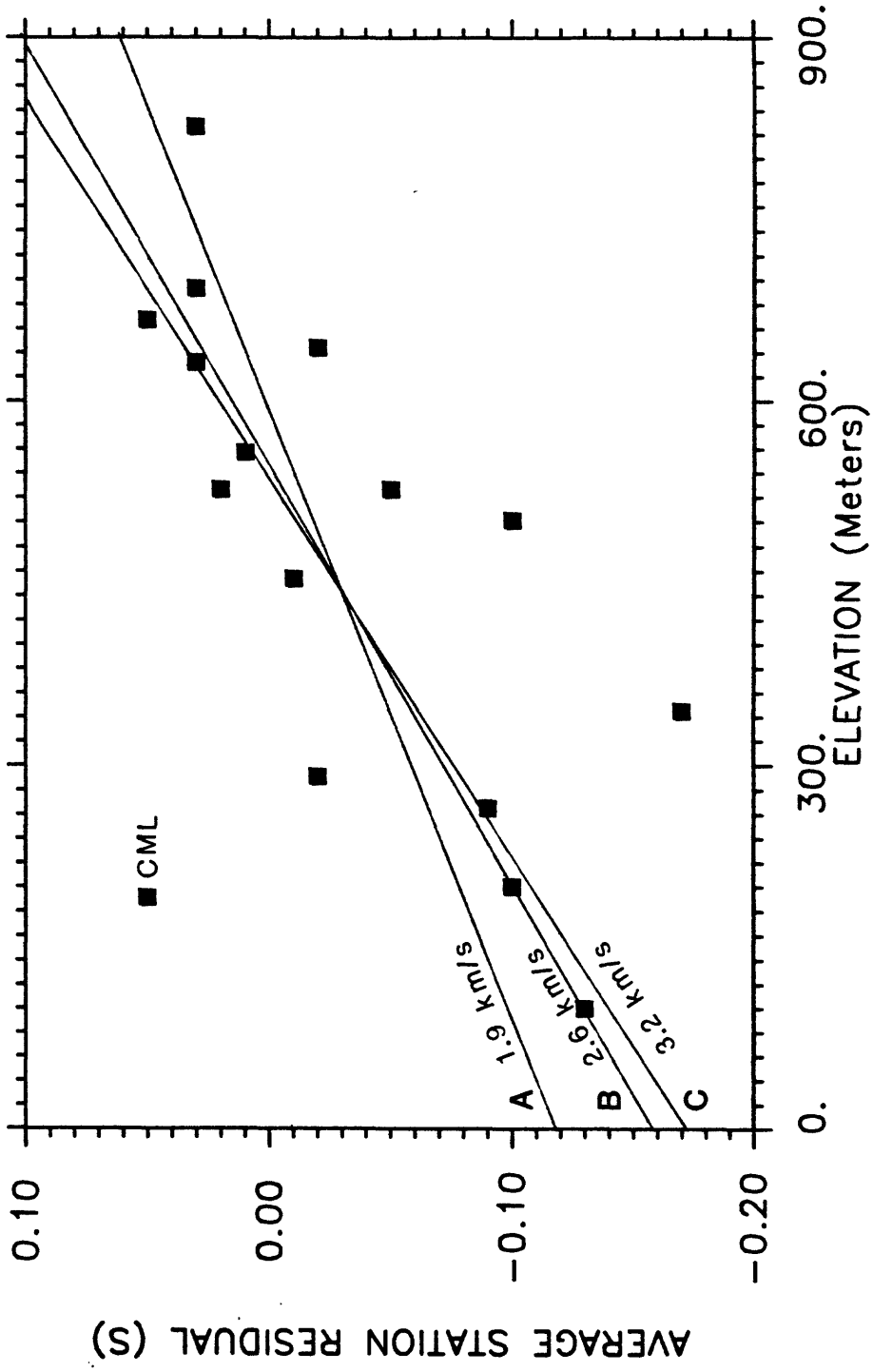
AVERAGE STATION RESIDUAL (S)
0.10
0.00
-0.10
-0.20
0.
300.
600.
900.
ELEVATION (Meters)
CML
A 1.9 km/s
B 2.6 km/s
C 3.2 km/s

Figure 19

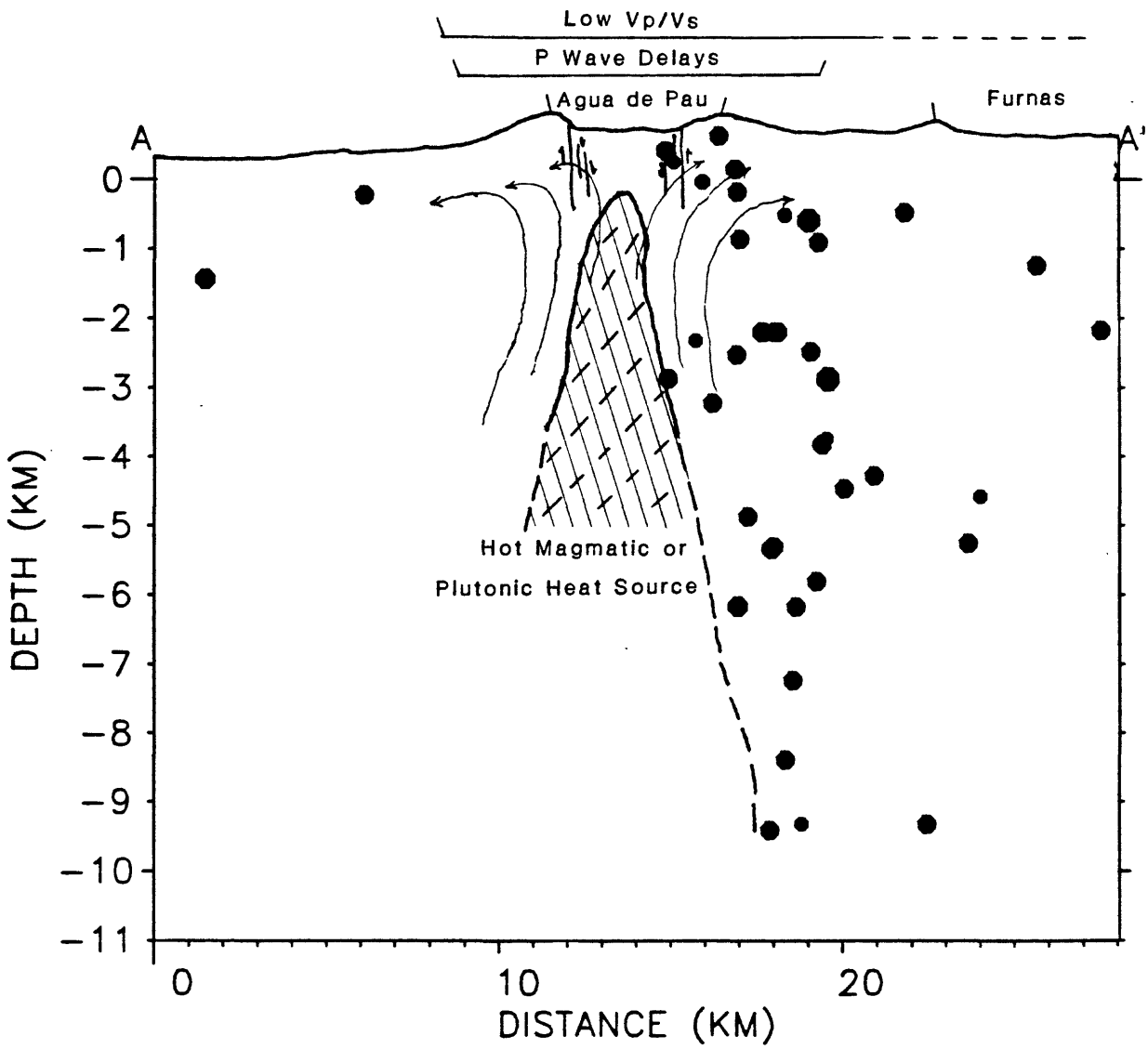
Low Vp/Vs
P Wave Delays
Agua de Pau
Furnas
A
A'
0
−1
−2
−3
−4
−5
−6
−7
−8
−9
−10
−11
DEPTH (KM)
Hot Magmatic or
Plutonic Heat Source
0
10
20
DISTANCE (KM)

Figure 20

APPENDIX A

Clock Drifts (ms)

Station:	ADA	CHC	CRA	EPD	LGD	MI1	MI2	MI3	PFM	PST	PVM	SBA
Recorder No.:	216	192	347	214-216	218	346	344	203	202	212	202	202
DAY												
169		on									on	
170		-									-	
171		-								on	-	
172		+14.7				on				- 7.4	+51.7	
173	on	-		on	on	-				-	-	
174	-	-		-	-	-			on	-	+24.7	
175	-	-	on	-	-	+67.8	+43.6		-	-		
176	-	-	-	-	-	-	-		-	-		
177	-44.5	+19.3	-	-	-				-	-31.9		
178	-	-	-	+81.0	+44.7	+56.0	+32.6		+59.1	-		
179	-	+ 8.0	+15.7	-	-	-	-		-	-16.0		
180	-40.6	-	-	+31.8	+16.8	+31.3	+15.8		+32.0	-		
181	-14.5	+ 7.4	+15.2	-	-	-	-		-	-12.4		
182	-	-	-	+26.8	+14.5	+33.1	+16.5		+28.0	-		
183	-	-	-	-	-	-	-		-	-		
184	-37.4	+ 9.2	+22.9	-	-	-	-		-	-18.3		
185	-	-	-	+41.0	+23.5	+43.9	+22.4		+47.8	-		
186	-23.3	+ 7.6	+17.7	-	-	-	-		-	-12.6		
187	-	-	-	+23.7	+16.0	+31.2	+16.2		+31.1	-		
188	-28.5	+ 5.0	+15.0	-	-	-	-		-	-12.9		
189	-	-	-	+18.2	+13.4	+33.1	+16.8		+27.9	-		
190	-	-	-	-	-	-	-		-	-		
191	-38.4	+ 6.8	+22.8	-	-	-	-		-	-17.7		
192	-	-	-	+34.1	+26.1	+49.7	N/R		+45.4	-		
193	-27.1	+ 4.6	+16.0	-	-	-	-		-	-14.9		
194		-	-	+22.3	+14.9	+31.5	+15.8		+30.2	-		
195		+ 4.8	+15.9	-	-	-	-		-	-11.4		
196		-	-	-20.8	+16.2	+32.6	+16.4		+29.5	-		
197		-	-	-11.2	-	-	-		+13.7	-		
198		+ 5.7	+21.8	-	-	-	-		-	-16.7		
199		-	-	-	-	+50.4	+25.2	on	-	-		
200		+ 6.3	+16.8	-	-	-	-	-	-	-11.6		
201		-	-	-37.7	+34.3	+27.9	+14.6	+ 5.6	+60.3	-		
202		+ 4.7	+15.6	-	-	-	-	-	-	-11.2		
203		-	-	-24.2	+13.2	+33.0	+17.3	+ 5.9	+31.1	-		
204		-	-	-	-	-	-	-	-	-		
205		+ 4.0	+20.9	-	-	-	-	-	-	-18.0		
206		-	-	-35.3	+13.3	+43.7	+23.0	+ 8.8	+41.7	-		
207		+ 4.3	+15.2	-	-	-	-	-		-11.3		
208		-	-	-21.1	+10.1	+29.7	+15.9	+ 5.9	+29.0	-		
209		+ 4.3	+16.1	-	-	-	-	-	-	-10.8		
210		-	-	-21.0	+11.3	+30.4	+16.4	+ 6.1	+30.0	-		
211		-	-	-	-	-	-	-	-	-		
212		+ 7.2	+23.7	-	-	-	-	-	-	-16.3		
213		-	-	-31.6	+15.6	+43.3	+21.6	+ 9.7	+44.1	-		
214		+ 9.7	+19.1	-	-	-	-	-	-	-11.6		
215		-	-	-20.3	+10.1	+27.4	+13.3	+ 6.6	+31.7	-		
216		+ 7.5	+16.8	-	-	-	-	-	-	-10.7		
217		-	-	-20.8	+10.9	+28.5	+14.1	+ 5.8	+32.3	-		
218		-	-	-	-	-	-	-	-	-		
219		+10.1	+26.4	-	-	-	-	-	-	-15.8		
220		-	-	-37.1	+12.7	+47.7	+25.6	+ 8.9	+47.9	-		
221		+ 6.0	+18.4	-	-	-	-	-	-	-13.4		
222		-	-	-21.7	+ 7.4	+36.1	+19.4	+ 6.6	+30.5	-		
223		+ 6.0	+16.4	-	-	-	-	-	-	-11.3		

Appendix A cont.

Clock Drifts (ms)

Station:	ADA	CHC	CRA	EPD	LGD	MI1	MI2	MI3	PFM	PST	PVM	SBA
Recorder No.:	216	192	347	214-216	218	346	344	203	202	212	202	202
DAY												
224		-	-	-25.0	+ 8.2	+29.1	+15.9	+ 5.6	+33.2	-		
225		-	-	-	-	-	-	-	-	-		
226		+ 8.5	+26.3	-	-	-	-	-	-	-18.3		
227		-	-	-39.5	+12.6	+47.2	+26.3	+ 9.2	+47.7	-		
228		+ 5.2	+17.0	-	-	-	-	-	-	-11.4		
229		-	-	-26.8	+ 7.5	+32.9	+19.1	+ 6.0	+32.2	-		
230		-	+15.8	-	-	-	-	-	-	-10.9		
231		-	-	-26.4	+ 6.8	+32.8	+19.0	+ 6.2	+32.7	-		
232		-	-	-	-	-	-	-	-	-		
233		+11.4	+23.6	-	-	-	-	-	-	-16.6		
234		-	-	-38.9	+ 9.6	+49.9	+26.9	+ 8.8	+45.7	-		
235		+ 6.0	+16.3	-	-	-	-	-	-	-12.4		
236		-	-	-64.7	+ 6.4	+32.4	+17.7	+ 5.9	- 7.7	-		
237		+ 5.7	+15.9	-	-	-	-	-	-	-10.8		
238		-	-	+13.7	+ 6.5	+31.0	+15.7	+ 6.4	+71.8	-		
239		-	-	-	-	-	-	-	-	-		
240		+ 9.7	+23.1	-	-	-	-	-	-	-19.0		
241		-	-	-39.5	+10.1	+62.6	+39.6	+ 8.6	+49.2	-		
242		+ 5.8	+16.3	-	-	-	-	-	-	-12.6		
243		-	-	-27.8	+ 6.0	+41.5	+27.0	+ 5.3	+31.4	-		
244		+ 6.3	+15.9	-	-	-	-	-	-	-13.0		
245		-	-	-26.2	+ 6.4	+25.4	+11.9	+ 6.9	+31.5	-		
246		-	-	-	-	-	-	-	-	-		
247		+10.9	+24.6	-	-	-	-	-	-	-17.8		
248		-	-	-33.6	+12.4	+40.9	+24.2	+10.7	+52.9	-		
249		+ 7.2	+16.6	-	-	-	-	-	-	-12.3		
250		-	-	-27.2	+ 6.1	+29.6	+17.5	+ 5.3	+32.7	-		
251		+ 6.3	+15.2	-	-	-	-	-	-	-13.1		
252		-	-	-27.1	+ 6.5	+32.7	+20.8	+ 5.9	+34.6	-		
253		-	-	-	-	-	-	-	-	-		
254		+11.3	+23.7	-	-	-	-	-	-	-17.3		
255		-	-	-40.2	+ 9.8	+48.5	+30.2	+24.6	N/R	-		
256		+ 7.3	+15.8	-	-	-	-	-	-	-12.0		
257		-	-	-24.8	+ 6.7	+24.4	+12.4	+ 6.5	+33.3	-		
258		+11.4	+19.2	-	-	-	-	-	-	-12.1		
259		-	-	-26.8	+ 6.7	+26.6	+15.2	+ 6.6	+33.2	-		
260		-	-	-	-	-	-	-	-	-		
261		+13.8	+27.2	-	-	-	-	-	-	-15.9		
262		-	-	-38.3	+ 9.4	+40.2	+19.8	+10.1	+49.0	-		
263		+ 8.5	+17.7	-	-	-	-	-	-	-13.0		
264		-	-	-29.8	+ 6.1	+24.8	+11.2	+ 6.8	+30.8	-		
265		+ 6.8	+16.1	-	-	-	-	-	-	-11.5		
266		-	-	-24.3	+ 9.6	+25.9	+13.3	+ 6.9	+37.2	-		
267		-	-	-	-	-	-	-	-	-		
268		+15.8	+28.3	-	-	-	-	-	-	-12.3		
269		-	-	-27.0	+19.1	+50.7	+28.1	+ 8.7	+64.4	-		
270		+ 7.2	+16.5	-	-	-	-	-	-	-11.4		
271		-	-	-23.6	+ 9.8	+33.3	+18.5	+ 5.7	+37.0	-		
272		+ 8.0	+16.9	-	-	-	-	-	-	- 9.9		
273		-	-	-26.7	+ 9.0	+34.5	+19.3	+ 6.0	+37.3	-		
274		-	-	-	-	-	-	-	-	-		
275		+ 8.9	+22.0	-	-	-	-	-		-17.2		on
276		-	-	-	-	+51.6	+29.6	+ 9.8		-		-
277		+ 8.7	+16.9	-	-	-	-	-		-12.3		+14.0
278		-	-	-	+24.7	+37.4	+21.5	+ 6.0		-		+16.9

Appendix A cont.

Clock Drifts (ms)

Station:	ADA	CHC	CRA	EPD	LGD	MI1	MI2	MI3	PFM	PST	PVM	SBA
Recorder No.:	216	192	347	214-216	218	346	344	203	202	212	202	202
DAY												
279		+ 8.2	+16.9	-	-	-	-	-		-11.3		+20.7
280				-83.8	+ 9.5	+35.4	+19.7	+ 6.4				-
281						-	-	-				-
282						-	-	-				+43.7
283						+50.5	+28.1	+10.1				+17.8
284						-	-	-				+18.8
285						+32.3	+17.2	+ 6.8				+19.8

_____ Station removed

Tapes were changed and clock drifts were measured every two days (three days over weekends) and each clock was reset to ±0.1 ms after drift was measured. The numbers in the above table indicate the amount of drift (ms) measured on the indicated day from the previous tape change.

APPENDIX B

FINAL HYPOCENTERS

YRMODA	ORIGIN	LAT	LON	DEPTH	MAG	NO	GAP	DM	RMS	ERH	ERV	Q
830628	0231:34.13	37° 44.72′	25° 25.79′	10.22	1.44	7	174	0.9	0.05	0.9	1.0	BC
830628	1410:10.14	37° 46.57′	25° 25.26′	6.98	1.09	5	259	1.6	0.02	1.4	1.0	CC
830628	1415:00.13	37° 43.39′	25° 25.33′	8.03	1.29	5	328	2.9	0.10	5.1	2.4	DC
830628	1730:07.51	37° 46.21′	25° 26.41′	3.33	1.48	6	172	1.2	0.09	1.0	2.1	CC
830628	2217:18.62	37° 54.95′	25° 00.44′	3.00	1.62	12	346	36.0	0.28	194.8	253.4	DC
830628	2344:55.36	37° 46.54′	25° 25.47′	9.19	1.41	9	99	1.4	0.06	0.9	1.0	BC
830629	0242:43.39	37° 45.22′	25° 23.07′	1.29	1.12	4	316	5.0	0.00	0.0	0.0	CC
830629	0411:53.50	37° 46.42′	25° 24.84′	6.61	1.04	5	271	2.3	0.00	0.1	0.1	CC
830629	0611:11.47	37° 46.04′	25° 26.20′	5.68	1.14	5	192	1.5	0.04	1.5	1.2	CC
830701	0533:23.32	38° 16.55′	26° 16.96′	3.00	2.40	6	357	85.7	0.08	999.9	999.9	DC
830702	1109:58.67	37° 43.44′	25° 20.42′	2.06	1.42	8	314	2.4	0.07	1.4	0.6	CC
830702	2229:30.83	37° 28.62′	25° 05.49′	1.14	1.80	17	344	37.5	0.14	56.6	42.4	DC
830705	0633:52.64	37° 54.49′	25° 58.79′	0.43	1.51	9	353	41.1	0.13	389.7	146.9	DC
830705	2328:26.29	37° 46.46′	25° 27.80′	0.38	1.54	5	116	1.8	0.29	2.56	40.9	DC
830706	0233:01.21	37° 46.31′	25° 26.39′	0.98	1.31	7	144	3.0	0.23	1.3	1.0	CC
830713	0120:25.21	37° 33.62′	25° 16.75′	21.32	1.79	7	345	24.9	0.17	15.4	15.3	DC
830717	0048:49.37	37° 45.81′	25° 22.67′	10.14	1.63	10	162	3.2	0.05	0.8	0.7	BC
830718	1229:07.77	37° 45.33′	25° 33.78′	1.01	1.16	4	305	2.3	0.47	0.0	0.0	DC
830719	2328:53.87	37° 44.97′	25° 24.94′	3.29	1.19	6	159	2.2	0.06	0.7	1.5	BC
830725	0737:03.88	37° 27.72′	25° 17.62′	0.67	1.55	8	354	33.9	0.29	676.4	511.0	DC
830726	1724:19.23	37° 32.74′	25° 06.90′	9.49	1.78	14	342	36.2	0.14	61.9	109.5	DC
830730	2321:27.25	37° 48.11′	25° 39.57′	4.27	1.85	6	285	3.3	0.03	13.4	4.9	DC
830805	2355:30.84	37° 44.15′	25° 26.34′	1.66	1.50	12	180	1.0	0.16	0.8	0.4	CC
830810	0040:34.46	37° 25.80′	25° 35.11′	5.75	1.77	20	321	34.3	0.13	1.3	141.0	DC
830812	2326:14.46	38° 11.73′	25° 02.96′	3.00	1.73	15	339	50.4	0.47	127.4	120.7	DC
830813	0214:45.68	37° 30.76′	25° 15.77′	5.64	1.83	17	335	29.7	0.23	2.8	267.6	DC
830824	2017:20.11	37° 46.47′	25° 25.70′	6.11	1.30	6	146	1.1	0.03	0.7	0.9	BC
830829	2214:19.99	37° 45.49′	25° 21.82′	6.08	1.15	7	126	1.9	0.07	0.8	1.1	BC

APPENDIX B

FINAL HYPOCENTERS

YRMODA	ORIGIN	LAT	LON	DEPTH	MAG	NO	GAP	DM	RMS	ERH	ERV	Q
830902	1403:15.40	37° 37.68′	25° 34.69′	1.50	1.01	6	345	17.8	1.13	61.0	27.6	DC
830906	1509:06.25	37° 48.06′	25° 24.29′	5.27	1.39	6	205	1.0	0.04	0.9	0.5	CC
830906	1751:33.65	37° 44.41′	25° 26.12′	12.05	0.63	6	223	0.6	0.10	3.1	2.2	DC
830906	1842:57.68	37° 45.73′	25° 26.42′	0.65	1.15	5	109	1.9	0.15	0.1	1.9	CC
830906	1847:02.37	37° 45.70′	25° 27.22′	3.12	0.96	5	148	2.2	0.01	0.1	0.3	CC
830906	1848:43.95	37° 44.79′	25° 25.16′	10.12	0.55	7	170	1.8	0.12	2.3	1.5	CC
830906	1902:37.35	37° 45.71′	25° 21.59′	5.39	0.72	9	209	5.2	0.13	3.6	3.6	DC
830906	1913:45.93	37° 45.76′	25° 27.07′	0.83	0.55	6	138	2.2	0.07	0.3	3.4	CC
830906	1914:00.96	37° 46.32′	25° 19.16′	3.00	1.52	3	339	10.5	0.00	0.0	0.0	CC
830906	1920:32.21	37° 45.97′	25° 27.65′	0.54	0.75	6	148	2.1	0.21	2.0	201.3	CC
830906	2022:10.59	37° 45.57′	25° 25.45′	1.32	0.95	6	223	2.1	0.19	2.5	5.8	DC
830906	2033:13.44	37° 43.71′	25° 24.63′	4.55	0.98	7	315	3.2	0.10	1.3	1.9	CC
830906	2058:18.76	37° 45.95′	25° 25.60′	3.00	1.60	3	238	2.0	0.00	0.0	0.0	CC
830906	2102:35.57	37° 46.29′	25° 25.90′	3.00	1.30	7	160	1.2	0.23	2.6	3.3	CC
830906	2133:16.98	37° 45.64′	25° 26.74′	0.17	1.52	5	129	1.8	0.09	0.5	1.6	CC
830906	2140:46.17	37° 46.36′	25° 25.74′	6.14	1.69	9	177	1.2	0.08	0.9	0.9	BC
830906	2158:02.96	37° 46.75′	25° 26.41′	6.97	1.51	5	137	0.2	0.12	4.5	5.3	DC
830906	2200:20.98	37° 49.28′	25° 26.41′	3.00	1.23	3	323	4.5	0.20	0.0	0.0	CC
830906	2204:21.98	37° 46.26′	25° 24.78′	1.72	1.40	7	272	2.5	0.13	1.4	0.4	CC
830906	2245:18.45	37° 46.02′	25° 27.77′	3.67	1.15	5	149	1.9	0.02	0.3	0.7	CC
830906	2310:51.63	37° 46.66′	25° 24.97′	1.40	2.07	13	137	2.0	0.13	0.6	0.4	BC
830907	0555:16.05	37° 47.43′	25° 24.59′	3.68	2.34	13	165	2.7	0.19	1.1	1.7	CC
830907	0606:12.80	37° 45.89′	25° 25.66′	3.00	1.51	3	233	2.0	0.00	0.0	0.0	CC
830907	0635:45.52	37° 46.81′	25° 26.89′	4.03	1.93	7	110	0.9	0.18	1.4	2.8	BC
830912	0315:31.79	37° 51.31′	25° 28.45′	2.36	1.30	6	294	9.6	0.03	2.5	102.8	DC
830912	1716:37.43	37° 56.91′	25° 40.33′	3.00	1.82	9	317	19.6	0.27	24.1	29.6	DC
830914	0507:56.61	37° 45.12′	25° 24.72′	4.63	1.36	8	244	5.0	0.08	1.4	1.4	CC
830930	0742:34.70	37° 47.29′	25° 23.70′	5.09	1.31	7	162	3.9	0.13	1.4	3.7	CC

APPENDIX B

FINAL HYPOCENTERS

YRMODA	ORIGIN	LAT	LON	DEPTH	MAG	NO	GAP	DM	RMS	ERH	ERV	Q
831001	0007:35.44	37° 45.44′	24° 31.36′	1.50	2.08	16	355	70.1	0.17	649.2	400.8	DC
831002	0543:23.45	37° 00.61′	25° 12.87′	1.10	3.00	11	349	90.0	0.12	81.3	26.9	DC
831002	2157:04.33	38° 05.07′	26° 03.81′	3.00	3.10	9	134	95.0	2.81	19.9	74.5	DC
831009	0421:03.36	37° 26.31′	24° 55.56′	5.71	2.23	14	341	50.6	0.09	43.0	76.5	DC

Program Parameters

Test Variable	Value Used	Definition
TEST(01)	0.0001	The cutoff value for RMS below which Jeffrey's weighting of residuals is not used. In this case Jeffrey's weighting is always used.
TEST(03)	0.2	Critical F-value for the stepwise multiple regression [*Draper and Smith*, 1966]. TEST(03) should be set according to the number and quality of P- and S-arrivals.
TEST(11)	15	Maximum number of iterations in the hypocentral adjustment.

Crustal Velocity Model

2.40	0.00	Column1: P-velocity (km/sec) in a given layer.
4.10	0.50	Column2: depth (km) to the top of a given layer.
5.40	2.20	
6.80	5.40	
7.80	11.00	
	3.	Trial focal depth in km.
	30.	Distance in km from epicenter where the distance weighting is 1.
	100.	Distance in km from epicenter beyond which the distance weighting as 0.
	1.73	Ratio of P-velocity to S-velocity.
	3	A, B, C, and D quality class of earthquakes to be included in the summary of residuals.
	2	Method of selecting earthquake magnitude:

Hypocenter Output

The following data in the HYPO71 locations are given for each event:

1. DATE of earthquake: Year, Month, and day. 830628 = June 28, 1983.
2. ORIGIN time in Coordinated Universal Time (UTC), (hour, minute, and second). 1410 10.14 = 14 hours, 10 minutes, and 10.14 seconds.
3. Epicenter in degrees and minutes of north latitude (LATITUDE) and west longitude (LONGITUDE).
4. DEPTH of the focus in kilometers.
5. MAG, local magnitude of the earthquake.
6. NO, total number of P- and S-arrivals used in location the earthquake.
7. GAP, largest azimuthal separation (degrees) between stations.
8. DM, epicentral distance (km) to the nearest station.
9. RMS, root-mean-square error of the time residuals:

   where R is the observed seismic-wave arrival time minus the computed time at the ith station.
10. ERH, standard error of the epicenter (km):

    where SDX and SDY are the standard errors in latitude and longitude, respectively, of the epicenter.
11. ERZ, standard error of the depth in kilometers.
12. Q, solution quality of the hypocenter. This measure is intended to indicate the general reliability of each solution.

Q	Epicenter	Focal Depth
A	excellent	good
B	good	fair
C	fair	poor
D	poor	poor

Q is based on the nature of the station distribution with respect to the earthquake and the statistical measure of the solution. These two factors are each rated independently according to the following schemes.

Station Distrubution

	NO	GAP	DMIN
A	> 6	< 90	< depth or 5 km
B	> 6	< 135	< 2 x depth or 10 km
C	> 6	< 180	< 50 km
D	others		

Statistical Measures

RMS (sec)	ERH (km)	ERZ (km)

A	< 0.15	< 1.0	< 2.0
B	< 0.30	< 2.5	< 5.0
C	< 0.50	< 5.0	
D	others		

Q is taken as the average of the ratings from the two schemes, i.e., an A and a C yields a B, and two B's yield a B. When the two ratings are only one level apart the lower one is used, i.e., an A and a B yield a B.

APPENDIX C
PHASE DATA

STA	PRMK	TIME	P-SEC	S-SEC	SRMK	DUR
VIF	PU1	830628023136.08		37.15	S 4	14.0
EPD	IPU0	830628023136.24		37.40	S 3	14.0
MTS	P-2	830628023136.30				15.0
PFM	IPU2	830628023136.33		37.73	S 0	14.0
FRA	IPD0	830628023136.37		38.15	S 2	16.0
RIB	P+4	830628023136.62				10.0
LFA	P+4	830628023136.79				16.0
MTS	IP+2	830628141011.68		13.78	S 4	10.0
RIB	IP+0	830628141011.77				10.0
VIF	IPD0	830628141011.80		13.00	S 3	8.0
LFA	IP+3	830628141012.15				10.0
VIF	IP-1	830628141461.94		62.94	S 3	10.0
MTS	IP-1	830628141462.09		63.89	S 3	14.0
LFA	IP+1	830628141462.33				15.0
RIB	EP+4	830628141463.55				9.0
MTS	IP+1	830628172968.49		70.42	S 4	15.0
RIB	IPU1	830628172968.57				15.0
VIF	IPD0	830628172968.58		70.12	S 4	14.0
CRA	IPU0	830628172968.69		69.40	S 3	15.0
LFA	IPU2	830628172968.96				15.0
FRA	P+3	830628221725.58		30.96	S 3	15.0
VIF	P-1	830628221725.80		30.94	S 3	15.0
MTS	PD0	830628221725.85		31.40	S 3	15.0
RIB	P+3	830628221726.01		30.94	S 3	15.0
LFA	P+2	830628221726.30		32.47	S 3	15.0
CML	P-1	830628221727.21		33.01	S 3	14.0
EPD	IPU0	830628234457.13		58.48	S 3	14.0
MTS	IPU0	830628234457.14		59.26	S 4	14.0
RIB	IPU0	830628234457.22		58.25	S 3	14.0
VIF	IPD0	830628234457.23		58.75	S 3	15.0
CRA	IPU0	830628234457.33		58.15	S 4	16.0
LFA	IPD0	830628234457.53		59.72	S 4	12.0
FRA	EP+3	830628234457.70				13.0
CML	EP+4	830628234458.31				11.0
VIF	IP-0	830629024244.81		45.83	S 3	11.0
FRA	EP+4	830629024244.93		49.87	S 4	08.0
MTS	P+0	830629024244.98		46.82	S 4	10.0
LFA	P-0	830629024245.68				10.0
MTS	EP+1	830629041155.00		57.18	S 4	10.0
VIF	IPD0	830629041155.12		56.30	S 3	10.0
RIB	EP+3	830629041155.16				7.0
LFA	EP+3	830629041155.38		57.65	S 4	9.0
MTS	P-2	830629061112.85		13.75	S 3	10.0
VIF	IPD0	830629061112.85		14.38	S 4	11.0
RIB	EP+3	830629061112.88		14.64	S 4	9.0
LFA	EP+3	830629061113.07		15.92	S 4	10.0

APPENDIX C
PHASE DATA

STA	PRMK	TIME	P-SEC	S-SEC	SRMK	DUR
PVN	IP+2	830701053336.20	44.81		S 4	28.0
CRA	EP+0	830701053337.34	47.53		S 2	30.0
MTS	P+0	830701053337.38	47.42		S 2	30.0
VIF	EP+0	830701053337.47	47.32		S 4	30.0
FRA	P+0	830701053338.69	49.27		S 2	30.0
FRA	IPD1	830702110959.51	60.27		S 3	14.0
VIF	IPD1	830702111000.92	02.34		S 3	17.0
MTS	IPU2	830702111001.12	03.14		S 3	10.0
LFA	IPD0	830702111001.71	03.83		S 3	14.0
FRA	PU1	830702222937.86				18.0
VIF	PU0	830702222938.62	44.21		S 3	18.0
EPD	IPD1	830702222938.65	44.62		S 1	18.0
PFM	IPD1	830702222938.95	44.65		S 1	18.0
MTS	PU0	830702222939.06	45.42		S 3	18.0
PST	IPD0	830702222939.23	45.19		S 1	18.0
RIB	P+0	830702222939.29				18.0
LFA	PU0	830702222939.37				18.0
CHC	EP-3	830702222939.42	46.15		S 1	18.0
PVN	IP-3	830702222939.79	46.78		S 4	18.0
CML	P-1	830702222939.91	47.19		S 3	18.0
CML	EP+3	830705063400.27	5.66		S 3	12.0
PVN	P+3	830705063400.60	5.90		S 3	18.0
LFA	P+1	830705063401.08	7.40		S 3	12.0
RIB	PD1	830705063401.08	7.41		S 4	12.0
MTS	EP+3	830705063401.58	8.37		S 4	12.0
VIF	EP+4	830705063403.21	8.95		S 3	12.0
LFA	EP+3	830705232826.65				17.0
RIB	EP+3	830705232826.66				15.0
VIF	EP+2	830705232827.29				15.0
MTS	EP+2	830705232827.36				17.0
CML	EP+2	830705232828.53	32.25		S 3	15.0
MTS	P+4	830706023260.09	64.54		S 4	12.0
VIF	P+2	830706023262.02	64.81		S 4	12.0
RIB	P+2	830706023262.14	65.31		S 4	12.0
LFA	P+3	830706023262.86	65.57		S 4	12.0
CML	P+3	830706023263.02	65.45		S 3	12.0
FRA	P+2	830706023263.47	65.10		S 3	12.0
CRA	IPD0	830713012030.29	34.39		S 1	19.0
VIF	IPU0	830713012030.45	33.37		S 4	19.0
MTS	IPU0	830713012030.55				19.0
RIB	EPD3	830713012031.15				19.0
CML	EP+3	830713012031.26	35.46		S 3	19.0
FRA	IP+3	830713012031.43				19.0
ADB	IP+4	830713012031.81	33.65		S 4	20.0

APPENDIX C
PHASE DATA

STA	PRMK	TIME	P-SEC	S-SEC	SRMK	DUR
VIF	P-4	830717004850.02	52.96		S 4	16.0
EPD	IPU0	830717004851.32	52.90		S 4	17.0
FRA	IPU0	830717004851.35	52.89		S 3	20.0
PFM	IPU0	830717004851.46	52.93		S 2	16.0
MTS	PD1	830717004851.53				15.0
ADB	P+3	830717004851.67				25.0
RIB	IPD0	830717004851.71	53.42		S 3	18.0
LFA	PU1	830717004852.05	53.49		S 4	19.0
PVN	P-3	830717004852.55	54.47		S 4	12.0
CML	EP+0	830718122908.05				10.0
VIF	PU0	830718122910.40	11.79		S 3	10.0
RIB	EP+0	830718122910.93				10.0
SVA	EP+4	830719232854.11		58.00	S 4	10.0
VIF	IPD0	830719232854.86	56.41		S 4	13.0
FRA	P-3	830719232854.87	56.57		S 3	9.0
MTS	P+3	830719232855.07	57.25		S 4	11.0
RIB	EP+4	830719232855.29	56.82		S 2	9.0
LFA	P+1	830719232855.60	56.54		S 4	11.0
VIF	EPU3	830725073710.53	15.23		S 3	14.0
MTS	IPU1	830725073710.82	15.91		S 3	14.0
LFA	IPU1	830725073711.14	16.00		S 3	14.0
RIB	EP+3	830725073712.29	17.27		S 3	14.0
VIF	PU1	830726172425.27	30.15		S 2	18.0
CRA	PU0	830726172425.60	32.24		S 4	18.0
PFM	P+3	830726172425.65	30.39		S 3	18.0
MTS	P+1	830726172425.72	30.53		S 4	18.0
RIB	PU0	830726172425.97	29.65		S 4	18.0
PST	PU0	830726172426.05	30.84		S 2	18.0
LFA	PD0	830726172426.11	30.93		S 3	18.0
FRA	P+4	830726172426.37	30.46		S 3	18.0
SVA	P+4	830726172426.38	31.89		S 4	18.0
CML	P+4	830726172426.66	31.62		S 3	18.0
FAC	PU1	830726172427.94	33.67		S 3	18.0
FAC	IP+0	830730232128.55				20.0
PVN	P+4	830730232130.00				30.0
PST	IP+4	830730232130.16	31.52		S 2	20.0
LFA	IPD1	830730232130.67				20.0
ADB	P+3	830730232130.74				25.0
RIB	IPD1	830730232130.77	32.63		S 3	20.0
MTS	IPD1	830730232131.16				20.0
VIF	IPU3	830730232131.62				20.0

APPENDIX C
PHASE DATA

STA	PRMK	TIME P-SEC	S-SEC	SRMK	DUR
VIF	IPU0	830805235531.44	32.92	S 4	20.0
LGD	IPU1	830805235531.55	32.95	S 2	19.0
ADB	IP+3	830805235531.91			22.0
CRA	IPU1	830805235531.97	32.41	S 2	15.0
MTS	IPD0	830805235532.32			13.0
RIB	EP+3	830805235532.66	34.03	S 1	10.0
LFA	P+2	830805235532.67			13.0
FRA	P-3	830805235532.71	35.06	S 4	16.0
CML	EP+4	830805235533.01			13.0
SVA	EP+2	830805235533.75			13.0
PST	P+0	830810004040.33	44.61	S 2	25.0
ADB	P+3	830810004040.50	44.30	S 3	14.0
CRA	IP+0	830810004040.79	45.65	S 2	20.0
CML	P+2	830810004040.81			18.0
FAC	P+2	830810004040.93	45.89	S 3	18.0
CHC	IPU0	830810004040.94	45.92	S 2	25.0
VIF	P-2	830810004040.98	45.63	S 3	18.0
LFA	P-0	830810004041.16			18.0
PVN	P+3	830810004041.20	45.60	S 4	10.0
RIB	P-0	830810004041.50	46.37	S 1	18.0
MTS	P+1	830810004041.54	47.13	S 4	18.0
FRA	P+3	830810004041.55	46.14	S 1	18.0
SVA	P+4	830810004042.35	48.42	S 4	18.0
SVA	PD1	830812232623.13	29.66	S 2	15.0
ADB	P+4	830812232623.24	30.00	S 4	18.0
VIF	P-1	830812232623.57	30.14	S 2	15.0
MTS	PU1	830812232623.90	30.92	S 3	15.0
FRA	P+4	830812232623.99	31.01	S 4	15.0
RIB	P+1	830812232624.18	31.75	S 3	15.0
LFA	P-1	830812232624.32	31.94	S 2	15.0
PVN	P+3	830812232624.60	30.60	S 4	20.0
CML	P-3	830812232624.70	31.87	S 2	15.0
FAC	P+3	830812232626.03	33.54	S 2	15.0
CML	EP+4	830813021450.00	56.33	S 3	00.0
LGD	PU0	830813021450.83	54.30	S 2	00.0
ADB	P+3	830813021450.90	54.50	S 3	25.0
VIF	P+1	830813021451.11	55.27	S 2	00.0
PST	PU0	830813021451.50	55.97	S 2	00.0
MTS	P-1	830813021451.55	55.81	S 3	00.0
LFA	P-1	830813021451.74	56.44	S 3	00.0
PVN	EP+4	830813021451.80	55.00	S 3	15.0
RIB	P+3	830813021452.10	57.41	S 3	00.0
FAC	PD0	830813021453.21	58.46	S 3	00.0

APPENDIX C
PHASE DATA

STA	PRMK	TIME	P-SEC	S-SEC	SRMK	DUR
MTS	PD0	830824201721.46		23.43	S 4	12.0
EPE	EPU0	830824201721.51		22.63	S 2	12.0
VIF	P+4	830824201721.55		22.72	S 3	12.0
RIB	P+2	830824201721.57		23.22	S 4	12.0
LFA	PU0	830824201721.83		22.25	S 4	12.0
SVA	P+4	830824201723.34		24.91	S 4	12.0
VIF	P+4	830829221420.19		23.52	S 4	10.0
FRA	PD0	830829221421.36		22.97	S 3	10.0
EPE	PD0	830829221421.48		22.79	S 2	10.0
SVA	PD0	830829221421.76		23.95	S 4	10.0
MTS	PU1	830829221421.99		24.55	S 4	10.0
RIB	P+1	830829221422.16		24.45	S 4	10.0
LFA	P+1	830829221422.59		24.82	S 4	10.0
VIF	P+3	830902140317.61		22.54	S 3	08.0
LFA	P+4	830902140319.50				08.0
MTS	P+3	830902140319.95		23.73	S 3	08.0
SVA	P+4	830902140320.72		20.72	S 4	08.0
CML	P+4	830902140321.43		25.01	S 4	08.0
RIB	P+3	830902140321.73		22.05	S 3	08.0
FRA	P+4	830902140322.17		22.17	S 4	08.0
EPE	IPU0	830906150907.35		08.18	S 2	13.0
PFM	EPU3	830906150907.36		08.15	S 2	14.0
CRA	IPU0	830906150908.34		09.04	S 3	13.0
VIF	IPD0	830906175135.77		37.53	S 3	08.0
MTS	IP+1	830906175135.90		37.67	S 3	05.0
FRA	EP+4	830906175136.00		38.12	S 3	05.0
LFA	EP+1	830906175136.21		38.68	S 4	05.0
SVA	P+4	830906175141.85		44.72	S 4	05.0
VIF	IPD0	830906184258.20		59.91	S 4	10.0
MTS	IPD0	830906184258.25		60.04	S 4	10.0
FAC	EP+4	830906184258.67				10.0
RIB	EP+2	830906184259.00		61.85	S 4	10.0
LFA	EP+1	830906184259.02		61.16	S 4	10.0
FRA	EP+4	830906184259.08		61.53	S 2	10.0
VIF	P-0	830906184663.35		64.95	S 4	08.0
MTS	P-0	830906184663.40		65.20	S 4	08.0
LFA	P+2	830906184663.44		64.24	S 2	08.0
RIB	P+4	830906184664.20		65.68	S 4	08.0
FAC	P+4	830906184664.56		66.56	S 4	08.0
SVA	P+3	830906184705.22		66.02	S 4	08.0
CML	P+4	830906184705.68				08.0

APPENDIX C
PHASE DATA

STA	PRMK	TIME P-SEC	S-SEC	SRMK	DUR
SVA	P+4	830906184843.05	48.57	S 3	00.0
RIB	P+4	830906184843.86	46.23	S 4	05.0
VIF	P-1	830906184845.83	47.38	S 1	05.0
MTS	P+2	830906184845.88			05.0
FRA	P+1	830906184846.21	47.13	S 3	05.0
LFA	P+3	830906184846.42	48.90	S 4	05.0
CML	EP+4	830906190238.76	40.81	S 4	06.0
SVA	EP+3	830906190239.00	40.01	S 3	06.0
MTS	IPU0	830906190239.31	40.82	S 2	06.0
VIF	IPU0	830906190239.36	40.92	S 4	06.0
PFM	IP+0	830906190239.38	40.50	S 2	06.0
LFA	IP+2	830906190239.45	40.24	S 4	06.0
RIB	EP+4	830906190240.73	41.24	S 2	06.0
RIB	P+4	830906191346.35	47.33	S 3	05.0
FAC	P+4	830906191346.59			05.0
VIF	P+0	830906191346.68	47.10	S 3	05.0
MTS	P-0	830906191346.71			05.0
LFA	P+1	830906191346.94	47.45	S 3	05.0
MTS	IPD0	830906191403.40			15.0
VIF	IPU0	830906191403.48			16.0
LFA	IPD0	830906191404.13			14.0
VIF	P+1	830906192033.19	33.52	S 2	10.0
MTS	PD0	830906192033.20			07.0
RIB	P+1	830906192033.24	33.69	S 2	05.0
LFA	P+3	830906192033.73	35.93	S 4	07.0
CML	P+4	830906192035.26			05.0
FAC	P+4	830906192036.35			05.0
MTS	P+0	830906202211.19	12.49	S 4	08.0
VIF	P+0	830906202211.33	12.41	S 3	08.0
PFM	IPU0	830906202211.96	13.15	S 3	08.0
LFA	P+0	830906202212.12	13.69	S 4	08.0
VIF	P+0	830906203314.76	16.42	S 4	08.0
MTS	P+0	830906203315.02	16.63	S 3	09.0
LFA	P+0	830906203315.52	117.00	S 2	08.0 .0
PFM	P+1	830906203315.54	16.81	S 2	08.0
MTS	IPD0	830906205819.70			17.0
VIF	IPU0	830906205819.78			17.0
LFA	IPU0	830906205820.20			17.0
MTS	P+0	830906210236.30	37.05	S 3	12.0
VIF	P+1	830906210236.34	38.05	S 4	12.0
LGD	P+1	830906210236.74	37.84	S 3	12.0
LFA	P+1	830906210237.02	38.39	S 3	12.0

APPENDIX C
PHASE DATA

STA	PRMK	TIME	P-SEC	S-SEC	SRMK	DUR
VIF	IPU2	830906213317.63				15.0
MTS	IPD2	830906213317.78				15.0
LGD	IPU1	830906213318.15	19.30	S	3	15.0
LFA	IPD1	830906213318.20				17.0
MTS	IPD0	830906214047.55	48.75	S	3	25.0
VIF	IPU0	830906214047.60	48.75	S	3	20.0
RIB	IPD0	830906214047.65	48.65	S	3	15.0
LGD	IP+3	830906214047.67	47.84	S	3	15.0
LFA	IPD0	830906214047.95	49.00	S	3	21.0
MTS	IPD0	830906215804.35				16.0
VIF	IPU0	830906215804.45				17.0
LGD	IPU1	830906215804.71	5.89	S	1	12.0
LFA	EPU0	830906215804.75				17.0
MTS	EPU0	830906220022.05				12.0
LFA	EPU0	830906220022.75				
VIF	EPU0	830906220023.25				10.0
MTS	IPD1	830906220422.80	23.50	S	3	15.0
VIF	EP+0	830906220423.25	24.59	S	4	15.0
RIB	EPD3	830906220423.53	24.70	S	2	10.0
LFA	IPD0	830906220423.55	24.75	S	3	18.0
LGD	P+4	830906220423.66	24.67	S	4	11.0
LFA	IPU1	830906224519.50				10.0
MTS	IPD1	830906224519.55				13.0
VIF	IPU1	830906224519.62				8.0
LGD	IPU0	830906224519.93	21.01	S	2	10.0
MTS	EP+1	830906231052.30				37.0
VIF	IPD1	830906231052.80	54.35	S	3	35.0
RIB	IPU0	830906231052.85	54.20	S	3	33.0
LFA	IPU0	830906231053.30	54.00	S	4	41.0
FRA	IPU2	830906231053.45	55.45	S	4	28.0
SVA	IPU1	830906231053.85	57.50	S	4	29.0
CHC	IPU0	830906231054.01	55.16	S	2	18.0
CML	IPD1	830906231054.10x				25.0
PST	IPU0	830906231054.25	55.98	S	2	20.0
MTS	IPU0	830907055517.15	22.00	S	4	47.0
RIB	IPU1	830907055517.25	18.70	S	3	40.0
VIF	IPD2	830907055517.30	18.75	S	3	42.0
LFA	IPU1	830907055517.60				55.0
SVA	IPU1	830907055518.20	20.50	S	4	37.0
CHC	IPU1	830907055518.48	20.39	S	3	41.0
CML	IPU0	830907055518.55	20.75	S	2	40.0
PST	IPU0	830907055518.77	20.73	S	1	42.0
FAC	EP+4	830907055520.00				18.0

APPENDIX C
PHASE DATA

STA	PRMK	TIME	P-SEC	S-SEC	SRMK	DUR
MTS	IPD0	830907060613.75	15.10		S 4	15.0
VIF	IPU0	830907060613.80	15.25		S 4	20.0
LFA	EPD1	830907060614.23	15.50		S 4	15.0
RIB	EP+4	830907060614.95	15.63		S 0	12.0
RIB	IPU0	830907063546.40	48.15		S 4	25.0
MTS	IPU0	830907063546.60	48.50		S 4	25.0
VIF	IPU0	830907063546.65	48.10		S 3	22.0
LFA	IPD0	830907063546.95	48.75		S 4	27.0
SVA	EP_3	830907063548.25	50.25		S 3	25.0
EPE	IPU0	830912031533.93	35.46		S 2	10.0
CHC	IPU0	830912031534.19	35.96		S 1	12.0
PST	IP-0	830912031534.77	37.00		S 2	13.0
CHC	EP+4	830912171641.46	44.39		S 3	20.0
FAC	EP+3	830912171641.64	44.63		S 3	20.0
LFA	IPU0	830912171641.97				20.0
CML	EP+3	830912171642.04				20.0
RIB	EP+0	830912171642.38	45.52		S 4	20.0
MTS	IPU0	830912171642.80	46.85		S 3	20.0
FRA	EP+4	830912171644.43				20.0
VIF	IPD4	830912171644.56	47.14		S 3	20.0
EPE	IPU1	830914050758.04	59.23		S 3	12.0
CRA	IPD1	830914050758.16	59.29		S 3	12.0
CHC	IP+1	830914050758.69	60.35		S 3	12.0
PST	P+1	830914050759.06	60.84		S 3	15.0
FRA	IPU0	830930074236.33	37.94		S 4	12.0
MTS	IPU0	830930074236.34	37.90		S 4	12.0
RIB	IPD0	830930074236.35	37.22		S 2	12.0
VIF	IPD0	830930074236.60	37.80		S 4	12.0
SVA	IPD0	830930074236.61	37.88		S 4	12.0
LFA	IPD0	830930074236.73				12.0
SVA	IP+0	831001000746.81	55.03		S 2	20.0
FRA	IP+3	831001000747.13	55.92		S 2	20.0
VIF	IPU0	831001000748.10	56.87		S 3	20.0
MTS	IP+3	831001000748.19	56.82		S 3	20.0
ADB	IP-3	831001000748.30	57.30		S 3	35.0
RIB	IP+0	831001000748.42	57.61		S 2	20.0
LFA	IP-3	831001000748.94	58.89		S 3	20.0
CML	IPU0	831001000749.33	59.76		S 2	20.0
FAC	IP-3	831001000750.45	59.82		S 3	20.0

APPENDIX C
PHASE DATA

STA	PRMK	TIME	P-SEC	S-SEC	SRMK	DUR
FRA	P+4	831002054336.33	47.68	S	4	20.0
ADB	IPU3	831002054336.50	48.40	S	4	40.0
SVA	IPD2	831002054336.67	47.90	S	4	20.0
VIF	IPD2	831002054336.71	48.90	S	4	20.0
MTS	IPU0	831002054337.18	49.30	S	4	20.0
LFA	IPU0	831002054337.29	49.35	S	4	20.0
CML	P-2	831002054337.43	49.40	S	4	20.0
PVN	IP-3	831002054337.59	49.60	S	4	30.0
RIB	IPU4	831002054337.63	49.66	S	4	20.0
FAC	P+4	831002054338.20				20.0
FAC	PD0	831002215709.77	23.70	S	3	18.0
PVN	P+3	831002215710.70	25.00	S	3	30.0
CML	PD0	831002215710.77	24.95	S	3	18.0
RIB	PD0	831002215711.32	25.50	S	3	18.0
LFA	PD0	831002215711.43	25.61	S	3	18.0
MTS	PD0	831002215711.80	25.98	S	3	18.0
ADB	P+3	831002215711.90	26.08	S	3	42.0
VIF	P-1	831002215712.24	26.42	S	3	18.0
SVA	PD0	831002215712.81	26.99	S	3	18.0
FRA	PU0	831009042111.55	17.09	S	4	22.0
SVA	PU0	831009042111.79				22.0
ADB	IP+3	831009042112.40	18.85	S	4	90.0
VIF	PU0	831009042112.44	18.93	S	2	22.0
MTS	PU0	831009042112.82	19.68	S	2	22.0
RIB	PU0	831009042112.95	19.92	S	4	22.0
LFA	PU0	831009042113.16	18.84	S	4	22.0
PVN	P+3	831009042113.20	19.97	S	3	55.0
CML	PU0	831009042113.56	21.04	S	3	22.0
FAC	PU1	831009042114.73	22.30	S	2	22.0